Universitetet
i Stavanger

FACULTY OF SCIENCE AND TECHNOLOGY

MASTER'S THESIS

Study programme/specialisation: Petroleum Geosciences Engineering	Spring semester, 2017 Open
Author: Herman Birkeland	..... (signature of author)
Faculty Supervisor: Chris Townsend	
Title of master's thesis: A study of several proposed alluvial fan deposits in the Kerpini Fault Block, Greece	
Credits: 30	
Keywords: Greece Gulf of Corinth Peloponnese Peninsula Alluvial Fan Kerpini Fault Block Sedimentology and Structural Geology Kalavryta	Number of pages: 125 + enclosure: 14 Stavanger, 19.06.2017

A Study of Several Proposed Alluvial Fan Deposits in the Kerpini Fault Block, Greece

By

Herman Birkeland

Master Thesis

Presented to the Faculty of Science and Technology

University of Stavanger

University of Stavanger

June 2016

Acknowledgements

Firstly, a sincere thanks to my main supervisor Chris Townsend, for his valuable and constructive input before, during and after the field trips. Another thanks goes to my secondary supervisor, Alejandro Escalona, for his constructive comments and discussion related to the thesis. I would also like to express my gratitude to Eirik Oppedal and Asbjørn Veiteberg, for being wonderful fellow students and travelling companions, and for their many helpful discussions during the past two semesters. Another thanks goes to the Petroleum Student Fund at the University of Stavanger for funding the two field trips. Thanks to my brother, Fredrik Birkeland, for his constructive criticism towards the end of the thesis. Finally, thank you Emma, for being such a wonderful and supportive girlfriend during this master's degree. Your patience and motivation has been dearly appreciated.

Abstract

A study of several proposed alluvial fan deposits in the Kerpini Fault Block, Greece

Herman Birkeland

University of Stavanger

Supervisor: Chris Townsend

The rift in the Gulf of Corinth is one of the most active rifts in the world. Regional N-S extension has caused normal faulting from the Gulf of Corinth and southwards into the Peloponnese Peninsula. The normal faulting resulted in a series of half grabens within a system of uplifted, rotated and north-dipping fault blocks, one of which is the Kerpini Fault Block. Within this southern fault block, many stratigraphic units are deposited in a complex relationship. Three of these units were proposed by Hadland (2016) to be footwall-derived alluvial fan deposits. These units, in addition to a fourth one, was studied in detail during this project. Additionally, a new and updated geological map was constructed. This was done to better understand the layout and extents of the stratigraphic units and faults in the area of study. The fault block mainly consists of pre-fault and syn-fault strata.

Through detailed outcrop analyses and investigation into facies variabilities, the four proposed fans were confirmed to be individual alluvial fan deposits within the Kerpini Fault Block. They were confirmed by classifying the facies into debris-flow, sheetflood and streamflow deposits. Three of the fans were classified as sheetflood-dominated fans, whereas the easternmost fan in the area of study was classified as a debris-flow dominated fan. Only two of the three proposed fans appear to be footwall-derived. The third one was suggested to be sourced from the north, but was in fact sourced from the south. The alluvial fans subject to this study are syn-fault deposits. The pre-fault strata originates from the Kalavryta Fault Block to the south.

Table of contents

Acknowledgements i

Abstract ii

Table of contents iii

List of figures vi

Chapter 1: Introduction 1

1.1 Background 1

1.2 Geological problem and previous studies 1

1.3 Objectives 2

1.4 Data 2

Chapter 2: Regional geology 3

2.1 Tectonics 3

2.2 Structural framework 6

2.2.1 Faults and fault geometries 7

2.3 Stratigraphic framework 8

2.4 Glacial history 9

2.5 Area of study 9

Chapter 3: Alluvial fan theory 10

3.1 Alluvial fans 10

3.2 Debris-flow dominated fans 13

3.3 Streamflow dominated fans 13

3.4 Sheetflood dominated fans 13

Chapter 4: Methodology 15

4.1 Pre-field work 15

4.2 Fieldwork 15

4.2.1 Structural measurements 16

4.2.2 Clast studies 16

4.3 Post-field work 19

Chapter 5: Field observations – faults and stratigraphic units 20

5.0 Introduction 20

5.1 Major faults 23

5.1.1 Kerpini Fault 23

5.1.2 Doumena Fault 24
5.1.3 Roghi Fault 25
5.1.4 Minor faults 26
5.1.4.1 Fault A 27
5.2 Stratigraphic units in the Kerpini Fault Block 36
5.2.1 Basement lithologies 38
5.2.2 Lower Conglomerates 41
5.2.3 Sub-horizontal Sediments 42
5.2.4 Vighia Member 43
5.2.5 Kalavryta Member 45
5.2.6 East Vouraikos Sediments 47
5.2.7 Skepasto Member 47
5.2.8 Profitis Conglomerates 47
5.2.9 Late Fan 50
5.3 Fan A 51
5.3.1 Structural description 52
5.3.2 Sedimentary description 54
5.3.3 Fan A summary 63
5.3.4 Facies interpretation 64
5.4 Fan B 65
5.4.1 Structural description 66
5.4.2 Sedimentary description 68
5.4.3 Fan B summary 75
5.4.4 Facies interpretation 75
5.5 Fan C 77
5.5.1 Structural description 78
5.5.2 Sedimentary description 79
5.5.3 Fan C summary 83
5.5.4 Facies interpretation 83
5.6 Fan D 84
5.6.1 Structural description 87
5.6.2 Sedimentary description 87

5.6.3 Summary 93
5.6.4 Facies interpretation 93
5.7 Summary of fans 94
Chapter 6: Discussion 95
6.1 Fan A and Fan B 96
6.1.1 Fan A - classification and sourcing 96
6.1.2 Fan B – classification and sourcing 96
6.1.3 Relative timing 97
6.1.4 Earlier Lobes 97
6.2 Fan C 98
6.2.1 Classification and sourcing 98
6.2.2 Relative timing 98
6.3 Fan D 99
6.3.1 Classification and sourcing 99
6.3.2 Relative timing and Late Fan influence 99
6.3.3 Fault possibility 100
6.3.4 Lobes I and II 101
6.4 Cross sections 102
6.5 Transfer faults 107
6.6 Kalavryta Member and Lower Conglomerates 109
6.7 Profitis Conglomerates 110
6.8 XRD results 111
6.9 Evolutionary model 112
6.9.1 Stage 1 113
6.9.2 Stage 2 114
6.9.3 Stage 3 115
6.9.4 Stage 4 116
6.9.5 Stage 5 117
6.9.6 Stage 6 118
6.9.7 Stage 7 119
Chapter 7: Conclusion 120
Reference list 122

List of figures

Figure 1 : Shows the evolution of the Aegean Sea, and in (d): The present day rift systems of the Aegean Sea, the Corinth Rift (outlined in red), and the Peloponnese Peninsula (outlined in yellow). Modified after (Armijo et al., 1996). 4
Figure 2: Regional map of the Gulf of Corinth showing major structural features. Study area in red box. Modified after (Moretti et al., 2003). 4
Figure 3: Geological map from the Gulf of Corinth in the north and southwards past the study area. The syn-rift sediments of the Kerpini Fault Block (inside red box), which is the focus of the study, are coloured according to the legend. The eastern and western river valley boundaries are coloured in blue. Modified after Ford et al., (2013). 5
Figure 4: N-S cross section from inland Peloponnese Peninsula in the south and into the Gulf of Corinth in the north, shows the detachment fault model. The micro earthquakes in the figure are from Rietbrock et al. (1996), recorded 15 km west of this cross section. Modified after Sorel (2000). 6
Figure 5: Down-fan reduction of gradient accompanying reduction in particle size of a wet fan. Modified after Boothroyd (1972). 10
Figure 6: Shows four different examples of alluvial fans and their associated morphological features, after Blair and McPherson (1994) 12
Figure 7: Triangular classification scheme used to differentiate between the three main types of alluvial fans: debris-flow, streamflow and sheetflood fans. The classification is based on flow type, gradient, size and textural heterogeneity. As seen in the figure, debris-flow fans are dominated by mass movement, high gradient, high textural heterogeneity and large clast sizes. Streamflow fans consist of more channelized flows, lesser clast sizes and smaller gradient. The same goes for sheetflood fans. (Galloway and Hobday, 1996) 14
Figure 8: Grain size classification scheme modified after Wentworth (1922). For this study, cobble sizes are the most prominent, and as such, a more detailed size interval for cobbles was defined. 17
Figure 9: Field photo of two coarse beds in Fan A, showing how average clast measurements were made. Areas of approximately 1 x 0.50 m were used, but for thinner beds, it was scaled down accordingly. Book for scale. The location of this photo is shown in Figure 45. 17
Figure 10: Shows the general terms used for describing the roundness of the conglomeratic clasts. 18
Figure 11: Left - glacially reworked green chert clast with striations and a facetted pebble. Right - shows a common angular red chert clast. These two clasts were subject to an XRD analysis. Pencil for scale. 19
Figure 12: Surrounding area and detailed geological map of the Kerpini Fault Block. This map shows stratigraphic units and faults identified during this study, as well as work done by previous master students from the University of Stavanger, specifically the south-western area (Syahrul, 2014; Stuvland, 2015; Hadland, 2016). 22
Figure 13: Satellite image showing how the Roghi Fault (highlighted by yellow dots) affects the topography. 25
Figure 14: Zoomed in geological map with all the collected dip data displayed. If displayed in Figure 12, it would be too cluttered to be viewable. 26
Figure 15: Location of Fault A and the apex of Fan A. The red basement shales are located here, but coloured white for simplicity as they all belong to the basement. The location of this photo is shown in Figure 45. 27
Figure 16: Photo taken from the apex of Fan A, looking southwards along the fan. The Red Basement Shales can be seen over the sharp contact that is interpreted as Fault B. One of the earlier fan lobes are truncating against the main fan. At the back of the figure, Fan B is located close to the Vighia Member. The basement of the Kalavryta Fault Block is observed in the south-east. The location of this photo is shown in Figure 45. 28
Figure 17: Photo taken from Fan B towards Fan A. It shows Fault C, and how the package of conglomerates to the north of the fault disappears in the immediate hanging wall. The location of this photo is shown in Figure 45. 29
Figure 18: The planar basement surface interpreted as Fault D. The location of this photo is shown in Figure 45. 30
Figure 19: Fault D faulting the basement further south. The location of this photo is shown in Figure 45. 30

Figure 20: Fault E cutting through Fan B. The unconformity plane dips steeply towards the point of observation. Note the fine beds below the unconformity. Scale is relevant to base of figure. The location of this photo is shown in Figure 60. 31
Figure 21: Planar and steeply dipping basement surface, interpreted as a basement fault plane (white), with an associated Dip / DD of 60° / 190°S. The Lower Conglomerates (brown) are located in the immediate hanging-wall of the fault, with a Dip / DD of 15° / 90°E. The location of this photo is shown in Figure 71. 32
Figure 22: Fault G down-faulting fine and thinly bedded sediments adjacent to coarse and more thickly bedded conglomerates. The location of this photo is shown in Figure 71. 33
Figure 23: Drone photo of the northern area of Fan D showing the linear feature that bounds Fan D in the north, interpreted as Fault H. Location of Faults G and I and the Roghi Fault is outlined as well. The location of this photo is shown in Figure 71. 34
Figure 24: Fault I and the nature of the contact on the eastern side of Profitis Ilias. The location of this photo is shown in Figure 12. 35
Figure 25: Fault I across the Roghi Fault. It has stepped 50 metres to the north in this location. The location of this photo is shown in Figure 12. 35
Figure 26: Field photo of Roghi Mountain taken from the east of the Vouraikos Valley – shows the Intra Roghi Faults 1 and 2 cutting through the Vighia Member. Scale is relevant to the area between the faults. The location this photo was taken from is too far east of the study area to be displayed in Figure 12. However, it is shot 2 km directly east of where the Intra Roghi Fault 2 intersects the Vouraikos River Valley. 36
Figure 27: Top – panorama photo of nearly the entire study area shows the mapped features from Figure 12 but in a 3D view. It features most of the important stratigraphic units and some of the faults in the area. Bottom – same panorama photo, but with interpretations. Scale is relevant to the mountain ridge of Profitis Ilias, at the very back of the figure. The location of this photo is shown in Figure 12. 37
Figure 28: Typical appearance of the basement carbonates. The location of this photo is shown in Figure 12. 38
Figure 29: Simplified model showing variations in the paleotopography. 39
Figure 30: Typical brittle red basement shales. The location of this photo is shown in Figure 12. 39
Figure 31: One of the coarse breccia variations found within the area of study. Some of the angular clasts are outlined in black. The location of this photo is shown in Figure 71. 40
Figure 32: One of the fine breccia variations found in the Kerpini Fault Block. The location of this photo is shown in Figure 71. 41
Figure 33: Interval of conglomerates with a sand lens, typical for the fluvial/alluvial character of the Lower Conglomerates (coloured yellow for visualization). Compass for scale. The location of this photo is shown in Figure 33. 42
Figure 34: An outcrop of Sub-horizontal Sediments that shows the fluvial character of these clast-supported conglomerates with relatively small clast sizes compared to other conglomerates in the study area. The location of this photo is shown in Figure 12. 43
Figure 35: Segmentation of Roghi Mountain in a map view of LIDAR data (Sigmundstad, 2016). 44
Figure 36: Shows the small clast sizes and good sorting of the northernmost part of the Vighia Member. Compass for scale. The location of this photo is shown in Figure 71. 44
Figure 37: Conglomerates of the Kalavryta Member on the footwall of the Kerpini Fault Block in the south. Compass for scale. The location of this photo is shown in Figure 12. 46
Figure 38: Close to the basement unconformity near the Profitis Ilias Mountain, the conglomerates of the Kalavryta Member that are believed to have been transported furthest north in the Kerpini Fault Block are found. Compass for scale. The location of this photo is shown in Figure 45. 46
Figure 39: Profitis Conglomerates at their highest elevation, featuring cobble sized conglomerates. The location of this photo is shown in Figure 71. 48
Figure 40: Photo from the base of the Profitis Conglomerates outcrop, with boulder-sized clasts and thicker less well defined bedding than at the top of the outcrop. The location of this photo is shown in Figure 71. 49
Figure 41: Rose diagram constructed based on all the collected dip data for the Profitis Conglomerates. 49
Figure 42: Top: Uninterpreted photo taken from east across the Vouraikos River Valley, showing the best possible angle to view the plane of the unconformity. It intersects the topography, dipping away from

the point of observation. Bottom: Interpreted photo with all the stratigraphic units and unconformity included. The location of this photo is shown in Figure 12 50
Figure 43: Geological map of the Kerpini Fault Block with the four fans highlighted (A, B, C, D). Shows the locations of the photos taken from the east of the Vouraikos River Valley. 51
Figure 44: Rose diagram based on all the dip data collected for Fan A. There are some outcrops near the mid-fan area that dip slightly more to the east (≈ 135°); otherwise, the rest of the fan dips exclusively to the south (180 - 190°). 52
Figure 45: Shows a detailed geological map of Fan A and its associated lithological sections. Red (west) and black (east) lines within the dashed boxes on the map represent red and black labelled logs. Y-axis represents log interval in metres, and X-axis represents clast sizes (increasing towards the right). Notice the down-fan reduction of bed thickness and clast size from sections 1 to 3. Also note that the log intervals vary, based on exposed fan thickness. For a more detailed description of the logs, see Figure 46. The locations of all the figures related to Fan A are shown in this figure. 53
Figure 46: All the lithological logs for Fan A. Bed thicknesses and average clast sizes are emphasized, whereas contact types between beds are not, as most beds have been heavily eroded. All layers have a Dip / DD of ≈ 19 – 22° / 190°S. The conglomerates are polymictic and matrix supported. The beds are generally thinning from east to west, whereas the clast sizes and the two black layers are laterally correlatable. Vertically, the facies do not change much, but from north to south, the changes are clearly visible: finer sediments, thinning of beds and more vegetation.....55
Figure 47: Field photo of Section 1 – East. It is the most complete package of exposed conglomerates in proximity to the apex of Fan A, which is why it was chosen. The location of this photo is shown in Figure 45. 56
Figure 48: Shows Section 1 - West. There are greater amounts of vegetation and soil on this side of the fan, hence the relationship between Fan A and the sediments to the west are unclear. The location of this photo is shown in Figure 45. 56
Figure 49: Composite photo of Section 2 – East from bottom to top. Notice the degree of erosion compared to Section 1, and the lack of thick and pronounced conglomeratic beds anywhere but at the base. The location of this photo is shown in Figure 45. 58
Figure 50: Field photo showing Section 2 - West. Notice that the bed boundaries are clearer in the west compared to east, with good exposure and less soil and gravel intervals. The location of this photo is shown in Figure 45.....59
Figure 51: Imbrication to the south observed near Section 2 of Fan A. The location of this photo is shown in Figure 45. 59
Figure 52: Thinning of beds from north to south near the mid-fan area. The location of this photo is shown in Figure 45. 60
Figure 53: Shows Section 3 – West, in the southern parts of Fan A, and how a lithological log similar to Section 1 and 2 were impractical to construct due to the sheer amounts of vegetation and lack of outcrops. Within the red box, the only 15 m interval of clear and exposed conglomerates this far south is exposed, and as such this interval was logged. The location of this photo is shown in Figure 45. 61
Figure 54: Shows Section 3 - East, and how the southern parts are not ideal for lithological logs. Streamflow deposits dominate this section. The location of this photo is shown in Figure 45. 62
Figure 55: Panorama photo taken from Fan B, viewing the mid-fan area of Fan A, it shows the bedding geometries. Below, a simplified sketch of how the fan has built out through time. The location of this photo is shown in Figure 45. 62
Figure 56: Individual lobes located immediately east of Fan A, believed to be earlier events. Scale is relevant to the base of the nearest lobe. The location of this photo is shown in Figure 45. 63
Figure 57: Facies distribution map for Fan A, showing the facies, depositional directions and faults. 64
Figure 58: Photo from the southwestern base of Fan B that shows the location of the hidden relationship between Fan A and Fan B. The contact is partly eroded and completely covered by vegetation and a small river. The location of this photo is shown in Figure 45. 65
Figure 59: Rose diagram for fan B. This fan tends to dip slightly more to the west than Fan A.....66
Figure 60: Shows a detailed geological map of Fan B and its associated lithological sections. Red and black lines within the dashed boxes on the map represent red and black coded logs. Notice the down-fan reduction of bed thickness and grain size. For a more detailed description of the logs, see Figure 63. The locations of all the figures in this area are shown as well. 67

Figure 61: Shows the relationship between fine sediments at the bottom of Fan B and with the first conglomeratic bed of Fan B. Notice the parallel dips of 20°. Compass for scale (10 x 6 cm). The location of this photo is shown in Figure 60. 69
Figure 62: Shows Section 1 – West. At the base of the red box, the outcrop of Figure 61 is located. The location of this photo is shown in Figure 60. 70
Figure 63: Detailed lithological logs for Fan B and Fan C. Notice in Fan B how the beds and clast sizes decrease drastically from section 1 to 2. In Fan C however, there is no decrease in clast sizes from Section 1 to Section 2 (north-west to south-east). However, there is a small change in bed thicknesses. 71
Figure 64: Shows the typical facies found in Section 1 – West in Fan B, with one of the many sandy intervals, coloured orange. Compass and pen for scale. The location of this photo is shown in Figure 60. 72
Figure 65: Shows Section 1 – East, with the most complete conglomeratic outcrop in this section. The location of this photo is shown in Figure 60. 72
Figure 66: Satellite image from Google Earth used to show the location of Section 2 within the red box. Fault E is also included in the map. 74
Figure 67: Shows the fine and unconsolidated nature of the deposits near the base of Section 2. The location of this photo is shown in Figure 60. 74
Figure 68: Distal deposits in the immediate footwall of Fault E, interpreted as streamflow deposits. Book for scale. The location of this photo is shown in Figure 60. 75
Figure 69: Facies distribution map for Fan B, as well as the interpreted depositional direction. 76
Figure 70: Panorama photo taken from Roghi Mountain, that shows the extent of Fan D, its faults, and how the lithological contacts span out in field view. The Roghi Fault is not drawn on this figure, as it disappears behind the Vighia Member. But as seen in Figure 71, it is the south-eastern boundary of the fan. The main lobe of Fan C is outlined with a dashed black line. The location of this photo is shown in Figure 71. 77
Figure 71: Satellite photo from Google Earth, showing a detailed geological map of Fan C and its associated lithological sections. Notice the similarities between Section 1 and 2 and the complex faulting in the area. The sub-horizontal layers are found within the black dashed circle, close to Section 1. For a more detailed description of the lithological logs, see Figure 63. This figure also shows the locations of all the figures located in this area. 78
Figure 72: Rose diagram constructed based on all the collected dip data for Fan C. The outcrops furthest to the northwest dip slightly west, whereas the rest of the fan dips to the east. 79
Figure 73: Field photo showing Fan C to the northwest and the location of Section 1. The section was constructed here due to the extensive outcrops. Notice the sub-horizontal dip of the sediments, close to centre of the red polygon. The location of this photo is shown in Figure 71. 80
Figure 74: Photo from Section 1 showing a typical sand lens (coloured yellow), that was found within some of the finer conglomeratic facies of Fan C. The location of this photo is shown in Figure 71. 80
Figure 75: Shows the south-western part of Fan C, where the second and last lithological section was constructed (within red box). The location of this photo is shown in Figure 71. 81
Figure 76: Anomalous facies previously not observed in any of the fans, but found in several outcrops in Fan C. Very thin layers of coarse sand (≈ 1cm), overlain by boulder sized conglomerates. Similar facies were observed in the Profitis Conglomerates (Figure 106). Compass for scale. The location of this photo is shown in Figure 71. 82
Figure 77: Shows a fining up section at the very southern base of Fan C. Book for scale. The location of this photo is shown in Figure 71. 82
Figure 78: Facies distribution map for Fan C, showing the interpreted depositional direction and the faults as well. 83
Figure 79: Photo of Fan D taken from the other side of the Vouraikos Valley, displaying Lobe I and II. Shows how the Late Fan has deposited, and eroded Fan D into two parts. The Intra Roghi Fault 2 can be seen to the south. The purple area north of the fault is what Sigmundstad (2016) refers to as segment V of Roghi Mountain, and this will be further discussed in Sub-chapter 6.3. The location of this photo is shown in Figure 43. 84
Figure 80: Zoomed in map-view of Fan D and its surrounding features. It shows the locations of all the figures related to Fan D. The locations of all the photos taken from the east of the Vouraikos River Valley are shown in Figure 43. 85
Figure 81: Drone photo over the area overlying Fan D to the west, featuring a glimpse into the Doumena Fault Block. The location of this photo is shown in Figure 80. 86

Figure 82: Panorama photo showing that Lobe II has a similar structural nature and depositional geometry. However, Lobe II has a much finer clast size than Lobe I. Scale is relevant to Lobe II. The location of this photo is shown in Figure 80. 86
Figure 83: Rose diagram constructed based on all the dip data collected from Fan D. 87
Figure 84: Shows the large boulders typical for the coarse deposits found throughout Fan D. The location of this photo is shown in Figure 80. 88
Figure 85: Shows the angular nature of the Fan D clasts. The location of this photo is shown in Figure 80. ... 89
Figure 86: Shows the northern vertical cliff side of the fan with its massive outcrops. The bed boundaries are poorly defined, clasts are cobble to boulder-sized. The sorting is poor, matrix is quite coarse (pebbles, 3 - 4 cm) and the clasts are matrix-supported and sub-angular. The location of this photo is shown in Figure 80. 89
Figure 87: Shows the nature of the facies on the western limit of the main Fan D, which is a drastic change from what is observed elsewhere in the fan. The location of this photo is shown in Figure 80. 90
Figure 88: Shows the facies of the western Fan D outcrop (possible apex), separated from the main lobe by the Late Fan. The location of this photo is shown in Figure 80 91
Figure 89: Shows the conglomerates that are a possible source for Fan D, with similar facies as the fan, although not outcropped clearly. Shoe tip for scale. The location of this photo is shown in Figure 80. 92
Figure 90: Simplified figure showing how the beds of Lobe I and Lobe II are building out from NW to SE. The location of this photo is shown in Figure 43. 92
Figure 91: Facies interpretation map constructed for Fan D. The dashed yellow line in the figure represents the ridge of the fan, which was the only possible path to take from base to top. 94
Figure 92: The dashed line represents the eroded sediments from the Kerpini Fault Block, and the orange package is the re-deposited Fan C. The coarsest clasts (2) are present in a steeper slope closer to the fault, whereas the most distal parts (1) are located on a much gentler surface. This is a result of later tilting events, which is responsible for the present-day configuration of Fan C. The figure is very simplified, and the dip of the Roghi Fault is exaggerated to illustrate the scenario. 98
Figure 93: Simplified figure showing one possible interpretation as to how Lobe I of Fan D deposited first and was later influenced by the Late Fan. 100
Figure 94: Shows one interpretation of a possible fault bounding Fan D to the south. Intra Roghi Fault II is shown in the south. The location of this photo is shown in Figure 43. 101
Figure 95: Shows the locations of the eight cross sections, A-H. 102
Figure 96: Shows the westernmost north-south cross section A-A`. The southernmost data here is credited Hadland (2016), as this area was not studied for this thesis 103
Figure 97: Cross section B-B`. This section goes through Fan A and is not perpendicular to Fault B. Fault B is believed to be quite steep (50 - 55°), and such the dip in the cross section is apparent, as The Lower Conglomerates have a similar dip to the fan. The depth of the Lower Conglomerates is unknown, and the unconformity depth is assumed to jump to a shallower depth north of Fault B. Notice the earlier lobe immediately east of Fan A with a similar dip (coloured pink to be visible). 103
Figure 98: Cross section C-C` that barely intersects the Vighia Member and Fan A before it cuts through Fan B. The Roghi Fault, which is believed to be a transfer fault, dips quite vertically, and has a tiny offset in this location, as it is believed to die out in proximity to this location. The Kalavryta Member also outcrops in the very south, as seen here 104
Figure 99: Cross section D-D`, which is the first cross section that intersects Roghi Mountain, and shows the thick conglomeratic package that is the Vighia Member. A tiny interval of Lower Conglomerates is also displayed, and faults F and H are visible in this section. The fault depths are unknown, and the depth of the unconformity is assumed to be shallow, as the unconformity contact is close to the location of the cross section 104
Figure 100: Cross section E-E`. This cross section goes through Roghi Mountain, and shows the two intra Roghi Faults where the unconformity is assumed to drop across each fault. Fan D is intersected to the north, and the Late Fan is also displayed here, assumed to be quite thin. The Vouraikos Fault displaces the basement far down, as it is not observable to the east of the valley. 105
Figure 101: Cross section F-F`, the first of three west-east cross section. This section intersects all the transfer faults and three of the Ilias Fans; A, C and D. Fault B is believed to be the dominating fault over Fault A, both of which has an unknown dip/depth. Fault D also has an unknown depth, but it displaces the basement, as observed in the field. Fault G has an unknown depth, but the unconformity is assumed to drop to a lower depth over the fault. The Roghi Fault dips slightly to the

east, and displaces the unconformity to a lower but unknown depth. The Vighia Member is not intersected, but the sub-horizontal sediments can be seen on top of the Lower Conglomerates in this location. To the very east, it intersects Fan D, which is overlain by the Late Fan. 105
Figure 102: Cross section G-G`, the center east-west section. The thickness of the Lower Conglomerates increases to the east due to the steps of the Kerpini Fault. The displacement of the fault decreases to the west, where it terminates in the Kerinitis Fault 1. The cross section intersects Fan A around the mid-fan area, where it is thinner than in F-F`. Fan B is then intersected where the unconformity depth is unknown. However, it is assumed to jump to a higher level over Fault E. As aforementioned, the depths of fault B and E are unknown. The unconformity drops to a deep level over the Roghi Fault, and even further down in the Vouraikos River Valley.....106
Figure 103: Cross section H-H`. The western data here is credited Hadland (2016). This section passes through the more distal areas of Fan A and B, where Fan B has nearly died out, and Fan A has thinned even further. As in the previous east-west sections, the unconformity drops in both the Roghi Fault and the Vouraikos River Valley.....106
Figure 104: Google Earth satellite photo from south to north that shows how the Vouraikos and Kerinitis Transfer Faults split off in two different directions, quite similar to each other. 108
Figure 105: Proposed development of the Kalavryta Member (Hadland, in prep). 109
Figure 106: One of the many thinly layered sand intervals in the Profitis Conglomerates outcrop. The location of this photo is shown in Figure 71. 110
Figure 107: Chronostratigraphic chart showing the relative age relationships in the Kerpini Fault Block. ..112
Figure 108: Shows the area of study prior to syn-rift deposition. The map extends further to the west, east and south, to include the Kalavryta Fault Block in the next stage. 113
Figure 109: Shows the active Kalavryta Fault in the south, and the subsequent deposition of the Kalavryta Member. It has a wide extent, and covers most of the Kerpini Fault Block that will later be confined to the north. Sand lenses observed in the field are derived from a widespread channelization across the fan surface. 114
Figure 110: Shows how Fan D deposited in the northeast and activation of the Kerpini Fault. 115
Figure 111: Shows how the Vighia Member deposited and is overlying Fan D. Fan C deposited shortly after or at the same time as the Vighia Member. 116
Figure 112: Shows how the Aetovouni Member deposited in the southwest, followed by the Skepasto Member. 117
Figure 113: Shows how the Doumena Fault activates, and initiate the deposition of the Earlier Lobes, Fans A and B, and the Profitis Conglomerates. 118
Figure 114: Shows how the Sub-horizontal Sediments deposited on top of the other stratigraphic units in the Kerpini Fault Block, followed by the Late Fan in the northeast. 119

Chapter 1: Introduction

This is a short summary of the background for the thesis, previous studies, challenges and objectives of the thesis.

1.1 Background

The Corinth Rift, located in the Gulf of Corinth, north of the Peloponnese Peninsula, is one of the most active rifts in the world. The rift is responsible for the present day configuration of Greece where the entire country splits in two (Ford *et al.*, 2013). It is one of several rifts associated with the movement of the African and Anatolian plates from the Mesozoic up to the Paleogene. Regional N-S extension caused normal faulting from the Gulf of Corinth and southwards into the Peloponnese Peninsula. The normal faulting resulted in a series of half grabens within a system of uplifted, rotated and north-dipping fault blocks, one of which is the Kerpini Fault Block. Rotation has caused the unconformable Pliocene-Quaternary syn-rift deposits within the half grabens to tilt up to approximately 30° near the study area (Moretti *et al.*, 2003; Ford *et al.*, 2013). This is a structural configuration where alluvial fans have developed in a complex relationship with several other stratigraphic units. The Kerpini Fault Block is the second of three fault blocks filled with terrestrial syn-rift sediments, with the Kalavryta Fault Block to the south, and the Doumena Fault Block to the north. As this rift is recent from a geological point of view, it is a suitable area for observation of an ongoing rift system with the associated sedimentation, such as the proposed alluvial fans which are subject to this study. For simplicity's sake, the proposed fans will be referred to as Fans A, B, C and D prior to discussion, where it will be assessed whether they are indeed fans or not.

1.2 Geological problem and previous studies

Previous studies have investigated, mapped and modelled the different fault blocks to various extents and contributed to the understanding of this extensional area. Much of the present-day knowledge of the area is a direct result of the studies conducted by students from the University of Stavanger (Syahrul, 2014; Dahman, 2015; Lopes, 2015; Rognmo, 2015; Stuvland, 2015; Bjåland, 2016; Hadland, 2016; Sigmundstad, 2016). Ford (2013) investigated the entire rift system from north to south, but many of the smaller details of the various fault blocks are neglected. There is still an ongoing debate amongst researchers about the structural configuration, classification of

stratigraphic units and the relative timing between faults and stratigraphic units. Three of these units are suggested to be syn-rift, footwall-derived, alluvial fan deposits (Hadland, 2016). In addition, there is a fourth unit to the east that has not been studied in detail.

1.3 Objectives

This study aims to highlight some of the neglected details in the Kerpini Fault Block, and contribute to the present-day understanding of the area. As such, the objectives are to:

- Resolve whether the four units are alluvial fans and if so; classify them, and
- Determine their relative timing concerning faulting and other stratigraphic units in the Kerpini Fault Block.

1.4 Data

Field data collected over two separate field trips is the foundation of the study. Structural measurements, a multitude of photos, constructed lithological logs, recorded facies variabilities, geological mapping and rock samples make up most of the collected data. Satellite imagery from Google Earth combined with a Digitized Elevation Model (DEM) of the study area in Petrel have also been important tools to analyse and process the physical data.

Chapter 2: Regional geology

The contents of this chapter explain the regional geology of the area south of the Gulf of Corinth, and the geological processes that shaped the region.

2.1 Tectonics

In the Mesozoic through Paleogene times, the African Plate subducted under the Anatolian Plate. The plate convergence gave birth to the Hellenic Arc, as well as the Alpine Orogeny and its associated thrust sheet through central Greece. Hence, it was crucial to the lithostratigraphy in the study area (Taylor *et al.*, 2011).

The subduction of the African plate happened at a faster rate than the northwards movement of the same plate, which resulted in a slab pull of the Anatolian plate in a southward direction (Royden, 1993). This interaction of tectonic plates is how the N-S Miocene back-arc extension (≈15 Ma ago) initiated and created the Aegean Sea (Le Pichon and Angelier, 1979). This process resulted in several active rift systems, one of which is the rift of interest for this study (Figure 1). This particular rift is located in the Gulf of Corinth (Armijo *et al.*, 1996).

The regional N-S extension caused normal faulting from the Gulf of Corinth in the north, and southwards into the Peloponnese Peninsula (Figure 2). This subsequently resulted in a series of half grabens within a system of rotated north-dipping fault blocks from the Gulf of Corinth and past the town of Kalavryta to the south (Figure 3). The fault blocks show an increasing uplift towards the south, up to 2000 m at the most (Sorel, 2000). Minimum extension calculations have yielded a range of 6.4 - 7.7 km (Avallone *et al.*, 2004), but these results do not match the current extensional rates, where the Peloponnese is moving at a rate from 10 - 30 mm per year to the south. As such, periodical extensional events through time is a more likely theory than continuous extension through time (Ford *et al.*, 2013).

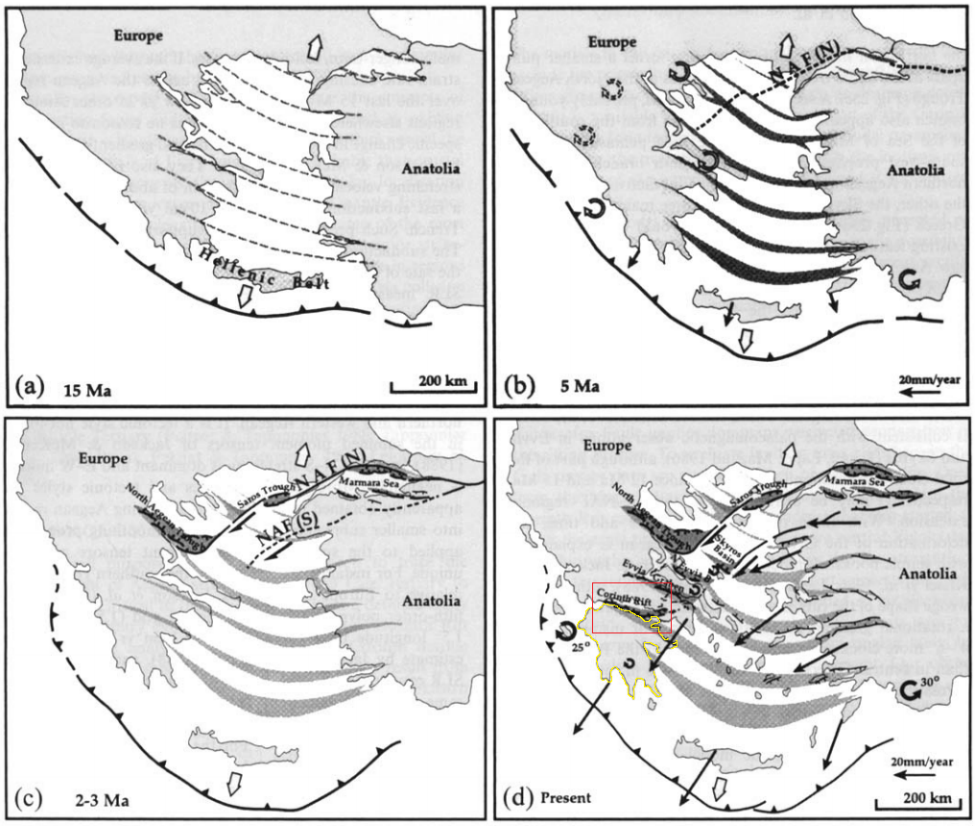

Figure 1 : Shows the evolution of the Aegean Sea, and in (d): The present day rift systems of the Aegean Sea, the Corinth Rift (outlined in red), and the Peloponnese Peninsula (outlined in yellow). Modified after (Armijo et al., 1996).

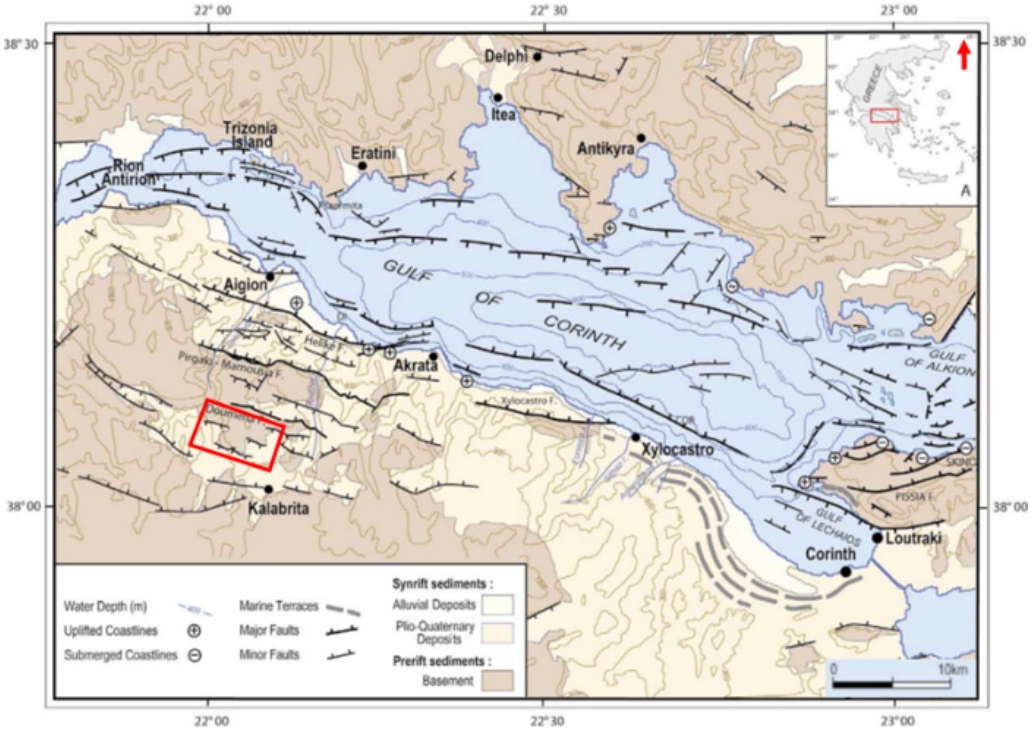

Figure 2: Regional map of the Gulf of Corinth showing major structural features. Study area in red box. Modified after (Moretti et al., 2003).

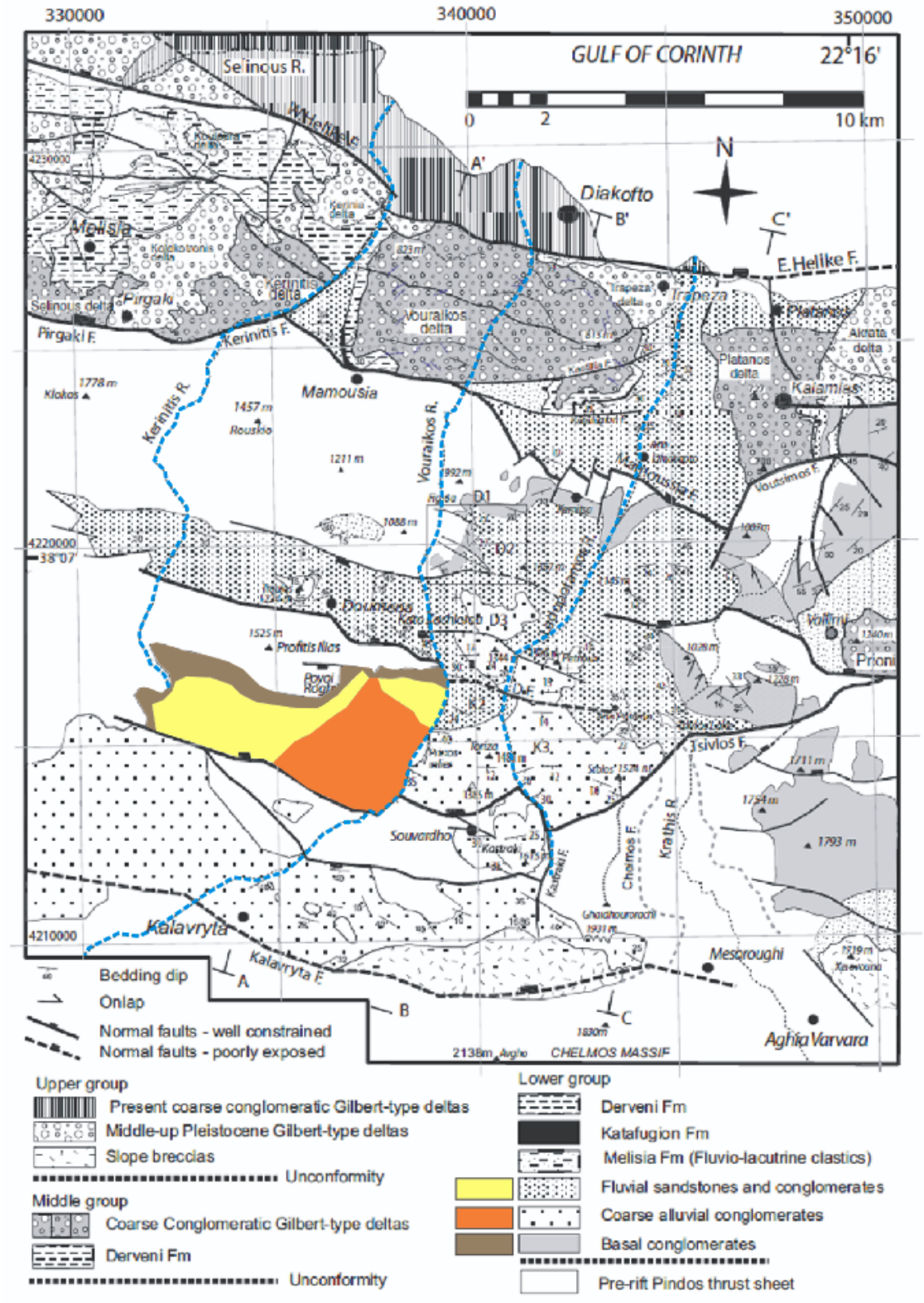

Figure 3: Geological map from the Gulf of Corinth in the north and southwards past the study area. The syn-rift sediments of the Kerpini Fault Block (inside red box), which is the focus of the study, are coloured according to the legend. The eastern and western river valley boundaries are coloured in blue. Modified after Ford et al.*, (2013).*

2.2 Structural framework

There are several theories that aim to explain the evolution of the 115 km wide graben which is the Gulf of Corinth. It stretches from the Strait of Rio in the west to the Corinth Canal in the east. This is an elongated symmetrical graben, oriented N100°E (Moretti *et al.*, 2003). As one would expect from an extensional setting like this, the faults are dipping towards the centre of the rift. South of the Gulf of Corinth, in the north-dipping fault system, much of the earlier rift (currently inactive) is preserved. Combined with north-south river incisions it provides a suitable area to study normal faults and associated syn-rift deposits. The major normal faults are all considered inactive (Leeder *et al.*, 2008). These faults define the boundaries of the half-grabens, and their dips are in the range of 40 - 60°. Within the study area, most of the sedimentary units dip at an angle of 20 - 25° to the south.

Different theories exist to explain how the major faults terminate downwards into the subsurface. One of the more popular explanations is the existence of a low angle regional detachment fault deep in the subsurface that strikes parallel to the Gulf of Corinth (Figure 4) (Sorel, 2000; Flotté *et al.*, 2005). Sorel (2000) estimated an approximate throw of 16 km for this fault, and used it to explain the atypical extensional rates previously modelled in the Gulf of Corinth. No concrete evidence exists for the detachment fault theory. However, the extensional rates could be explained by the combined displacement of the onshore and offshore faults.

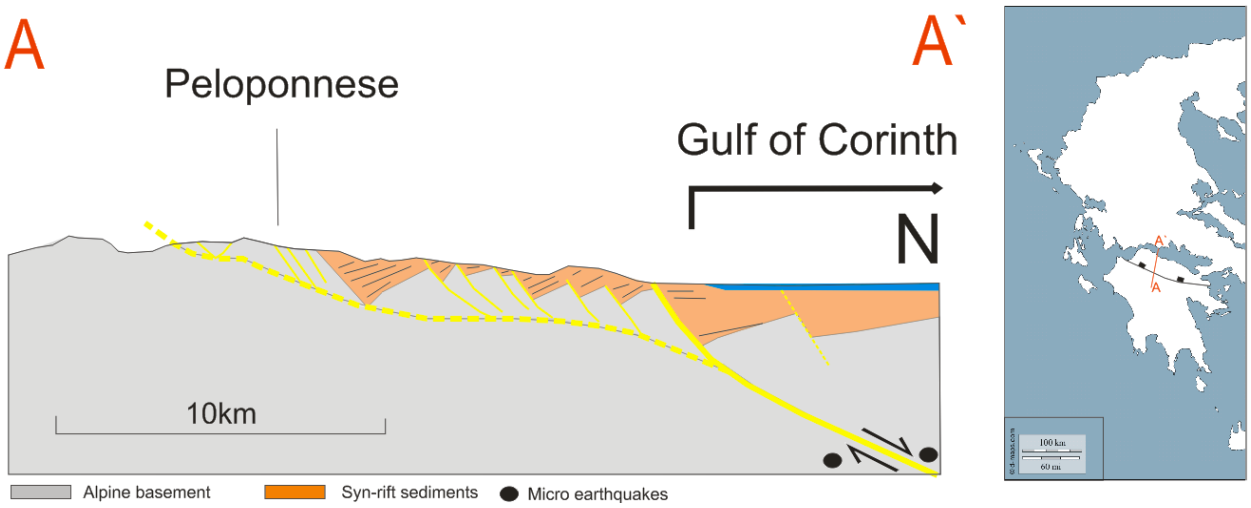

Figure 4: N-S cross section from inland Peloponnese Peninsula in the south and into the Gulf of Corinth in the north, shows the detachment fault model. The micro earthquakes in the figure are from Rietbrock et al. (1996), recorded 15 km west of this cross section. Modified after Sorel (2000).

2.2.1 Faults and fault geometries

The Mamousia-Pirgaki, Doumena, Kerpini and Kalavryta Faults segment the four major fault blocks from north to south, respectively. There is uncertainty tied to the displacement of the various faults, and calculations vary from study to study. The maximum displacement of the Mamousia-Pirgaki Fault has been estimated to 1500 m (Ford *et al.*, 2013; Dahman, 2015). The Doumena Fault is obscure, and yields several different calculations as the displacement changes significantly along the fault. The values range from 800 - 2000 m (Collier and Jones, 2004; Ford *et al.*, 2013; Syahrul, 2014; Dahman, 2015). The Kerpini Fault has a better exposure along the entirety of the fault, and several inconclusive displacement calculations exist for this fault as well. Estimations range from 1.5 km (Ford *et al.*, 2013; Syahrul, 2014; Dahman, 2015) to 2.5 km (Collier and Jones, 2004). Hadland (2016) concluded that the displacement of the Kerpini Fault is segmented by transfer faults. The Kalavryta Fault lacks proper exposure, and is interpreted to step in several locations. Thus, this fault is ambiguous as well. The displacement has been estimated from 800 m (Finnesand, 2013) to 1200 m (Ford *et al.*, 2013).

Several previous studies have concluded that north-south transfer faults are segmenting the different fault blocks (Syahrul, 2014; Dahman, 2015; Hadland, 2016; Sigmundstad, 2016). But some authors do not support this model (Ford *et al.*, 2013; Ford *et al.*, 2016), as they prefer a model involving smaller cross-faults or relay zones, and that the segmentation of the rift is controlled by paleo-topographic features within the pre-rift stratum. Their map has continuous faults from east to west.

The river valleys in the study area are perpendicular to the major faults, where lithologies and faults cannot be traced continuously across. There are also large thickness variations of the syn-rift layers on either side of the deep valleys in many locations. Dahman (2015) proposed three major transfer faults in three different river valleys: Kerinitis, Vouraikos and Ladopotamos (marked with blue in Figure 3). The presence of such transfer faults provides some explanation to the fault steps and abrupt terminations, as well as lithological and thickness variations across. Transfer faults often serve a purpose as fault block terminations, and strike more or less perpendicular to the major faults (Morley, 1995). Other possibilities are that some of the fault steps are caused by an individual cross fault (Ford *et al.,* 2013), or by relay zones (Wood, 2013).

2.3 Stratigraphic framework

The area from the Gulf of Corinth in the north and southwards into the Peloponnese Peninsula has been an area of interest for geoscientists of many disciplines for several years. The main focus has been on the Gilbert-type deltas and turbiditic deposits towards the north, whereas the southern region in proximity to the town of Kalavryta has not been studied as thoroughly. In recent years, some papers that focus on the entire rift system and its evolution through time have been published. Ford et al. (2013) studied the tectono-sedimentary evolution of the rift system, and defined three main groups of syn-rift stratigraphy, Upper, Middle and Lower Groups. These stratigraphic groups are overlying the pre-rift metamorphosed carbonate basement of Upper Triassic-Jurassic age (Skourlis and Doutsos, 2003).

The Upper Group consists of both Pleistocene and present-day Gilbert-type delta conglomerates mainly deposited offshore, and are concentrated near the Helike fault range, where they unconformably overlie the Middle and Lower Groups (Ford *et al.*, 2013). South of Kalavryta, a 300 m thick limestone breccia also belonging to the Upper Group can be observed, which is believed to be glacier-derived (Mastronuzzi *et al.*, 1994).

The Middle Group is characterized by marine deposits located in the Mamousia-Pirgaki Fault Block, and comprises coarse-grained Gilbert-type delta deposits of vast size that built northwards into a brackish marine basin. Finer deposits were deposited in the basin (mudstones, siltstones, fine sandstones) as distal turbidites and hemipelagic deposits. The base of the Middle Group is an erosional unconformity (Ford *et al.*, 2013).

The Lower Group appears from the Mamousia-Pirgaki Fault Block in the north to the Kalavryta Fault Block in the south, and constitutes the syn-rift sediments in the study. In the Mamousia-Pirgaki Fault Block the Lower Group occurs as alluvial/fluvial and lacustrine successions, and coarsens to the south. In the Kerpini Fault Block it coarsens into more of an alluvial character, where the Lower Group splits into three units based on grain size and different facies in the study area; K1, K2 and K3. K1 is a basal unit consisting of thickly bedded coarse-grained alluvial conglomerates that reach thicknesses up to 400 m. K2 overlies K1 and is a poorly exposed fluvial unit of reddish sandstones, siltstones and conglomerates with erosive bases. Finally, K3 is the thickest (up to 1300 m) conglomeratic unit and features thickly bedded coarse-grained conglomerates such as those of K2, but with occasional fluvial sandy intervals. On a regional scale,

the Lower Group consists of coarse-grained alluvial to fine-grained lacustrine successions that is coarse in the south and fines progressively towards the north (Ford *et al.*, 2013).

2.4 Glacial history

Mount Chelmos, which is 3 - 4 km south-east of the town of Kalavryta, was covered by an extensive Pleistocene glacier that advanced/stabilized around 40 - 30 Ka and retreated at approximately 23 - 21 Ka, before it advanced again at 13 - 10 Ka (Pope *et al.*, 2015). As such, glacial history is important for understanding the current shape of the region. Glaciers are responsible for generating certain lithologies such as the breccia found in the Kalavryta Fault Block and in some other localities. Meltwater from ice and snow is a prominent supplier of both fluids and sediments, and is probably the second largest contributor (after rain) to the fluid flows that transported clasts and reworked sediments to deposit as alluvial fans in the area of study. One would expect to find glacial derived clasts while surveying the southernmost fault blocks in the region.

2.5 Area of study

The area of study stretches E-W for 7.5 km and N-S for 4 km, covering an area of approximately 30 km^2. The major north-dipping faults, Doumena and Kerpini, act as the northern and southern boundaries respectively. Two deep south-north incising river valleys in the region further segment the fault block and define the eastern and western boundaries of the study area. The Vouraikos River Valley cuts through thick successions in the east, and the Kerinitis River Valley lies to the west. Hadland (2016) focused on the western and south-western part of the study area, whereas this study is focused more to the east of Kerpini Village. Roghi Mountain was also studied in detail by Bjåland (2016) and Sigmundstad (2016), whereas the structural elements in the region were studied by Dahman (2015). Stuvland (2015) studied the sub-horizontal sediments scattered throughout the study area, and Rognmo (2015) studied the sedimentary infill in the Kalavryta Fault Block. Kolbeinsen (2013) studied a later fan deposit in the Doumena Fault Block to the north, and Lopes (2015) did a thesis on the more coastal sediments. Finnesand (2013) researched the Chelmos and Kalavryta Faults and their effect on sediment drainage and accumulation. There are some areas in the study area that was not visited during the fieldwork tied to this study, but mapping done by previous students (mainly by Stuvland (2015) and Hadland (2016)) has been carried over into a new and improved geological map for the Kerpini Fault Block (Figure 12).

Chapter 3: Alluvial fan theory

This chapter describes necessary background theory for understanding the complexity and variations of alluvial fans.

3.1 Alluvial fans

An alluvial fan is a prominent landform type commonly present where a channel emerges from mountainous uplands to an adjoining valley (Blair and McPherson, 1994). It represents the coarsest, most poorly sorted, proximal unit in the range of subaerial depositional systems (Galloway and Hobday, 1996). These coarse sedimentary deposits have a geometrical shape that resembles a cone in 2D space. There are several processes that can lead to the formation of an alluvial fan, mainly gravity and fluvial processes. The poorly sorted nature of the deposits of alluvial fans is a consequence of short transport distances from the source, mass wasting processes instigated by high relief, and rapid loss of carrying capacity of the flow (Blair and McPherson, 1994). Due to a more progressive loss of flow power downslope (Figure 5), an alluvial fan is ideally more coarse-grained (boulder sizes) and thickly bedded in the proximal area, and finer-grained (cobble, pebble and sand sizes) as well as more thinly bedded in the distal parts (Blissenbach, 1954).

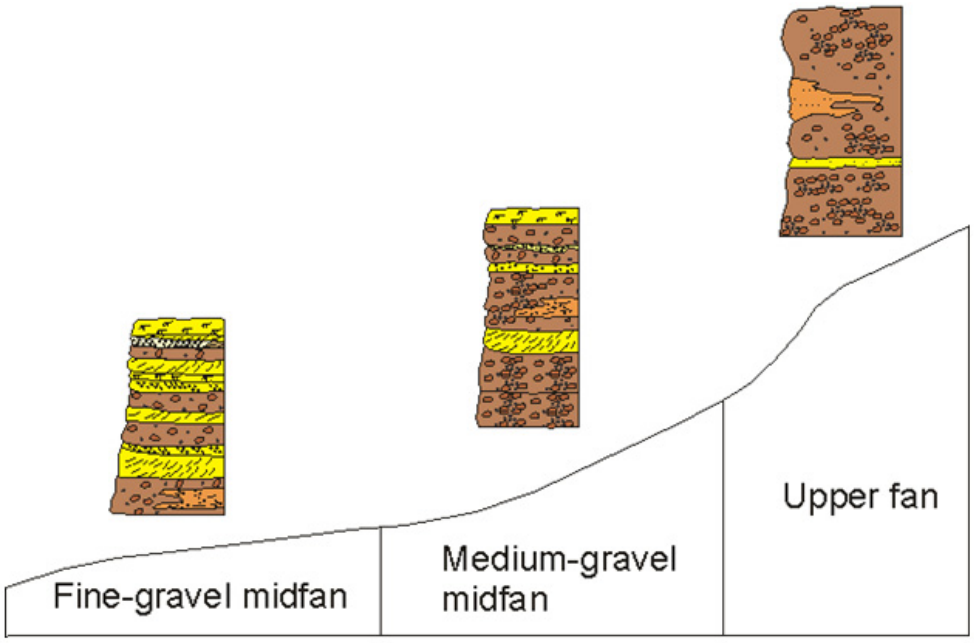

Figure 5: Down-fan reduction of gradient accompanying reduction in particle size of a wet fan. Modified after Boothroyd (1972).

The major morphological features of an alluvial fan system are the drainage basin, feeder channel, apex, incised channel, distributary channels, intersection point, active depositional lobe and head-ward eroding gullies (Figure 6). The drainage basin constitutes the upland area from which sediment and water discharges are derived. A feeder channel supplies the active depositional lobe with sediments from the drainage basin. The apex of a fan is the point at the mountain front where the feeder channel emerges from the highlands (Drew, 1873). This point represents the most proximal, and usually highest, part of the fan. The remaining features are best visualised in Figure 6.

Ideal alluvial fan geometries with intact major morphological features are ordinarily found in desert areas in proximity to nearby mountains. The alluvial fans in the study area have undergone secondary processes such as major erosion, faulting and rotational/tilting processes, thus the textbook examples are not always present in the study area.

Hadland (2016) used the triangular fan classification scheme by Galloway and Hobday (1996) to classify the alluvial fan subject to his study. This study will use the same classification to keep a consistent framework into which new knowledge can be included. This classification scheme differentiates between debris-flow, stream-flow and sheet-flood dominated fans, based on the respective dominating depositional processes.

There are other classification schemes, often based on sedimentary processes (Blair and McPherson, 1994), but the alluvial fans of the Kerpini region are weathered after extensive erosional events, resulting in a lack of clear bedding and sedimentary structures such as cross beds, ripples etc. commonly used to deduce sedimentary processes. There are schemes more suited to arid desert areas, where the morphological features are intact, but this is not the case for the study area. The following sections will give a brief explanation to the triangular classification scheme used in this study, with examples and further descriptions covered in the following chapters.

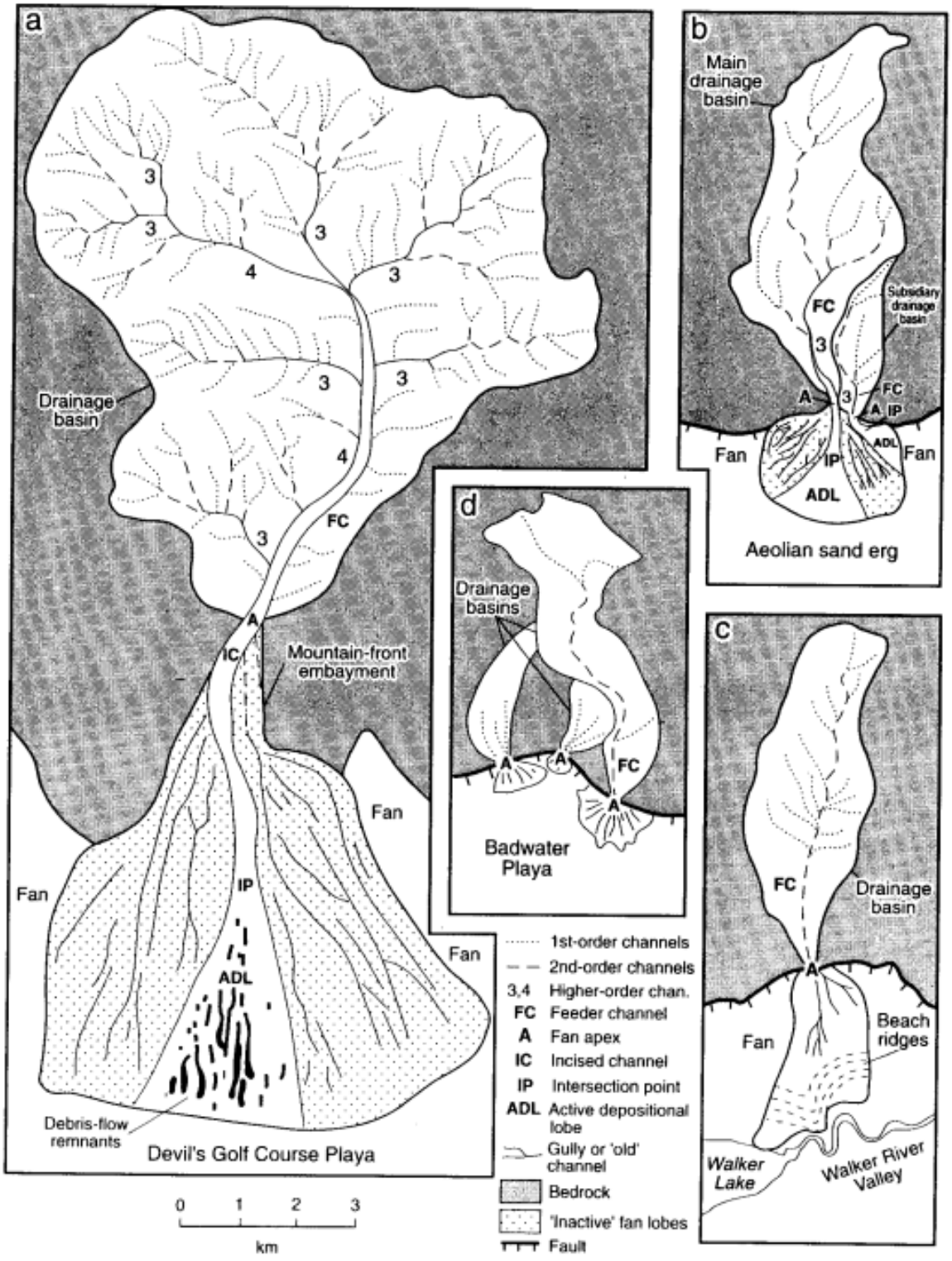

Figure 6: Shows four different examples of alluvial fans and their associated morphological features, after Blair and McPherson (1994).

3.2 Debris-flow dominated fans

Debris-flow dominated fans relate to high-energy mass movement generated by tectonic activity. Due to erosion, large amounts of sediments accumulate in the drainage basin where floods or tectonics can initiate movement of these sediments. Regardless of trigger mechanism, the crucial element for flow initiation is the presence of water. These alluvial fans are usually matrix-supported with pebble and gravel to boulder sized clasts (Galloway and Hobday, 1996). A typical debris-flow dominated alluvial fan should show a reduction in clast size distally, fining-upward beds and imbrication in the more proximal areas. The debris-flows are chaotic and poorly sorted, with obscure bed boundaries.

3.3 Streamflow dominated fans

Fans dominated by streamflows are subject to perennial streams due to year-round rainfall, and therefore the sediment supply is steady from the eroding highlands. Flows are usually confined to channels, but may also spread across the entire fan and rework the surface regularly. Vegetation is an effective stabilizer on the fan surface, but the steepest deposits often collapse during violent floods (Galloway and Hobday, 1996). Streamflow fans normally show a down-stream reduction in maximum clast size as well. The matrix is usually clast-supported, and the channels lose their structure and are poorly defined distally. In streamflows, high-energy currents are rare, and streams swiftly lose their energy down-slope. As a result, the proximal areas exhibit coarse and poorly sorted conglomerates. Sedimentary structures such as cross bedding, ripples and horizontal stratification can be found within sand/gravel bars (Galloway and Hobday, 1996).

3.4 Sheetflood dominated fans

The two terms used to describe sheetflood-dominated alluvial fans are sheetflooding and streamflooding. To simplify, sheetflood is used as a unifying term (Hadland, 2016). Sheetflood dominated fans are mostly found in arid areas. Sheetflooding directly relates to intense rainfall events, and is a non-channelized flow as opposed to the more channelized streamflooding. The flows are shallow, and usually result in a planar laminated sand deposit (Galloway and Hobday, 1996). Sheetfloods do not necessarily depend on a flooding event from the apex, as heavy rainfall on the fan surface itself can result in sheetfloods over large areas of the fan. As such, sheetfloods are often associated with the later stages of the fan. Grain sizes range from medium/coarse sand to periodical gravel and boulder sizes. Sheetflood facies are more homogenous than debris-flow

facies, with frequently occurring sandstone beds and lenses as natural bed boundaries for the conglomerates.

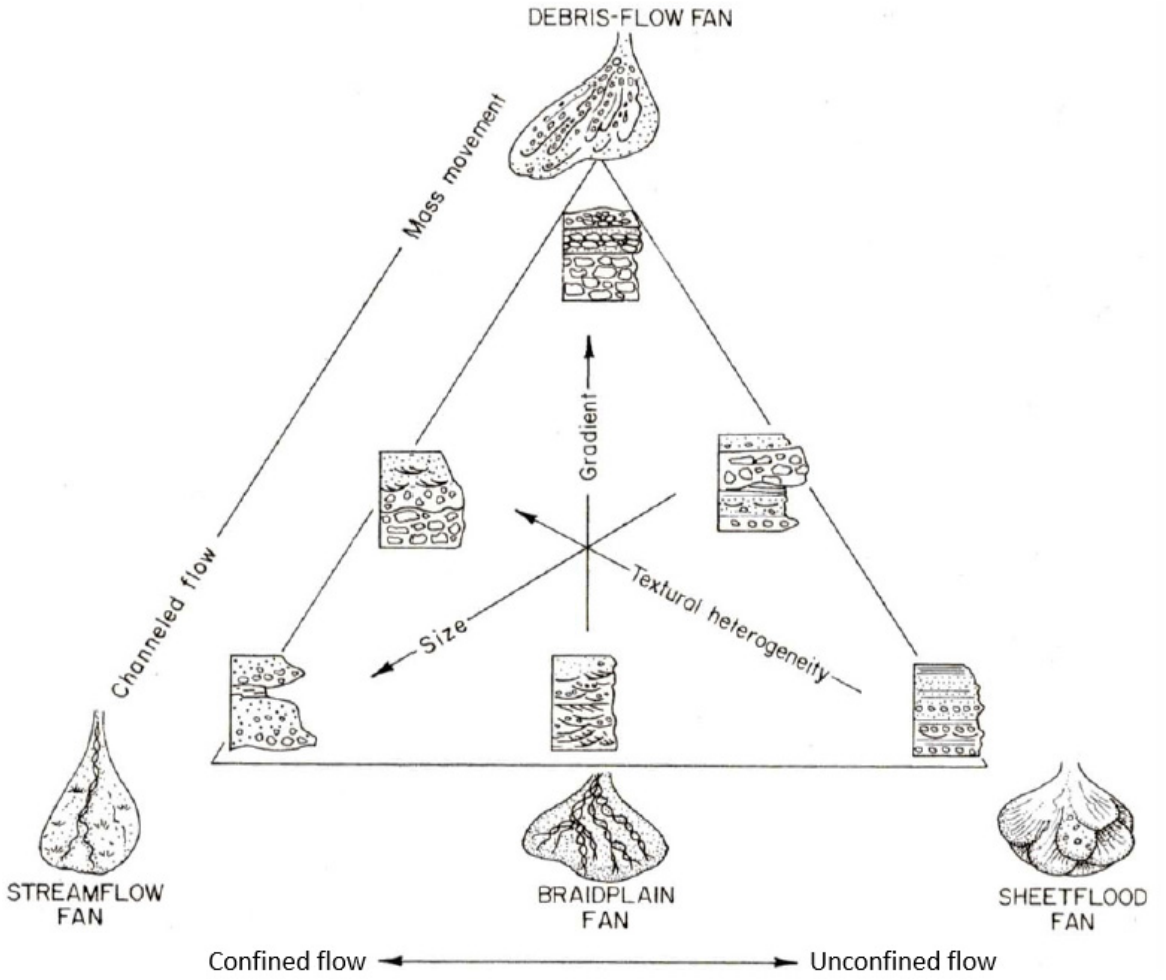

Figure 7: Triangular classification scheme used to differentiate between the three main types of alluvial fans: debris-flow, streamflow and sheetflood fans. The classification is based on flow type, gradient, size and textural heterogeneity. As seen in the figure, debris-flow fans are dominated by mass movement, high gradient, high textural heterogeneity and large clast sizes. Streamflow fans consist of more channelized flows, lesser clast sizes and smaller gradient. The same goes for sheetflood fans. (Galloway and Hobday, 1996)

Chapter 4: Methodology

This chapter describes the methodology that was employed in order to reach the objectives.

4.1 Pre-field work

Sufficient planning was necessary to carry out proper fieldwork in a limited amount of time in such a large study area. Prior to the field trips, a proper understanding of the objectives was achieved so that the practical work carried out every day was relevant and time efficient with regards to the objectives. Practice with a geological compass and a GPS was important to ensure proper collection of consistent data. A thorough literature review of both previous master studies and research papers in the area was crucial to find the areas of interest, and to understand how to carry out such individual field-work. Relevant literature concerning alluvial fans and extensional systems was perused, to better know what to look for and what the findings might implicate. A preliminary map was prepared with the relevant features of importance, and daily schedules were constructed. Due to three different areas of study several kilometres apart, the logistics of the fieldtrip had to be carefully planned. With only one car available and three different students, the most practical routes had to be pre-marked on a map. Even so, hours every day were spent exclusively by driving between study areas.

4.2 Fieldwork

Geological data such as dip and dip-direction (Dip / DD), paleocurrent indicators, vast numbers of photos, outcrop descriptions, sketches of lithological logs, and fault data were collected during the first field trip, following a sedimentary field guide as a reference (Tucker, 2011). It was important to follow a consistent framework to ensure proper data collection. The basement unconformity in the Kerpini Fault Block was mapped in detail as well, and geological contacts all over the study area were mapped by GPS. This work facilitated a detailed geological map. For the second field trip, the missing data required to compile the final thesis were collected, as well as a general quality check of some of the more anomalous data from the first field trip. A DJI Phantom 3 Drone was brought into the field to get a proper view of some of the more inaccessible areas and outcrops. Some conglomeratic clasts were sampled from the field for later analysis.

4.2.1 Structural measurements

A geological Silva compass was used for all the structural measurements made in the field. In inaccessible areas, a measurement from distance was made. There is room for error when measuring from afar; hence repeated measurements were taken, to further reduce the margin of error. The resulting structural key data is visualized on a map (Figure 12 and Figure 14) and in cross sections (Figures 96-103). Subsequently, rose diagrams were constructed to represent the collected Dip / DD data as well.

4.2.2 Clast studies

For every fan, the conglomeratic clasts were studied in detail to provide an overview of facies variabilities and differences from fan to fan; both vertically and laterally. This section briefly covers how the clast analyses were done.

4.2.2.1 Clast sizes

Clast sizes are based on Wentworth (1922), and cobble sizes are divided into three intervals (Figure 8). Average clast sizes were measured in an area of ≈ 1 m x 0.5 m, where the ten largest clasts were accurately measured and averaged (Figure 9). Hence, whenever clast sizes are discussed, it is always the average of the ten largest clasts. The average clast sizes were used to make lithological logs both vertically and laterally across the alluvial fans at certain strategic locations. For Fan A, a lithological log was made in three different locations: a) proximally, close to the apex, b) mid-fan, where the gradient has decreased, and c) distally, 200-300 m from the fan toe. Comparisons between these three logs show the facies variabilities from north to south, as well as east to west, and a description of the entire fan from apex to toe can be constructed. The lithological logs are of lower quality for fans B and C, due to poorer exposure and presence of lush vegetation. As a result, the lithological sections consist of more interpolated intervals. For Fan D, no lithological logs were made due to steep cliffs and impassable terrain. A general lithological description was recorded from west to east, but vertical variabilities such as approximate bed thicknesses could only be recorded from a distance.

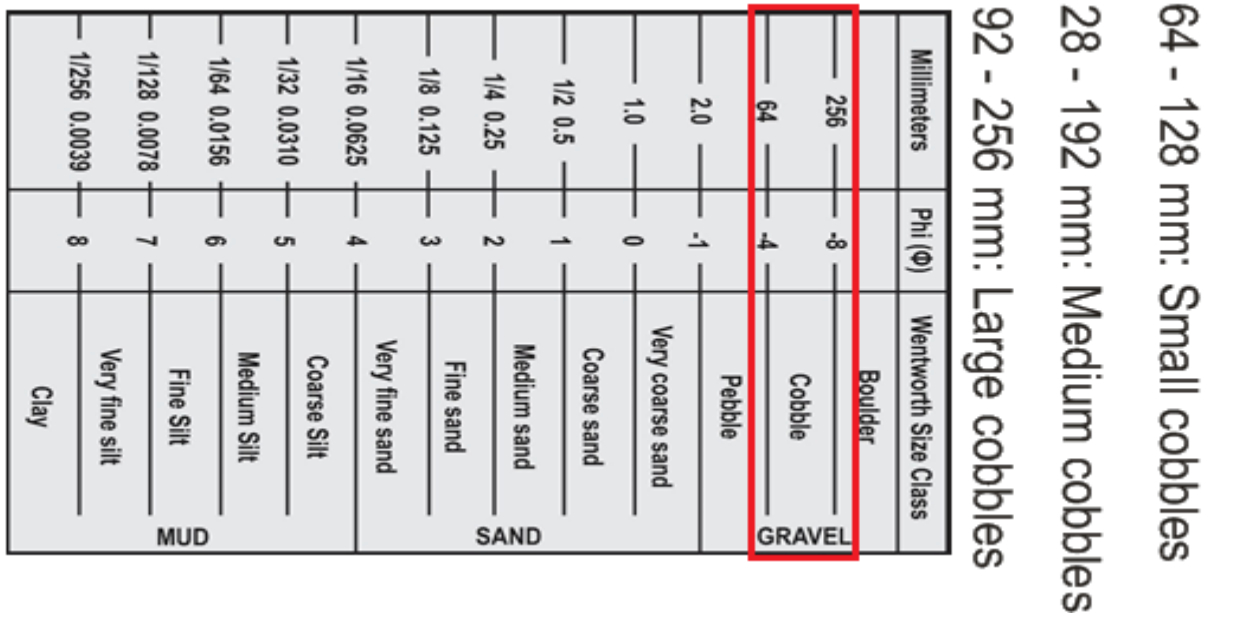

Figure 8: Grain size classification scheme modified after Wentworth (1922). For this study, cobble sizes are the most prominent, and as such, a more detailed size interval for cobbles was defined.

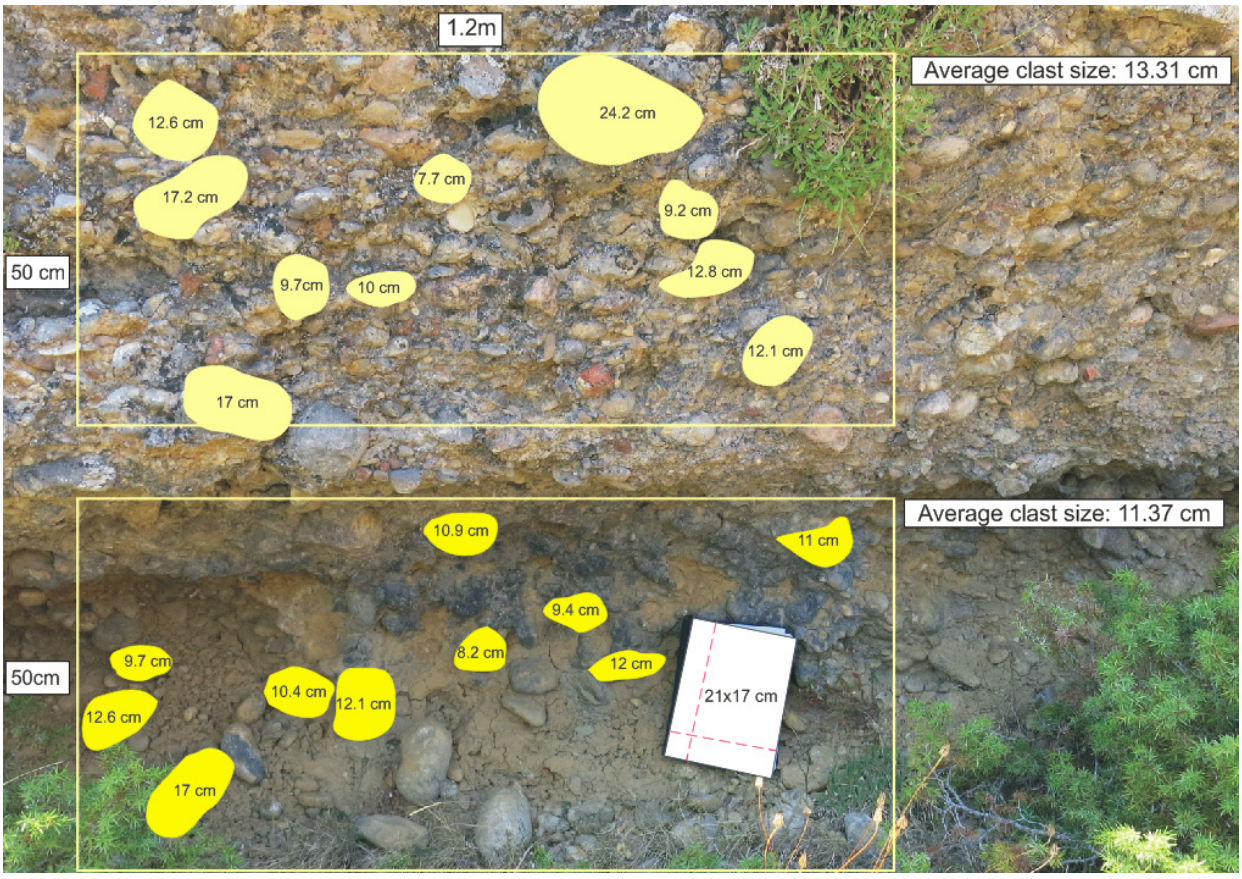

Figure 9: Field photo of two coarse beds in Fan A, showing how average clast measurements were made. Areas of approximately 1 x 0.50 m were used, but for thinner beds, it was scaled down accordingly. Book for scale. The location of this photo is shown in Figure 45.

4.2.2.2 Clast reworking

The roundness of clasts was recorded using general roundness terms (Figure 10). The conglomeratic clasts in the alluvial fans are mainly sub-rounded, although it depends on what type of clast it is. Limestone and sandstone clasts are generally rounded and sub-rounded, whereas the chert clasts are angular to sub-angular, due to the hardness of chert. The various extents of reworking and deformation also aid when speculating about the length of transportation as well as the energy of the different flows. Sandstone clasts are often split in half whereas limestone and chert are more arbitrarily chipped off and smoothed around the edges.

There are clear signs of glacial reworking, as clasts with striations and facetted pebbles (Figure 11) are found throughout the area of study at any elevation.

4.2.2.3 Clast type comparisons

The various clast types in the four different fans were identified to investigate the differences from fan to fan. This was done to say something about provenance. The fans consist of grey, white and green limestone clasts, along with red, grey and green chert clasts. No sandstone clasts were observed in situ, but were found scattered around in loose sediments. They are expected to be part of the clast composition, but of minor importance.

An X-ray Powder Diffraction (XRD) analysis was ran post-fieldwork on the green chert and the red chert, to examine the mineralogical bulk composition of these two lithologies. XRD is a relatively rapid analysis where the clasts are crushed and milled by hand in an agate mill to very fine powder size (fine silt to mud sizes) prior to analysis. The bulk mineral composition of the analysed sample is then determined through phase identification of the resulting mineral spectrum.

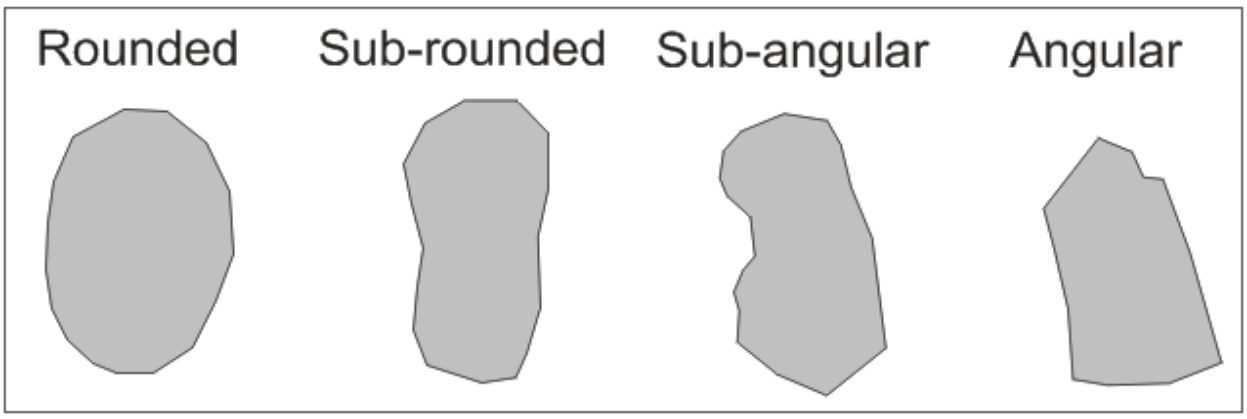

Figure 10: Shows the general terms used for describing the roundness of the conglomeratic clasts.

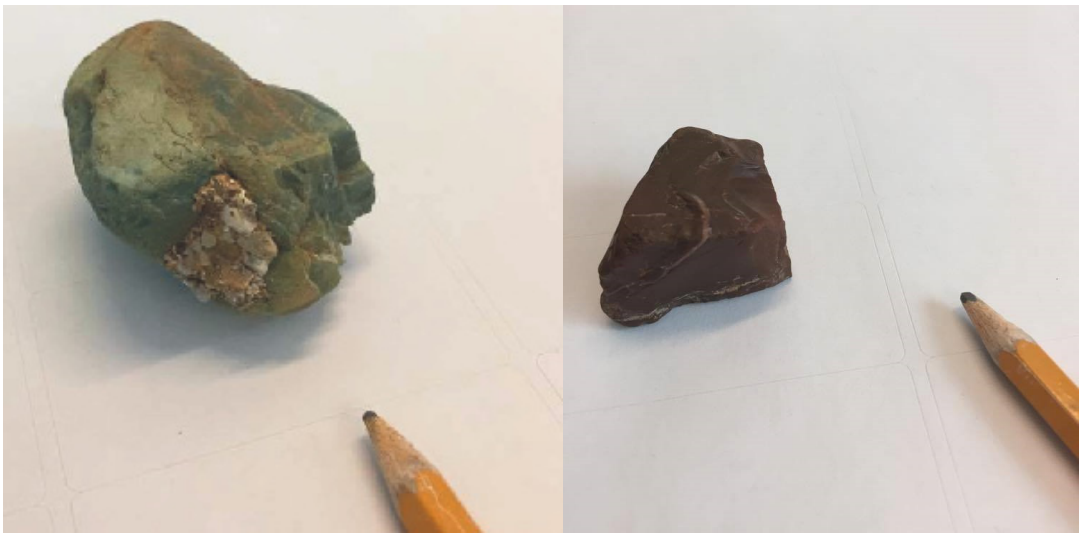

Figure 11: Left - glacially reworked green chert clast with striations and a facetted pebble. Right - shows a common angular red chert clast. These two clasts were subject to an XRD analysis. Pencil for scale.

4.2.2.4 Sorting

The area of study comprises basement carbonates, alluvial and fluvial conglomerates, and occasional sandstone beds, unconsolidated sediments and vegetated areas. A conglomerate consists of matrix and conglomeratic clasts. The size differences between the matrix and the clasts have nothing to do with sorting. As the main lithology in this study is conglomerates, sorting is slightly more difficult than for conventional sandstones. Conglomerates may look poorly sorted, but the relative size differences between the clasts might indicate a better sorting than one would presume. If all the clasts of a conglomerate are between 10 cm and 20 cm, it has the same sorting as a sandstone with grains between 1.0 - 2.0 mm. If the matrix consists of a coarse material and the clasts are relatively small in comparison, the difference between matrix to actual conglomeratic clasts may be unclear.

4.3 Post-field work

The first phase of post-fieldwork was to organize and digitize all the collected field data, and creating backups. Losing the field book, for example, would be an irreversible catastrophe. All GPS locations were properly geo-referenced in a geographic information system (ArcGIS). A multitude of photos were interpreted together with field measurements. Lithological logs and figures were drawn in detail in the Corel Draw software. Cross-sections were constructed using an elevation profile from a DEM in Petrel, and a geological model showing order of events were created. Some of the clast samples taken from Greece were milled and subjected to XRD analysis.

Chapter 5: Field observations – faults and stratigraphic units

In this chapter, the field observations will be presented. Firstly, all the faults relevant to the area of study will be covered. Then, stratigraphic units and a detailed description of the alluvial fans at the end. Some interpretations appear alongside the observations in this chapter, due to the nature of the thesis. This is done to facilitate easier reading.

5.0 Introduction

The proposed footwall derived fans are the focus of this study and will make up the better part of this chapter. All the stratigraphic units and faults have been mapped (Figure 12); but several field photos with interpretations are presented to improve visualisation of the study area in 3D. Most of the stratigraphic units will be covered briefly in the following subsections, with a few exceptions. The Aetovouni and Skepasto members are the only stratigraphic units not surveyed at all through this study, and the data regarding these and nearby faults are credited to previous theses (Syahrul 2014; Stuvland 2015; Rognmo, 2015; Hadland 2016). This thesis focuses on the eastern half of the Kerpini Fault Block.

Syahrul (2014) first identified Fan A as an individual fan in the study area, as well as its bounding faults. Hadland (2016) described it briefly during his work. He concluded that Fan A was a footwall-derived alluvial fan with generally smaller clast sizes (7 - 10 cm) than the other conglomeratic deposits found within the Kerpini Fault Block. A south-ward fining trend was observed, and the beds thin towards the south.

Fan B was first observed by Hadland (2016), and was interpreted as an individual alluvial fan. A fault that incises Fan B was inferred. The study concluded that Fan B exhibited the largest clasts of Fans A, B and C; in the range of 10 - 15 cm. He concluded that this fan had a south-ward fining trend, and that its depositional characteristics are similar to Fan A.

Hadland (2016) also identified Fan C. He found that the apex was difficult to pinpoint, which is indicative of poor geomorphological features. A south-ward fining trend was observed for this fan too. Fan C was not as well described as Fans A and B in his thesis, as the thesis focused further S-W than the location of Fan C.

Fan D has not been described as an individual unit before. It has been observed from across the Vouraikos River, but has not been investigated before. It was included in an overview photo in the

thesis by Sigmundstad (2016) as part of one of the eight segments of Roghi Mountain. Two distinct outcrops were identified and marked by LIDAR-scan. As this study will show, these two outcrops constitute Fan D (Figure 79).

Hitherto unidentified stratigraphic units were described during the field-work of this study. Several units that appear to be individual lobes were observed east of Fan A, in addition to a large conglomeratic outcrop on the very eastern limit of the Profitis Ilias Mountain. These units will be described in this chapter.

This thesis will show that some of the previous years' observations are erroneous whereas some are correct. First, all the bounding faults and stratigraphic units in the Kerpini Fault Block will be described in order to have a framework in place, followed by a thorough description of each fan at the end of the chapter. In the end, Fans A, B, C and D will be thoroughly characterized.

The names used for many of the stratigraphic units mentioned in this thesis, such as the Vighia Member and the Aetovouni Member come from Hadland *et al.* (in prep). This is done to have consistent names with the paper that is soon to be released, and make it unambiguous for future readers.

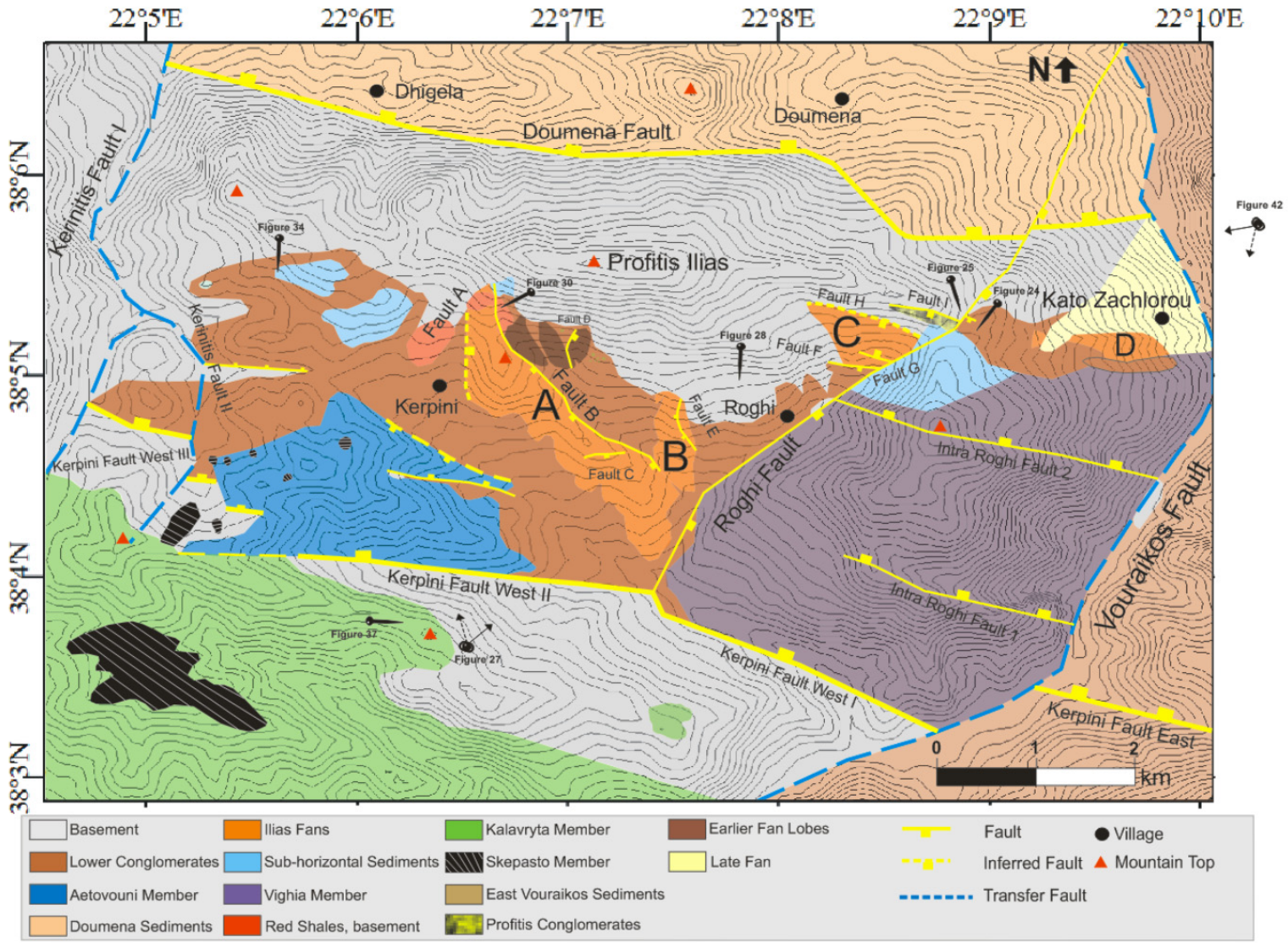

Figure 12: Surrounding area and detailed geological map of the Kerpini Fault Block. This map shows stratigraphic units and faults identified during this study, as well as work done by previous master students from the University of Stavanger, specifically the south-western area (Syahrul, 2014; Stuvland, 2015; Hadland, 2016).

5.1 Major faults

Faults and other structural observations from the field will be highlighted in this chapter. For simplicity, Dip / DD is used to describe the structural orientation of sedimentary layers and faults (with a right-hand rule, the strike of a fault = DD - 90°). All the minor faults have been photographed, and the observations / interpretations are drawn directly on the photos. The major faults and transfer faults are shown in a map view. Several faults in the westernmost region of the study area around the Aetovouni Member as well as the Kerpini Fault has been thoroughly studied by previous master students from the University of Stavanger (Syahrul, 2014; Stuvland, 2015; Hadland, 2016), as well as Ford (2013), and has not been further investigated during this study. However, a general description of the Kerpini Fault will be given below. Syahrul (2014) was the first to identify Faults A and B as well as the Roghi Fault, whereas Hadland (2016) was the first to identify Fault E. The Intra Roghi Faults 1 and 2 were identified by Syahrul (2014). Transfer faults striking north-south located in the Vouraikos and Kerinitis River Valleys were interpreted by Dahman (2015), which are important features covered in Sub-chapter 6.5.

5.1.1 Kerpini Fault

A detailed study of the Kerpini Fault is outside the scope of this thesis, but a short summary will be given here. It is traced with a high confidence in the area of study. Hadland (2016) concluded that a step in the Kerpini Fault was responsible for creating a pathway for the Aetovouni Member to deposit in the southwest. The displacement profiles for the Kerpini Fault and Doumena Fault were covered in sub-chapter 2.2.1. The fault has a Dip / DD of 45° / 10 - 25°N. It is separated into two main parts: Kerpini Fault West and Kerpini Fault East. The eastern fault is found to the east of the Vouraikos Valley, and is outside of the area of study. The western fault appears approximately 700 metres further north after a right-step in the valley.

The western Kerpini Fault splits into three separate segments: I, II and III, all with slight differences in dip direction. The DD of Segment I ≈ 25°N, Segment II ≈ 10°N and Segment III ≈ 15°N. The step between segment I and II is most likely caused by the southernmost part of the Roghi Fault, which intersects the Kerpini Fault in this location, and causes a small fault step. Syahrul (2014) proposed that the Vighia Member was sourced from this step of the Kerpini Fault, something Bjåland (2016), Sigmundstad (2016) and Hadland (2016) supported. The steps between

Segment II and III are not as simple, because it develops into two smaller normal faults, where the displacement decreases to the west.

5.1.2 Doumena Fault

The Doumena Fault bounds the study area in the north, and has one of the best exposed fault planes in southern Greece, thus the dip measurements for this fault have strong confidence. This fault was not studied as part of this thesis, as it is more important for sediments in the Doumena Fault Block to the north. The fault has a Dip / DD of 40° - 50° / 0-10°N. Towards the western limits, the fault is relatively well understood, but in the east towards the Vouraikos Valley the uncertainty increases significantly. There are different theories for where the Doumena Fault is traced to the east, and as the fault plane is not exposed here, there are different ways of tracing it. In this study, the Doumena Fault has been interpreted as stepping ≈ 50 m to the north when it intersects the Roghi Fault in the east, before either terminating or stepping in the Vouraikos Valley 500 m further to the east. Significant E-W striking faults to the east of the valley exist, but it is unclear whether the Doumena Fault is one of them.

5.1.3 Roghi Fault

The Roghi Fault will be discussed in Sub-chapter 6.5, but it is brought up briefly in this chapter. It can be observed clearly affecting the topography in the region (Figure 13). The contact is sharp, and there are clear lithological differences across the fault. In Figure 13, one of the later fans outside of the study area (yellow) has deposited over the Roghi Fault, which is why these conglomeratic layers are unaffected by faulting. The stratigraphic units and faults in the area of study are excluded from the figure, as it is included only to demonstrate the simple point above.

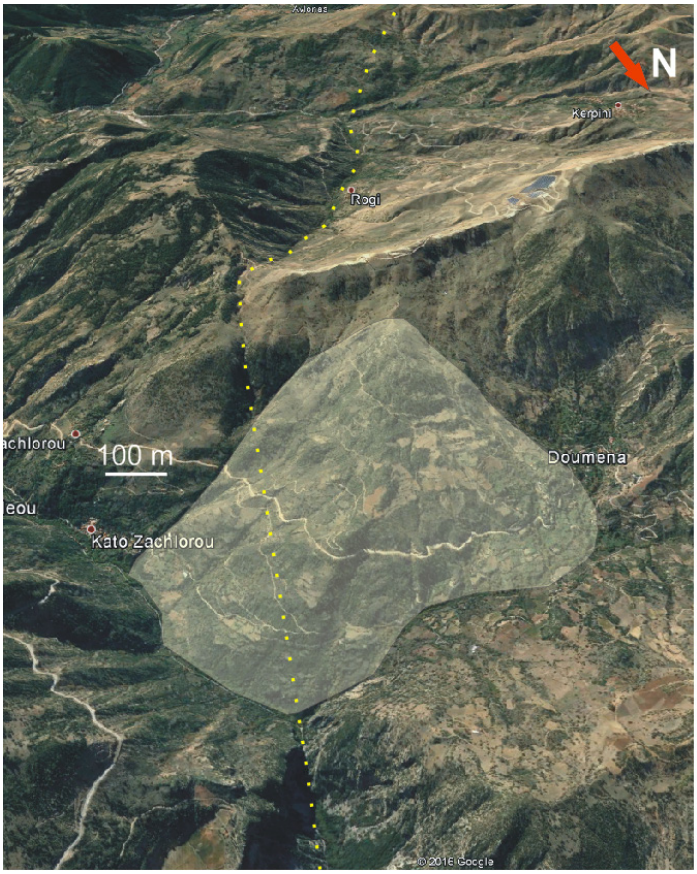

Figure 13: Satellite image showing how the Roghi Fault (highlighted by yellow dots) affects the topography.

5.1.4 Minor faults

In this study, six previously unidentified faults are mapped and described. Other previously identified faults, important to the stratigraphic units of interest are described; namely Fault A, B and E. All these faults will be presented in the following sub-chapters.

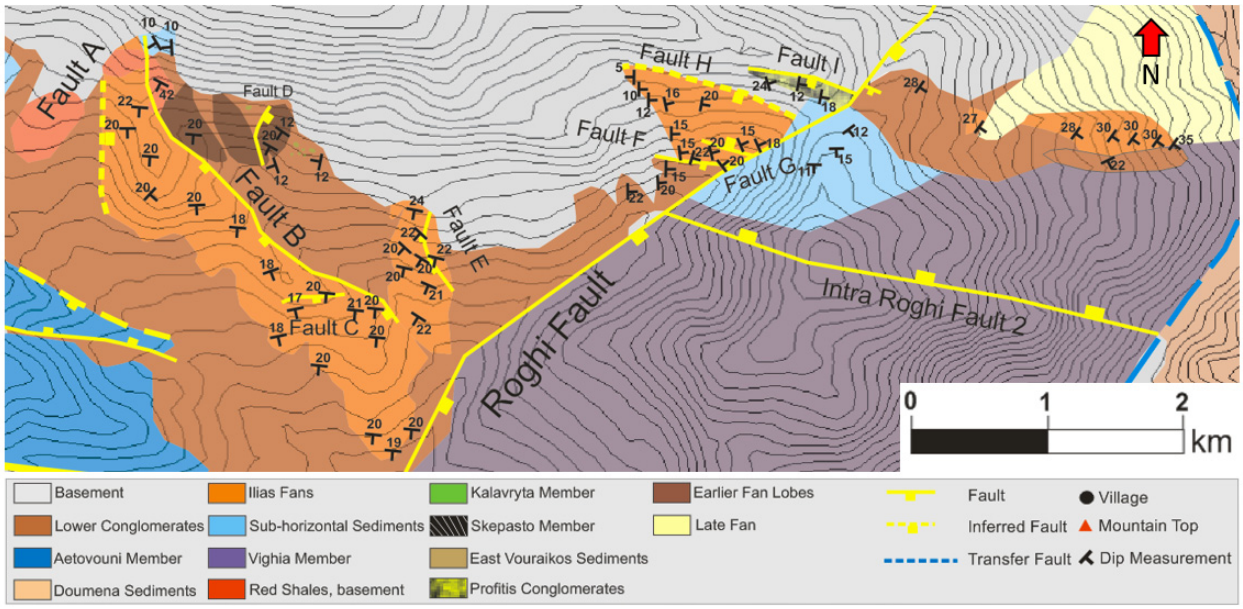

Figure 14: Zoomed in geological map with all the collected dip data displayed. If displayed in Figure 12, it would be too cluttered to be viewable.

5.1.4.1 Fault A

Fault A has no exposed fault plane, and exhibits little conclusive evidence that a fault is located here (Figure 15). It has an assumed Dip / DD of ≈ 50° / 90 - 95°E. As basement is exposed directly to the west of Fan A, the inference of the east-dipping Fault A accommodates for Fan A. Fault A forms a graben together with Fault B that allowed the fan to deposit. It is difficult to say anything about the minimum displacements of these fan-bounding faults, as there are no reference contacts to compare in the footwall and hanging wall of the faults. Additionally, there is no real control on the basement unconformity, but it drops to a greater depth across the fault. The displacement of the fault cannot be less than the height of the fan, since there is no exposed fault or unconformity contact on either side. Fan A is at least 150 m thick, hence a minimum fault displacement of 150 m is assumed.

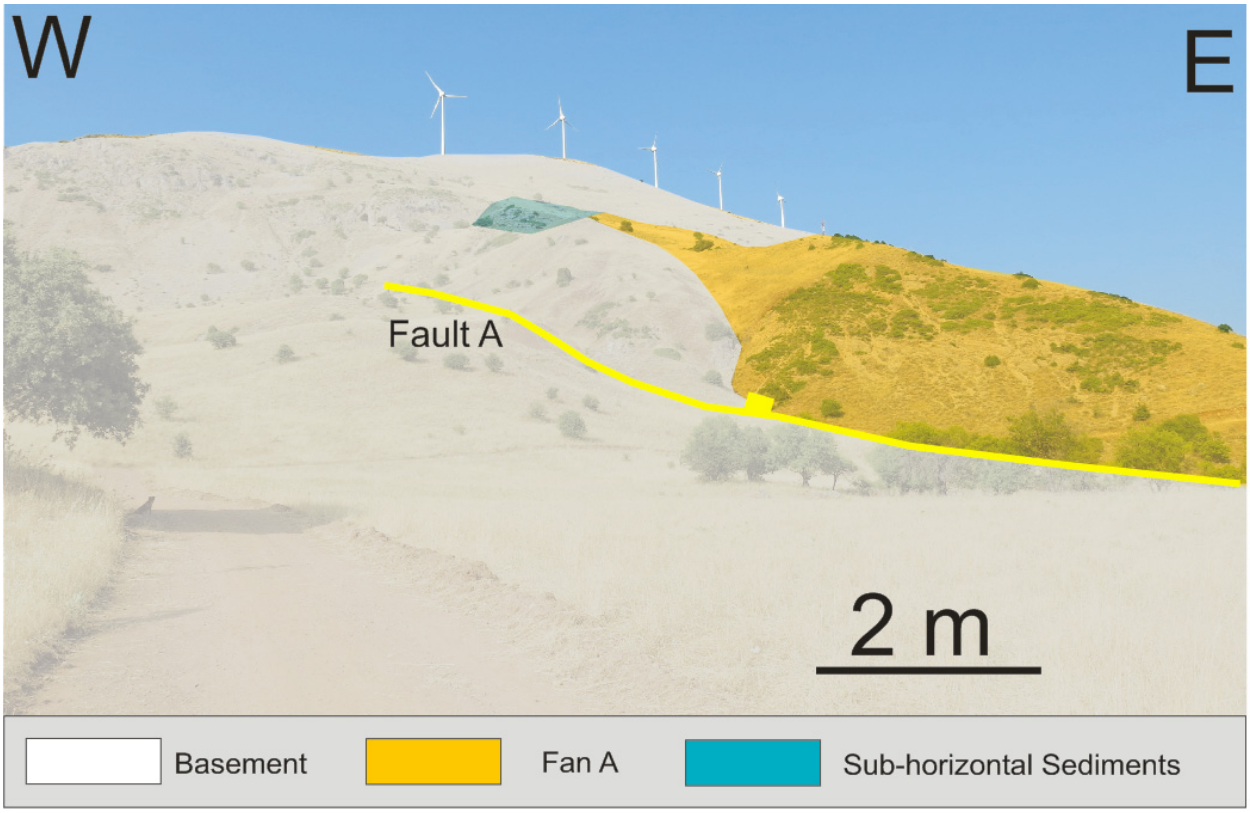

Figure 15: Location of Fault A and the apex of Fan A. The red basement shales are located here, but coloured white for simplicity as they all belong to the basement. The location of this photo is shown in Figure 45.

5.1.4.2 Fault B

Fault B bounds Fan A to the east, and has a Dip /DD of ≈ 50 - 60° / 225°SW. Basement is exposed adjacent to the fan, in addition to a sharp boundary against the Lower Conglomerates both at the location of Figure 16 and further south. The fault is not as curvy as it is drawn in Figure 16, but it is drawn where the contact is traced through the topography. The fault evidence becomes less clear to the south. The minimum displacement of the fault is estimated to be ≈ 25 m, based on the basement elevation across the contact from the base of Fan A. The unconformity could be located anywhere below the base of the fan, and the minimum displacement of the fault must be 25 m. The maximum displacement is estimated to be ≈ 200 m, based on the dip of the unconformity plane (24°) from the basement contact near the apex of Fan A, and southwards. This is seen in cross section B-B` (Figure 97).

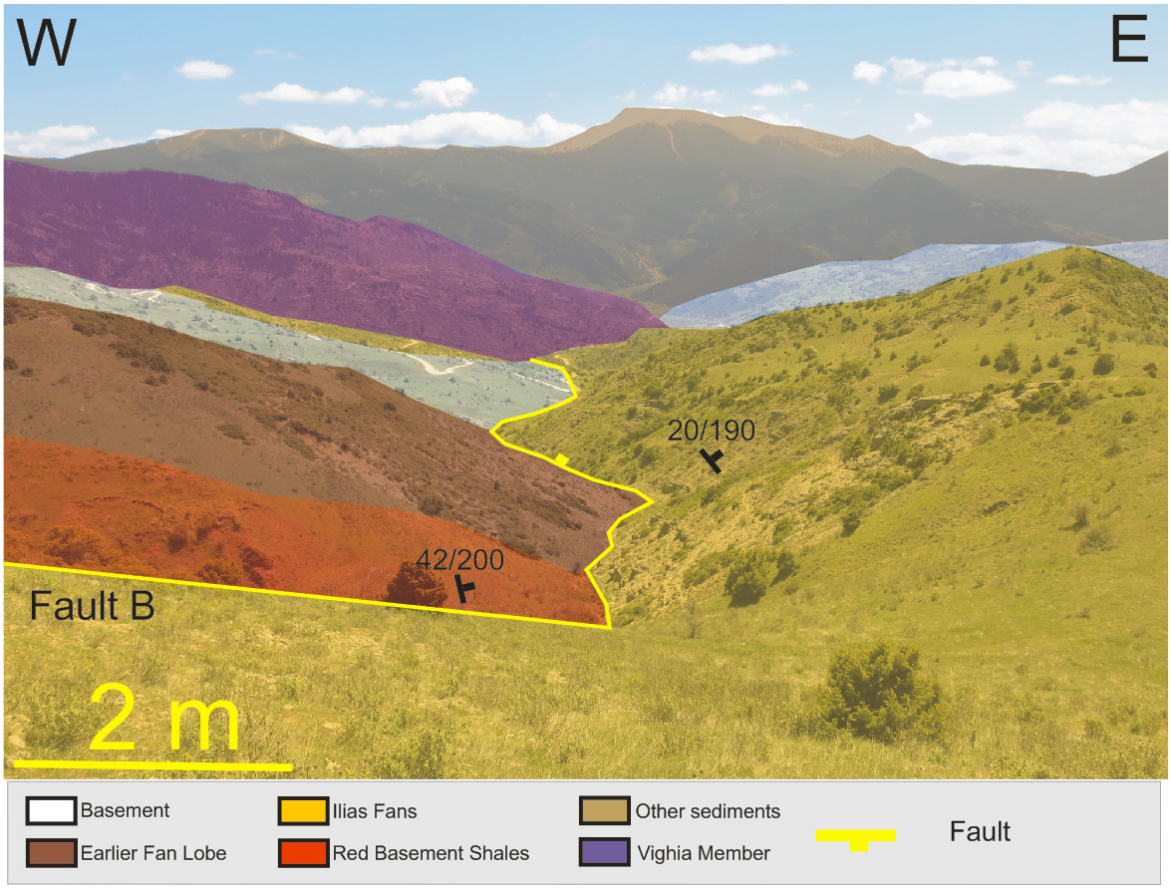

Figure 16: Photo taken from the apex of Fan A, looking southwards along the fan. The Red Basement Shales can be seen over the sharp contact that is interpreted as Fault B. One of the earlier fan lobes are truncating against the main fan. At the back of the figure, Fan B is located close to the Vighia Member. The basement of the Kalavryta Fault Block is observed in the south-east. The location of this photo is shown in Figure 45.

5.1.4.3 Fault C

Fault C is a minor fault, identified in the southern half of Fan A (Figure 17). The dip is unknown, as no fault plane is exposed – but a Dip / DD of ≈ 45 - 50° / 170°S. The fault is identified based on the sudden termination of the conglomeratic beds in the immediate hanging wall of the fault. A theory is that this fault may have affected lobe development through time, and shifted the lobe more to the south. Another possibility in this location is that Fault C is a small listric fault, and that the sharp feature 30 m to the north is a second listric fault (yellow dashed line in Figure 17). In the big picture however, Fault C is restricted to Fan A, and is only a small detail in the Kerpini Fault Block. A minimum displacement of 30 m is assumed, based on the offset of the conglomeratic beds.

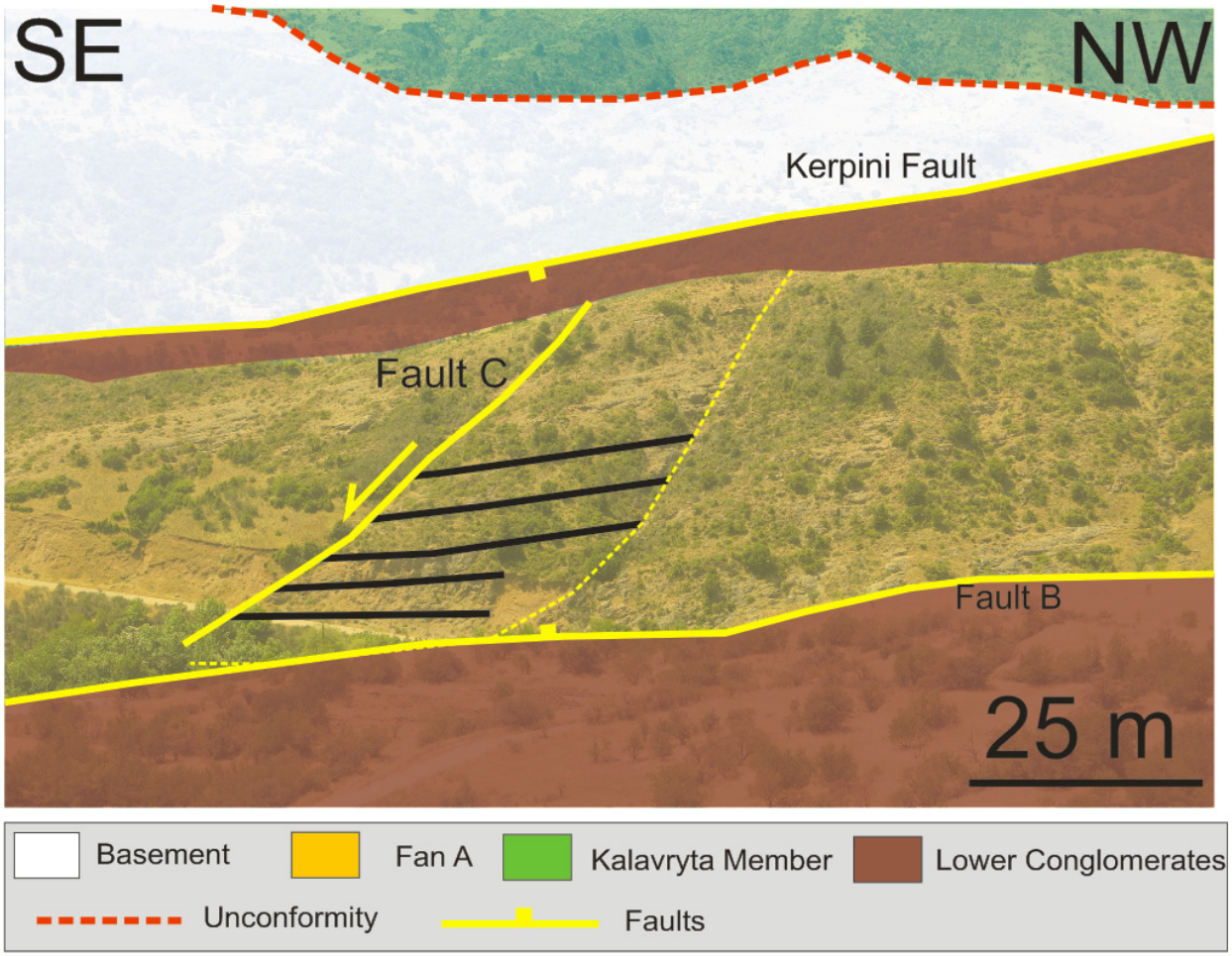

Figure 17: Photo taken from Fan B towards Fan A. It shows Fault C, and how the package of conglomerates to the north of the fault disappears in the immediate hanging wall. The location of this photo is shown in Figure 45.

5.1.4.4 Fault D

Fault D is identified between two of the lobes directly east of Fan A. These lobes are described later. A planar basement surface with a Dip / DD of ≈ 55° / 180°S is exposed and interpreted as a fault surface (Figure 18). The conglomerates of the individual lobes are found in the immediate hanging wall of Fault D adjacent to the basement. The fault can be traced further south (Figure 19), where it can be observed faulting the basement as well. This fault likely created accommodation space for the easternmost lobe. The minimum displacement is ≈ 15 m, based on the thickness of the adjacent conglomerates.

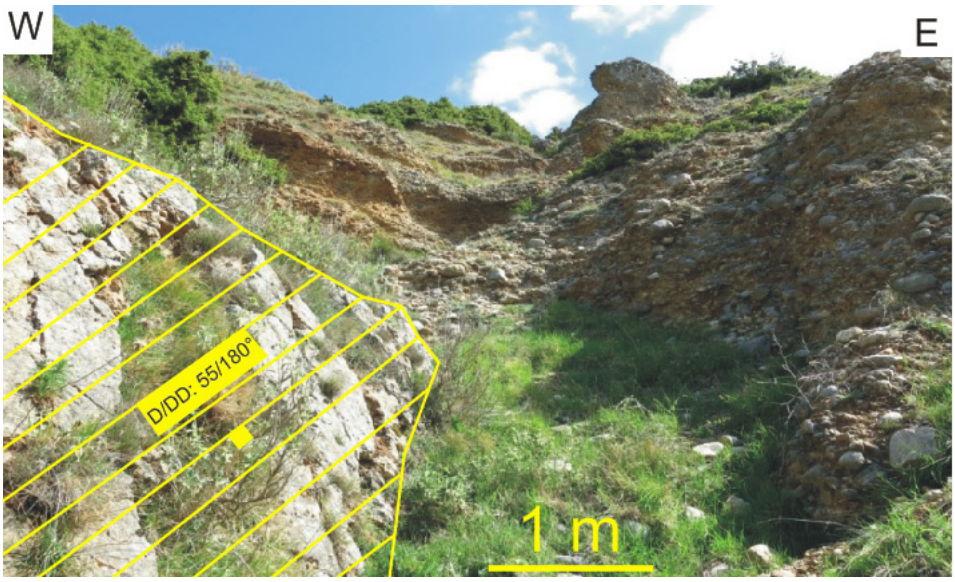

Figure 18: The planar basement surface interpreted as Fault D. The location of this photo is shown in Figure 45.

Figure 19: Fault D faulting the basement further south. The location of this photo is shown in Figure 45.

5.1.4.5 Fault E

Hadland (2016) inferred a fault based on an observed change in dip from a distance. Up close, the fault can be observed cutting straight through Fan B. The unconformity can be observed in this outcrop as well, separating the fan conglomerates from the carbonate basement.

The dips of the conglomeratic layers on either side change sharply across Fault E (Figure 20). Due to the angle of the unconformity plane, the basement would be expected to be exposed in the immediate hanging wall of this fault, but due to down-faulting it is not. The incision is very clear in the topography, with the fault having a D / DD of ≈ 45-50° / 240°SW. The dips of the sedimentary layers are indicated in yellow lines, but the dip of the fault is unknown as no fault plane is exposed. The dip is assumed based on the dip nature of the other faults in the area of study. The unconformity steps to the south in this area, as seen in map view – and this is interpreted to be due to a fault. The minimum displacement is estimated to be ≈ 15 m.

Due to the perspective from which the photo is taken, it seems like the basement is overlying the conglomerates. This is not the case. The plane of the unconformity is dipping steeply into the conglomerates due to the paleotopography of the basement.

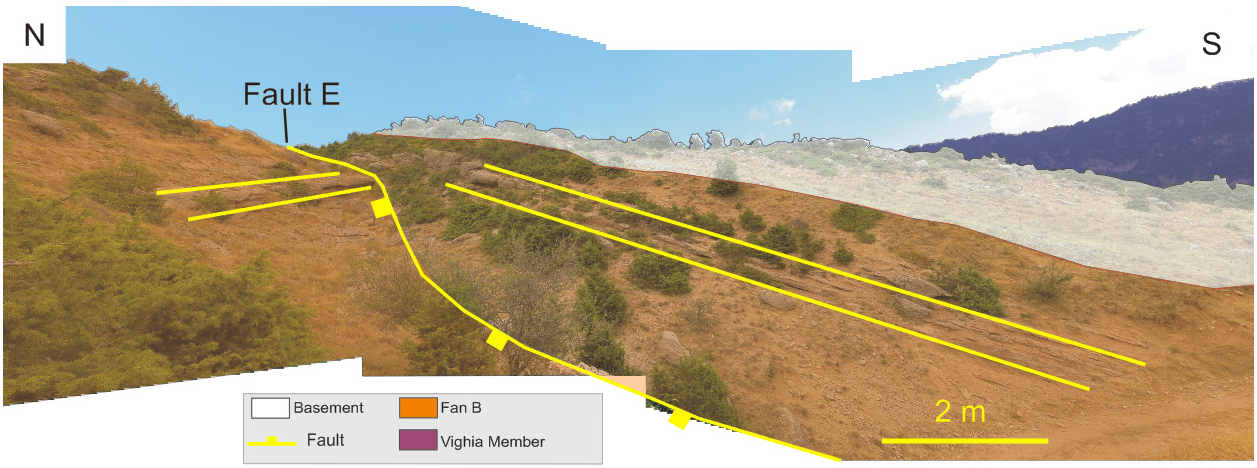

Figure 20: Fault E cutting through Fan B. The unconformity plane dips steeply towards the point of observation. Note the fine beds below the unconformity. Scale is relevant to base of figure. The location of this photo is shown in Figure 60.

5.1.4.6 Fault F

Fault F bounds Fan C to the south, separating it from the underlying Lower Conglomerates. The conglomerates have a vastly different structural orientation, with a Dip / DD of 15° / 90°E, compared to the orientation of Fault F (60° / 190°). The fault is evidenced by a conglomerate-basement contact in the very western part of the fault (Figure 21). The sharp contact between them is most likely a fault, which can be traced to the east and west, displacing the basement to a higher elevation than the conglomerates in several outcrops. These conglomerates exhibit similar Dip / DD as the fan conglomerates, but the clast sizes and bed thicknesses decrease across the fault. Hence, a fault is a plausible interpretation. Due to the thickness of the conglomerates found above the fault, the minimum displacement is estimated to be ≈ 40 m.

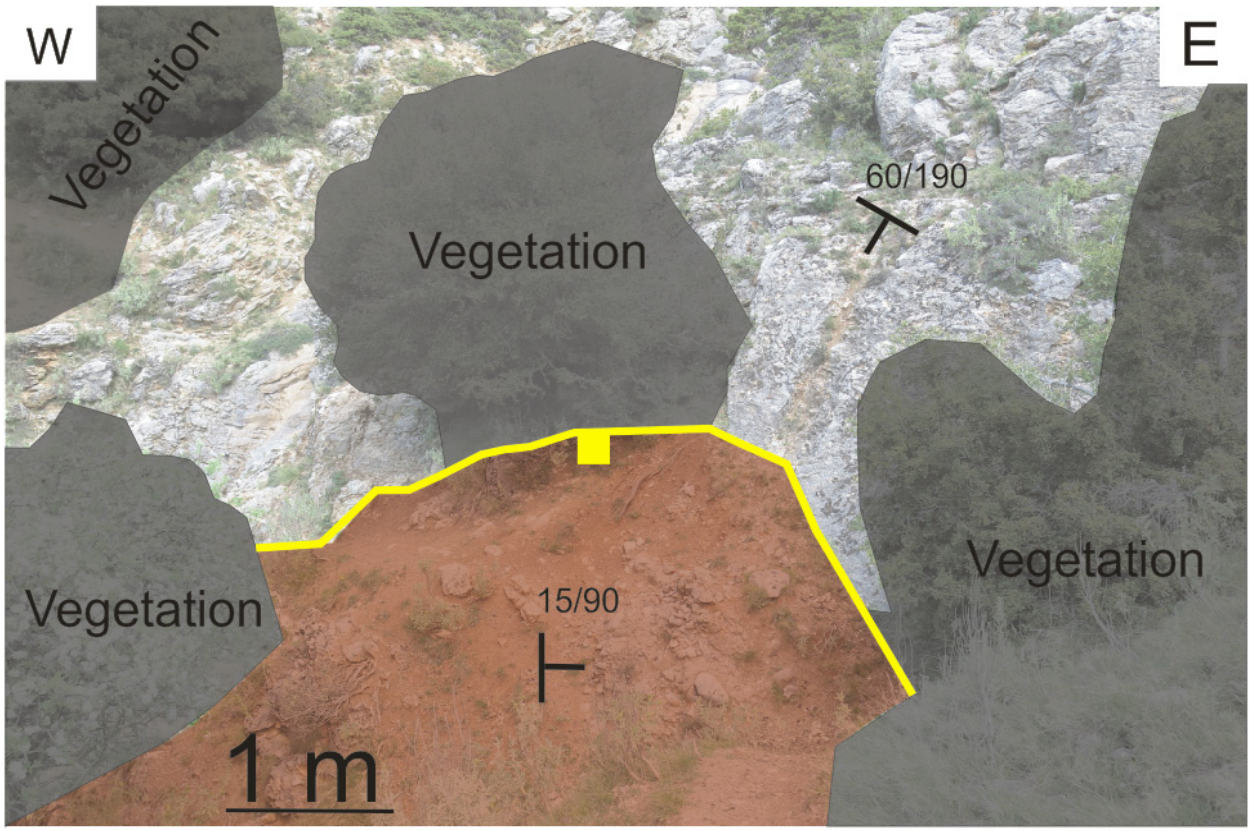

Figure 21: Planar and steeply dipping basement surface, interpreted as a basement fault plane (white), with an associated Dip / DD of 60° / 190°S. The Lower Conglomerates (brown) are located in the immediate hanging-wall of the fault, with a Dip / DD of 15° / 90°E. The location of this photo is shown in Figure 71.

5.1.4.7 Fault G

Fault G is an internal north-dipping fault of Fan C that juxtaposes thinly bedded fine conglomerates against coarse conglomerates. The sharp and planar appearance of the coarser conglomerates is interpreted as a fault surface, with a Dip / DD of 65° / 30°NNE (Figure 22). The fault itself is of no major importance, and likely activated post-deposition of Fan D. The minimum displacement is estimated to be ≈ 5 m.

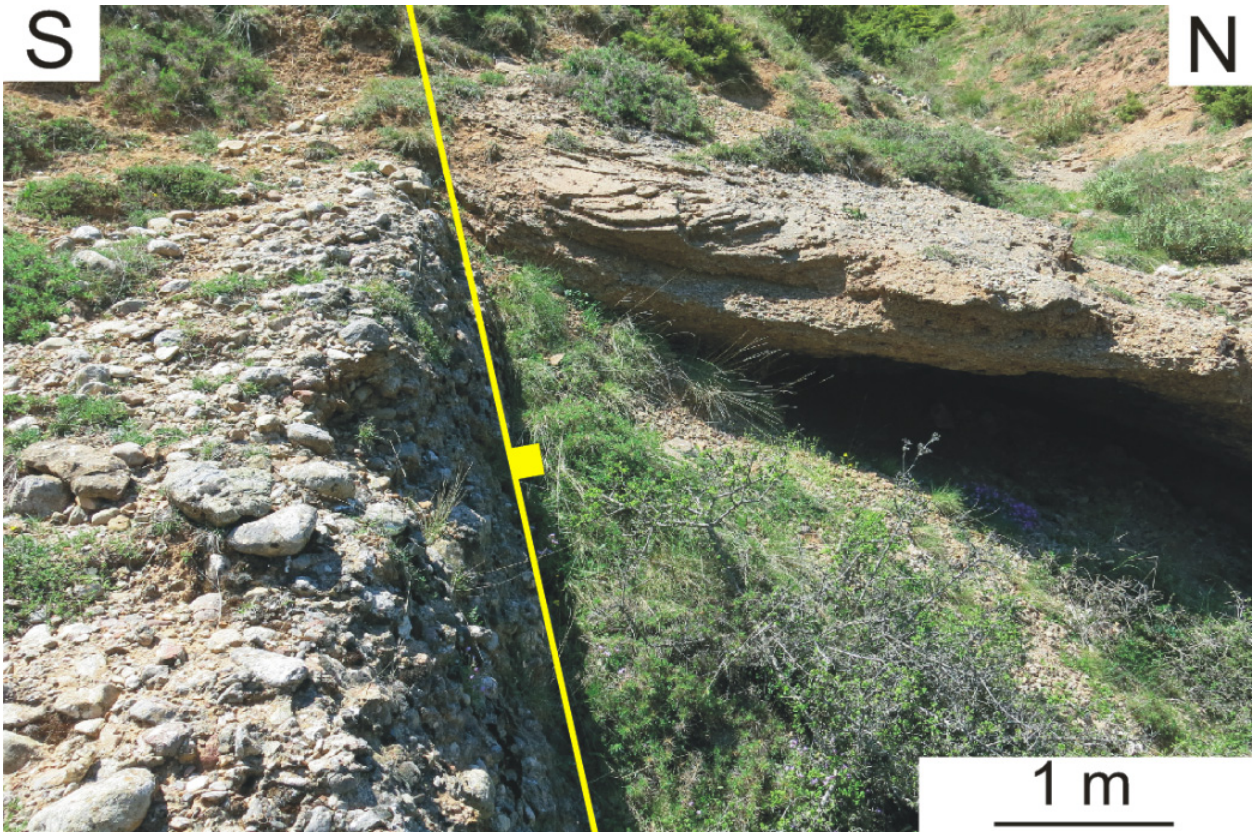

Figure 22: Fault G down-faulting fine and thinly bedded sediments adjacent to coarse and more thickly bedded conglomerates. The location of this photo is shown in Figure 71.

5.1.4.8 Fault H

At the northern boundary of Fan C, there is a linear feature in the topography that separates the basement of Profitis Ilias from the conglomerates of Fan C (Figure 23). The basement between Faults H and I essentially functions as a fault plane. There is no clear fault contact, as grassy mounds and eroded sediments from the nearby mountain have covered the area. A Dip / DD of 50° / 190°S is assumed for this fault. The minimum displacement is estimated to be ≈ 50 m.

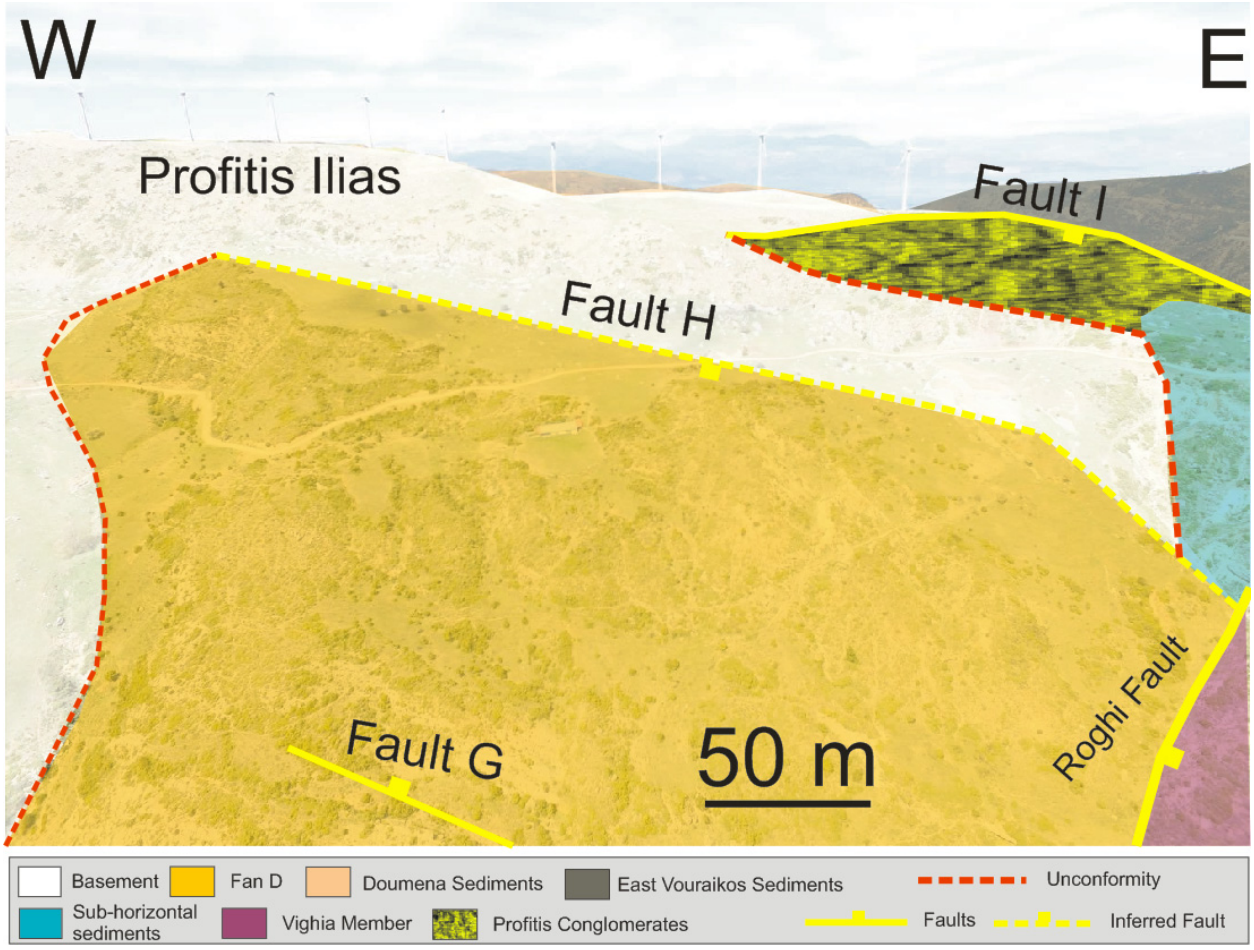

Figure 23: Drone photo of the northern area of Fan D showing the linear feature that bounds Fan D in the north, interpreted as Fault H. Location of Faults G and I and the Roghi Fault is outlined as well. The location of this photo is shown in Figure 71.

5.1.4.9 Fault I

Fault I is one of the most obvious faults identified in the study area. It bounds the Profitis Conglomerates to the north, separating it from the basement of Profitis Ilias (Figure 24). The contact is sharp and steep, with an assumed Dip / DD of 60° / 190°S, which is steeper than Fault H. As seen in the geological map, this fault can be traced westwards to the end of the Profitis Conglomerates and across the Roghi Fault, where it steps 50 metres to the north (Figure 25). The displacement has nearly died out to the east of the Roghi Fault, where it is ≈ 10 m. To the west of the Roghi Fault, the minimum displacement is estimated to be 30 - 40 m.

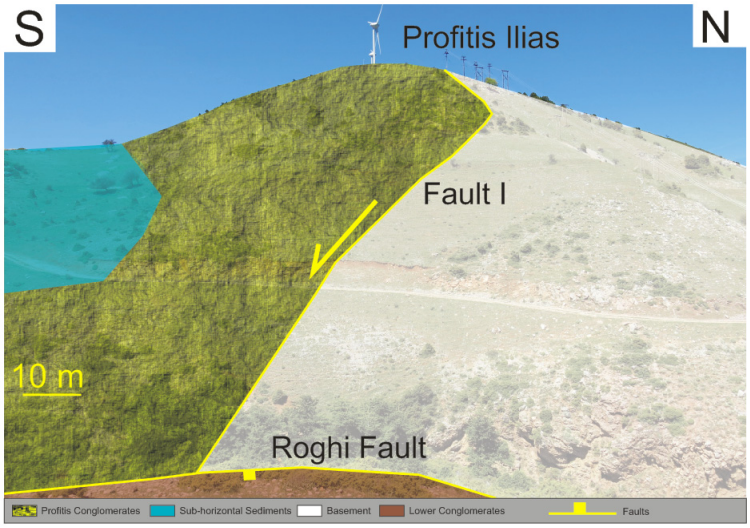

Figure 24: Fault I and the nature of the contact on the eastern side of Profitis Ilias. The location of this photo is shown in Figure 12.

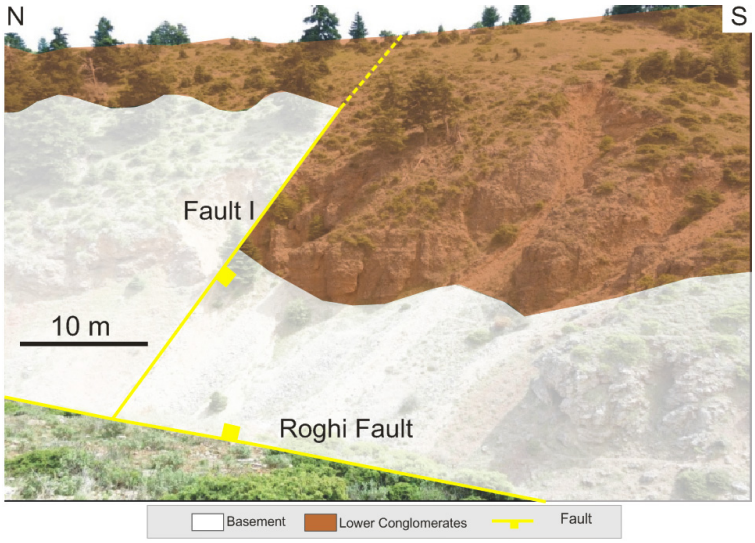

Figure 25: Fault I across the Roghi Fault. It has stepped 50 metres to the north in this location. The location of this photo is shown in Figure 12.

5.1.4.10 Intra Roghi Faults 1 and 2

As later shown in subchapter 5.2.4, Sigmundstad (2016) separated Roghi Mountain into eight segments. Intra Roghi Fault 1 acts as a boundary between segment II and III, whereas Intra Roghi Fault 2 is located in the northern part of segment IV (Figure 35). The bed characteristics and dip character change across these faults. As such, they are very obvious features in the mountain side (Figure 26). The dip is unknown, but a Dip / DD of 45° / 15 - 20°N is assumed.

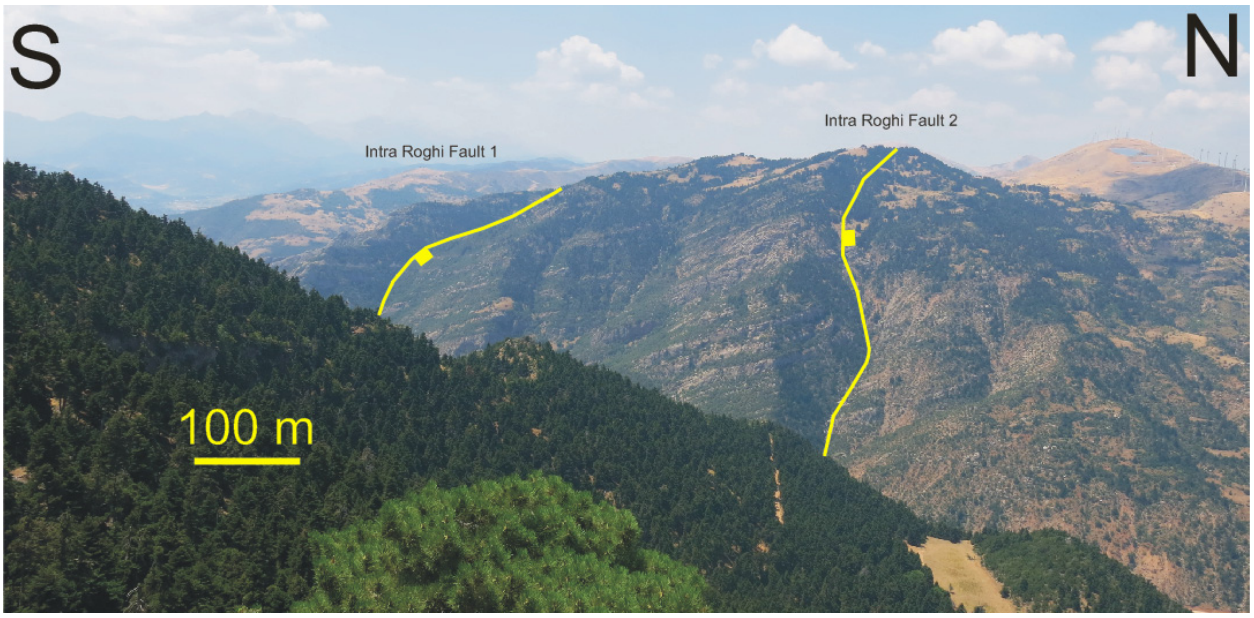

Figure 26: Field photo of Roghi Mountain taken from the east of the Vouraikos Valley – shows the Intra Roghi Faults 1 and 2 cutting through the Vighia Member. Scale is relevant to the area between the faults. The location this photo was taken from is too far east of the study area to be displayed in Figure 12. However, it is shot 2 km directly east of where the Intra Roghi Fault 2 intersects the Vouraikos River Valley.

5.2 Stratigraphic units in the Kerpini Fault Block

In the following subchapters, all of the stratigraphic units in the area of study will be briefly covered. With the exception of the area around Fan D, most of them can be observed from a southern vantage point in the fault block (Figure 27).

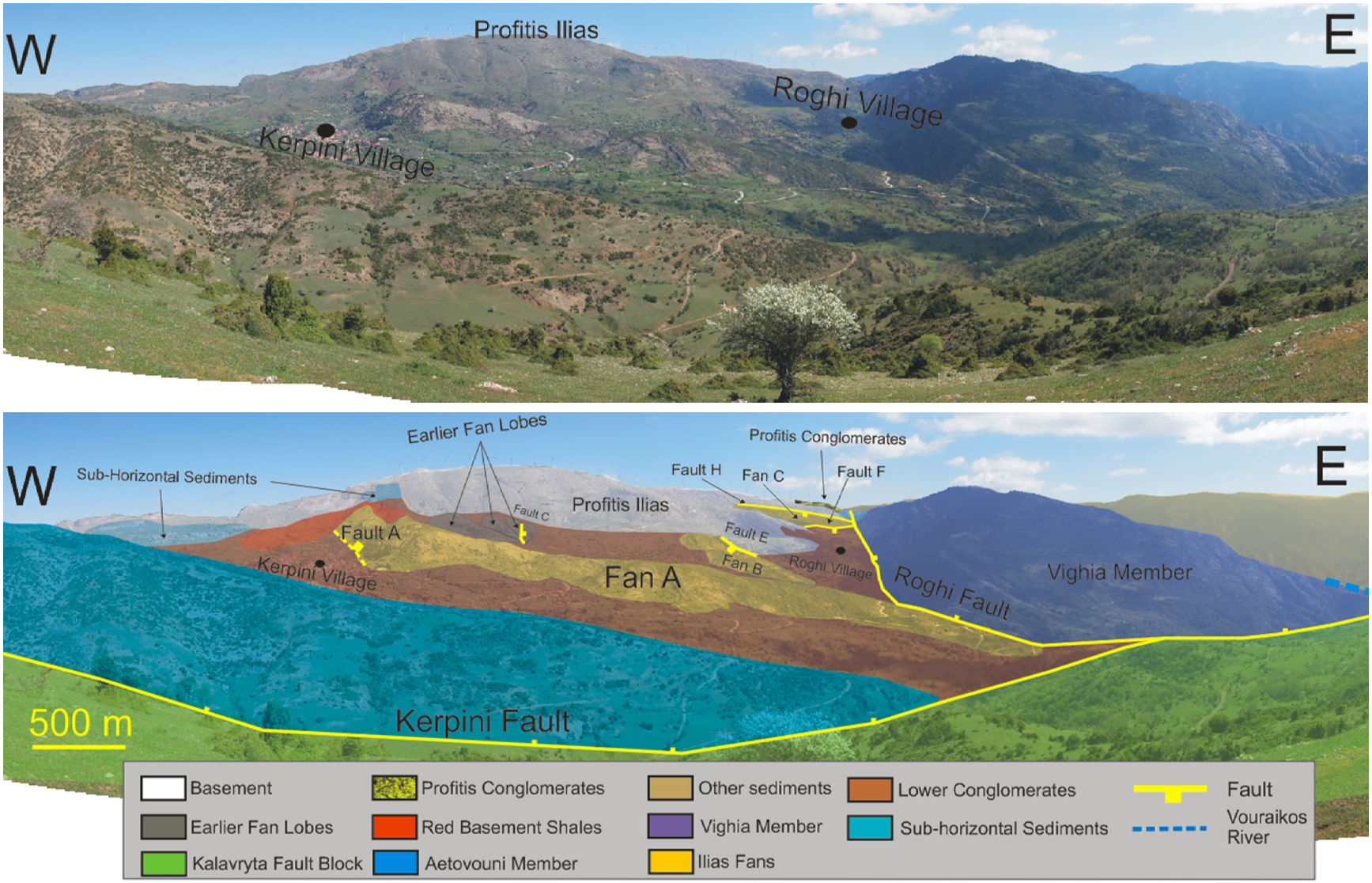

Figure 27: Top – panorama photo of nearly the entire study area shows the mapped features from Figure 12 but in a 3D view. It features most of the important stratigraphic units and some of the faults in the area. Bottom – same panorama photo, but with interpretations. Scale is relevant to the mountain ridge of Profitis Ilias, at the very back of the figure. The location of this photo is shown in Figure 12.

5.2.1 Basement lithologies

There are three main basement lithologies observable in the study area; the dominating carbonates, red basement shales, and the scarcely observed basement breccia. These will be described in the following subchapters. Additionally, various chert clasts are found in all the conglomerates in the Kerpini Fault Block. These chert lithologies are believed to be part of the pre-rift basement, but they are not outcropped in the area of study. All of the basement outcrops are devoid of chert.

5.2.1.1 Basement Carbonates

An extremely folded and altered carbonate lithology is typical for the basement of the Kerpini Fault Block (Figure 28). It consists mainly of thin (2 - 20 cm) folded layers, as well as thicker and more eroded beds of white and grey colour. It is easily distinguishable from the conglomeratic units in the region, as the colour of the lithology and type of flora that grows on top of it differs from the conglomerates. Google Earth is a useful tool to distinguish these lithologies, as the differences can be observed even on satellite images.

Due to the altered nature of carbonate lithologies, there is significant variability in the paleotopography. There are several locations in the study area where basement appears faulted or juxtaposed by an event, but it is often a paleotopographical feature due to the nature of the carbonates (Figure 29). Consequently, the unconformity has several abrupt changes in map view.

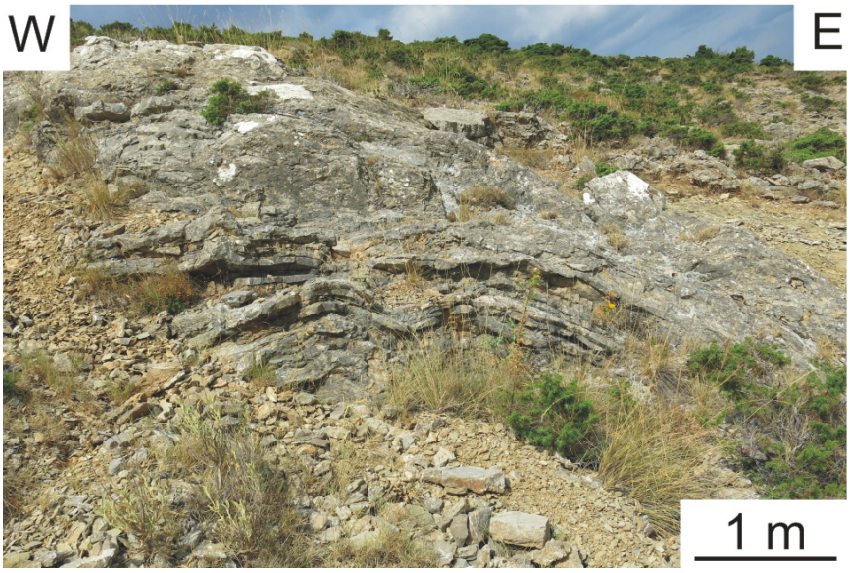

Figure 28: Typical appearance of the basement carbonates. The location of this photo is shown in Figure 12.

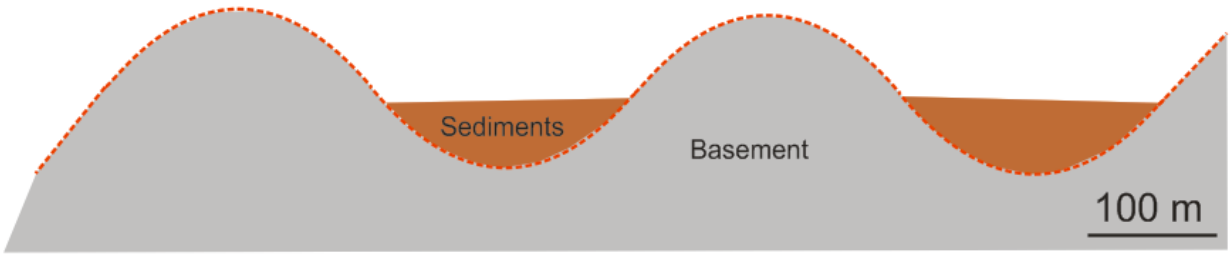

Figure 29: Simplified model showing variations in the paleotopography.

5.2.1.2 Red Basement Shales

In several outcrops, a distinct, thinly layered (5 – 20 mm) shale with a strong, red colour can be observed (Figure 30). It is brittle and often tilted to a steep dip angle. This constitutes a basement shale. In the geological map these red shales are coloured red to differentiate between the basement types.

Figure 30: Typical brittle red basement shales. The location of this photo is shown in Figure 12.

5.2.1.3 Chert

The described conglomerates contain various amounts of chert clasts. These are often angular, tabular and blocky in appearance, due to the hardness of chert. However, the limestone clasts are rounded and affected by transport to a higher degree. There are three main variations of chert; the most common is the lightly coloured white/grey chert, followed by the red chert that appears throughout the entire study area. The rarest type is the scarcely found green chert. No exposed chert outcrops were found in the Kerpini Fault Block during this study, and consequently it is

difficult to say anything about the source of these chert clasts. However, they are believed to be part of the basement.

5.2.1.4 Basement Breccia

The most extensive breccia unit found in the rift system is located south of the Kalavryta Fault Block, and is far from the area of study. However, there are several small and local variations of breccia found in the Kerpini Fault Block (Figure 31 and Figure 32). They are exclusively located in proximity to the basement, and due to very limited extent (a few square metres); they are excluded from the geological map. The locations of these outcrops are displayed in Figure 71. No relation to the syn-rift sediments was observed. They are interpreted as remnants of earlier erosional events of the basement, that were transported a short distance and lithified close to the source.

Figure 31: One of the coarse breccia variations found within the area of study. Some of the angular clasts are outlined in black. The location of this photo is shown in Figure 71.

Figure 32: One of the fine breccia variations found in the Kerpini Fault Block. The location of this photo is shown in Figure 71.

5.2.2 Lower Conglomerates

The most abundant lithology in the Kerpini Fault Block is what this study refers to as the Lower Conglomerates. The conglomeratic clasts are rounded, with sparse clasts that exhibit high angularity. The Lower Conglomerates sit unconformably on top of the basement, and is traced with a high accuracy throughout the area of study. Typical for the Lower Conglomerates is a mix of fluvial (channelized sand lenses) and alluvial character (Figure 33). The vegetation is useful when determining the unconformity contact, as certain flora grow exclusively on soil that rests on the carbonate basement. The unconformity plane has an estimated Dip / DD of ≈ 24° / 178°S, based on a best-fit plane created in the DEM in Petrel. The area between Fan A and Fan B is considered to represent the unconformity surface, as patches of conglomerates are outcropped in several places amongst the surrounding basement.

Figure 33: Interval of conglomerates with a sand lens, typical for the fluvial/alluvial character of the Lower Conglomerates (coloured yellow for visualization). Compass for scale. The location of this photo is shown in Figure 33.

5.2.3 Sub-horizontal Sediments

In 2015, Stuvland (2015) from the University of Stavanger did his thesis in the Kerpini Fault Block on the Sub-horizontal Sediments that are located throughout the fault block. He identified eight outcrops in the Kerpini and Kalavryta Fault Blocks. This stratigraphic unit consists of clast-supported, pebble to cobble sized conglomerates, with a poorly sorted matrix (Figure 34). Stuvland (2015) suggested that the Sub-horizontal Sediments are deposited as a result of fluvial incision during the late stages of the Kerpini Fault; or subsequent to it.

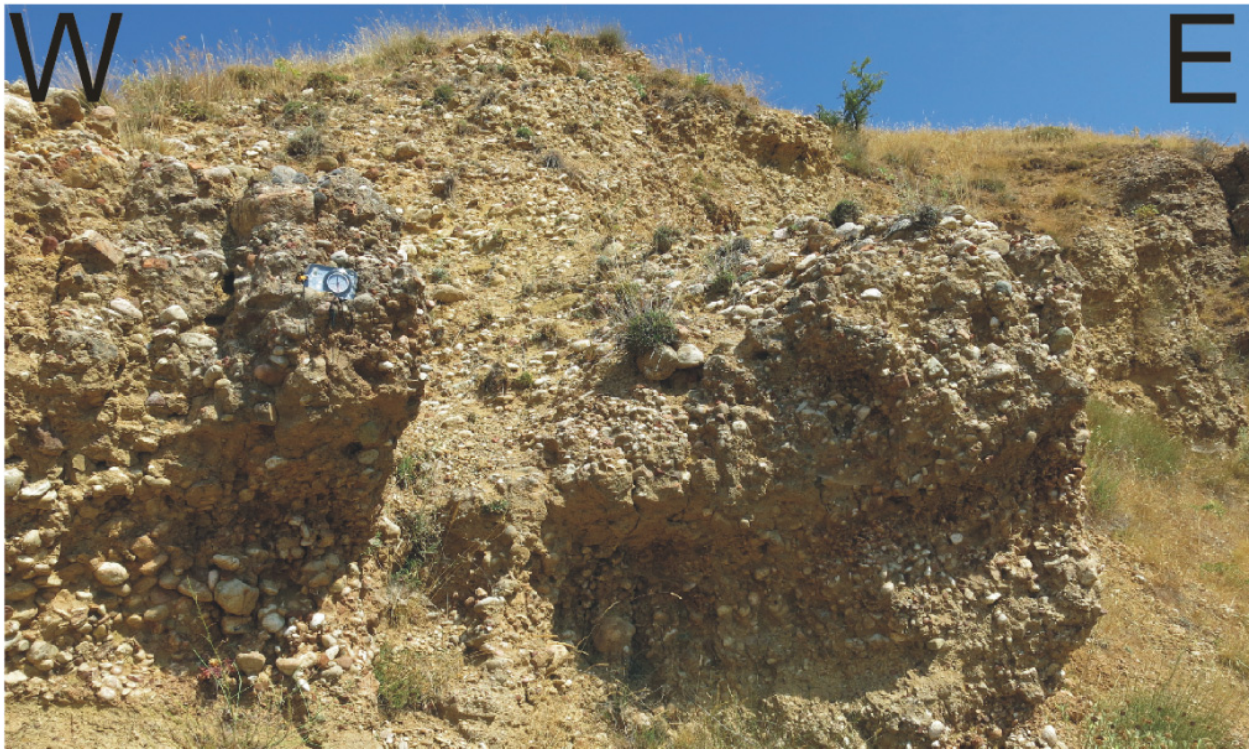

Figure 34: An outcrop of Sub-horizontal Sediments that shows the fluvial character of these clast-supported conglomerates with relatively small clast sizes compared to other conglomerates in the study area. The location of this photo is shown in Figure 12.

5.2.4 Vighia Member

In the eastern part of the area of study, a more than one kilometre thick conglomeratic succession with thick beds (20 - 30 m) can be observed. The coarsest facies of the Vighia Member is found in the south, and comprises cobble to boulder-sized conglomerates. In the north, the clasts sizes have decreased to pebble and cobble sizes (Figure 36). This unit forms an entire mountain named Mt. Aghios Ioanis, commonly referred to as Roghi Mountain. In 2016, there were two theses done on the Vighia Member (Bjåland, 2016; Sigmundstad, 2016). Sigmundstad subdivided the area into eight segments (Figure 35), one of which is of particular interest for this thesis as it includes Fan D – segment V. The Vighia Member is believed to be sourced from a step in the Kerpini Fault to the south, and that it was deposited from south to north prior to tilting (Syahrul, 2014). This is reasonable, considering that the thickest beds (25 - 35 m) with the coarsest clasts are found in the south, and the thinnest beds (10 – 25 m) are found to the north. Segment V is different from the rest, as the clear layering and pronounced bedding typical for Roghi Mountain are not present here. It has a distinct conical shape in the topography, and is interpreted as a late syn-rift fan that is unrelated to the other segments (Dahman, 2015).

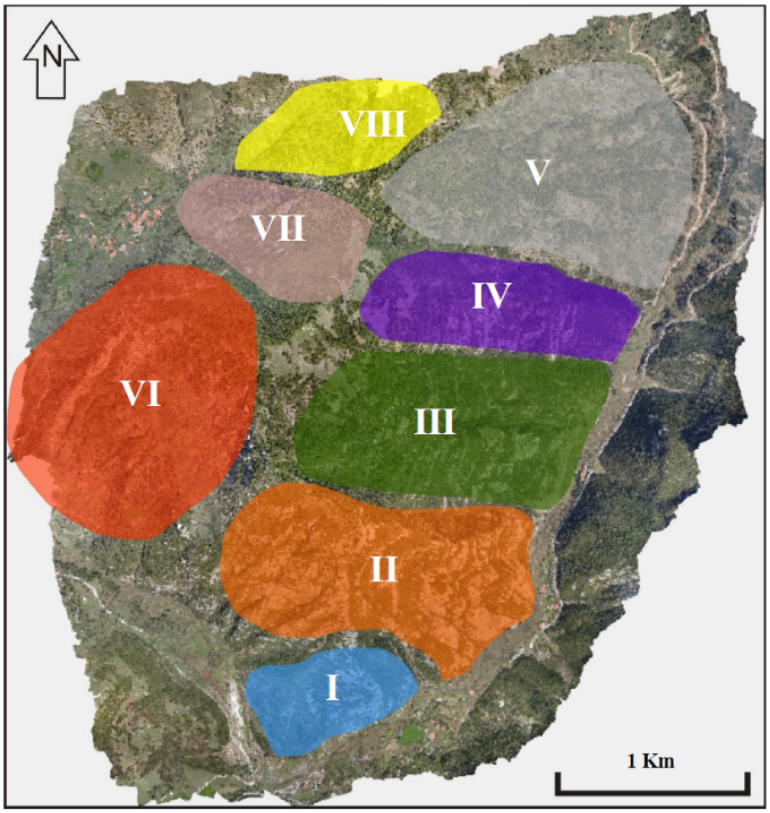

Figure 35: Segmentation of Roghi Mountain in a map view of LIDAR data (Sigmundstad, 2016).

Figure 36: Shows the small clast sizes and good sorting of the northernmost part of the Vighia Member. Compass for scale. The location of this photo is shown in Figure 71.

5.2.5 Kalavryta Member

The Kalavryta Member is found in the immediate footwall of the Kerpini Fault, as it originally deposited in the Kalavryta Fault Block. A 50 - 60 m thick package of conglomerates is located directly south of the Kerpini Fault, which cuts the unit. Therefore, it is present in the Kerpini Fault Block as well. It is hard to determine how far north this unit extends, as the outcrops are quite scarce and eroded. To get familiarised with this unit, the outcrops south of the Kerpini Fault were studied (Figure 37). The clasts appear white, sub-angular and small to medium cobble sized. As the unit is deposited from south to north, the coarsest facies are found southwards into the Kalavryta Fault Block, but this area was not studied during this thesis. The bed boundaries are not clear, and the conglomerates are moderately sorted.

In the northern study area, close to the unconformity, several small patches of conglomerates are found (Figure 38). These have the same sorting, colour and roundness as the conglomerates of the Kalavryta Member; but the clast sizes are smaller. One theory from Hadland (in prep) is that the Kalavryta Member and the Lower Conglomerates are in fact the same lithology, due to the development of the Kalavryta Member. This theory will be discussed in Sub-chapter 5.7.

Figure 37: Conglomerates of the Kalavryta Member on the footwall of the Kerpini Fault Block in the south. Compass for scale. The location of this photo is shown in Figure 12.

Figure 38: Close to the basement unconformity near the Profitis Ilias Mountain, the conglomerates of the Kalavryta Member that are believed to have been transported furthest north in the Kerpini Fault Block are found. Compass for scale. The location of this photo is shown in Figure 45.

5.2.6 East Vouraikos Sediments

The East Vouraikos Sediments split into two main lithologies: fluvial and alluvial sediments. The fluvial sediments dominate more than half of the valley side, but alluvial deposits are found on the very top of the mountain ridge. For better view of Fan D and to compare these sediments to the alluvial fans of the study area, a day on the first field trip was spent east of the Vouraikos Valley. The fluvial sediments found here are unlike anything found to in the western valley side. The channels and beds are several tens of metres thick, well sorted and considerably finer, with pebble sized clasts on average. All sediments found east of the Vouraikos Valley are referred to as East Vouraikos Sediments, and are outside the scope of this thesis.

5.2.7 Skepasto Member

Red coloured shales, believed to be lacustrine derived, constitute this stratigraphic unit. They are outcropped in the Kerpini Fault Block and the Kalavryta Fault Block. Rognmo (2015) studied them thoroughly in the attempt to explain their presence in the two fault blocks, but a definite conclusion was not reached. The shales are unconsolidated and highly weathered, and could be later soil deposits. In the Kalavryta Fault Block they are in-situ, but whether or not this is the case in the study area, is debatable.

5.2.8 Profitis Conglomerates

At the very eastern limit of the Profitis Ilias, a large and previously neglected conglomeratic outcrop is situated. The outcrop is approximately 60 metres thick, stretches E-W for nearly 500 metres, and 100 metres N-S. The beds have a Dip / DD of 12 - 24° / 75 - 100°E. The clasts are on average cobble sized (8 - 12 cm), with occasional boulders. The 30 – 100 cm thick, coarse conglomeratic beds are interbedded with frequent 1 - 5 cm thick beds of coarse sandstone. The chert clasts are angular, and the limestone clasts are generally well rounded. The outcrop has been exposed to significant erosion. The topmost beds are cobble sized (Figure 39), and the coarsest boulder-sized facies are found at the base (Figure 40). These conglomerates are distinguishable from most conglomerates in the study area, but they bear a striking similarity to the proximal facies of Fan C. The beds generally have the same structural orientation as the Fan C beds (Figure 41). The relationship between this unit and Fan C will be discussed in Sub-chapter 6.7.

Figure 39: Profitis Conglomerates at their highest elevation, featuring cobble sized conglomerates. The location of this photo is shown in Figure 71.

Figure 40: Photo from the base of the Profitis Conglomerates outcrop, with boulder-sized clasts and thicker less well defined bedding than at the top of the outcrop. The location of this photo is shown in Figure 71.

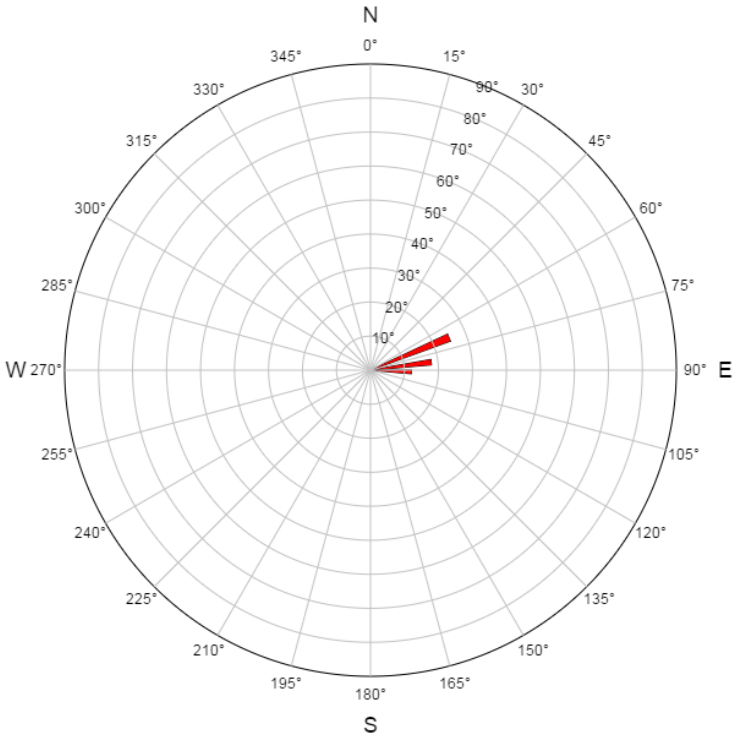

Figure 41: Rose diagram constructed based on all the collected dip data for the Profitis Conglomerates.

5.2.9 Late Fan

The Late Fan is the latest addition to the stratigraphic column. It has deposited on the western incised valley side of the current Vouraikos River Valley. The Late Fan is comprised of unconsolidated and loose sediments, and the morphological features are much better preserved compared to fans A-D. It has a clear conical shape in a map view. The fan has eroded parts of Fan D, and the relationship between these two units will be discussed in Sub-chapter 6.3. The best view of this area is achieved from across the Vouraikos Valley. Standing on the other side of the valley, it is possible to get a view straight down the strike of the unconformity plane, and the Late Fan that has deposited on top of it (Figure 42).

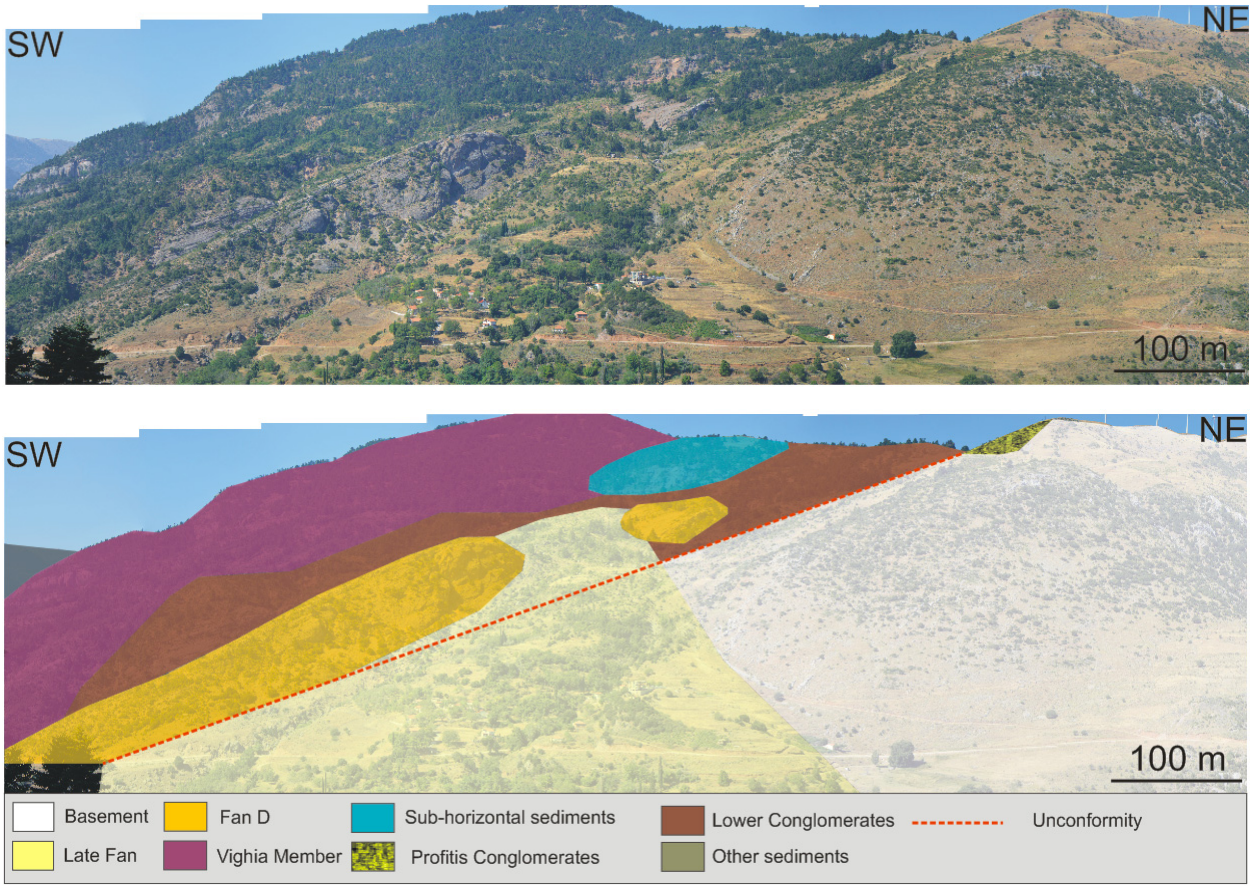

Figure 42: Top: Uninterpreted photo taken from east across the Vouraikos River Valley, showing the best possible angle to view the plane of the unconformity. It intersects the topography, dipping away from the point of observation. Bottom: Interpreted photo with all the stratigraphic units and unconformity included. The location of this photo is shown in Figure 12

5.3 Fan A

Fan A lies directly east of the Kerpini Village (Figure 43), and stretches from the Profitis Ilias mountain ridge to the north and southwards for more than half the N-S length of the study area. It is a significant stratigraphic unit covering an area of approximately 2600 x 500 m (1.3 km^2). Since there are no reference contacts in the east and west, the minimum thickness of the fan is estimated to be 150 m, based on its elevation from base to top. Most of the beds have a Dip / DD of 20° / 190°S, and as expected from such an extensive conglomeratic unit – the unit has been subjected to significant erosion through time. Even though loose clasts, soil, vegetation and poorly defined beds make up a large portion of the fan, it is well exposed from the apex and roughly down to Fault C. Thick beds (0.5 - 3.0 m) with coarse clasts are found in the north, whereas thin beds (5 - 50 cm) with fine clasts are more prominent towards the south. The clast composition of Fan A is comprised of 80 % limestone clasts, 18 % red and grey chert, and 2 % green chert/limestone clasts. Several lobes have been observed immediately east of the fan, and these will be described towards the end of Sub-chapter 5.3.

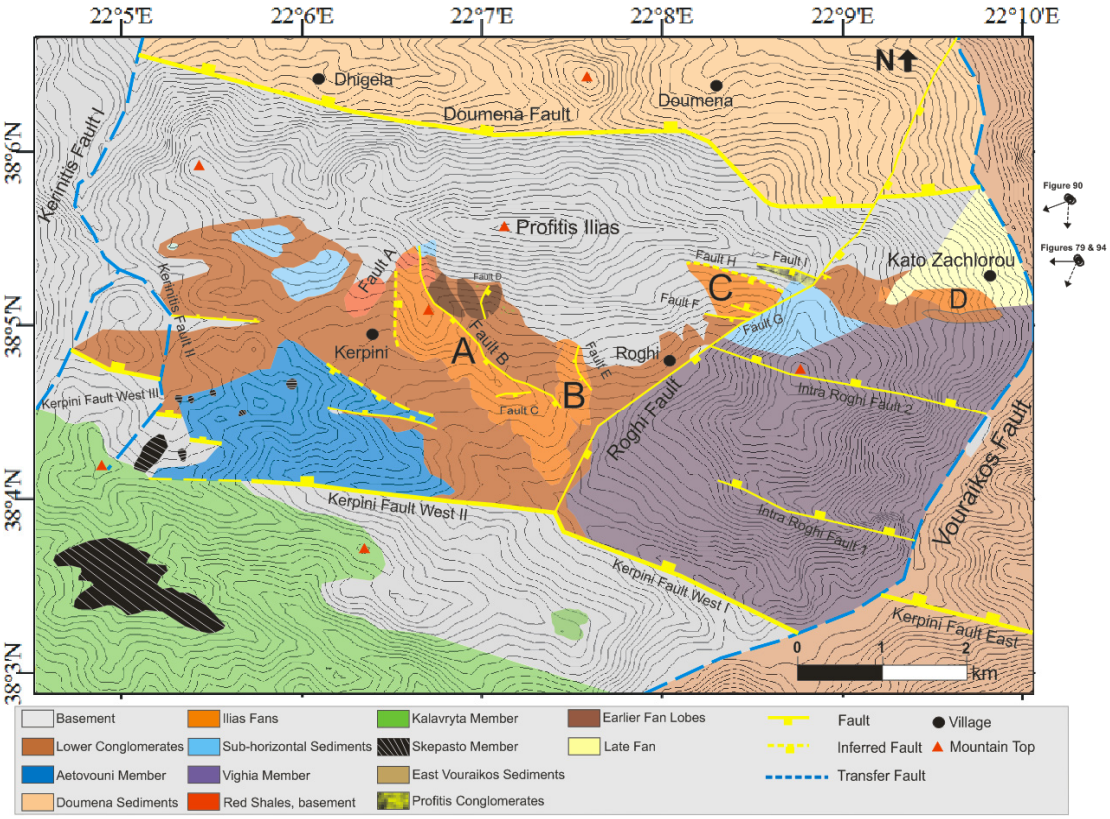

Figure 43: Geological map of the Kerpini Fault Block with the four fans highlighted (A, B, C, D). Shows the locations of the photos taken from the east of the Vouraikos River Valley.

5.3.1 Structural description

Fan A is bounded by an east dipping fault in the west (Fault A) and a west dipping fault to the east (Fault B), that forms a graben between them. This setting has created accommodation space for this large alluvial fan to deposit. The fan sediments are generally dipping towards S-SE. This is likely due to Fault B having a larger displacement, thus rotating the conglomerates more to the east. A minor internal fault was identified as well (Fault C). The dip data is shown in a rose diagram (Figure 44).

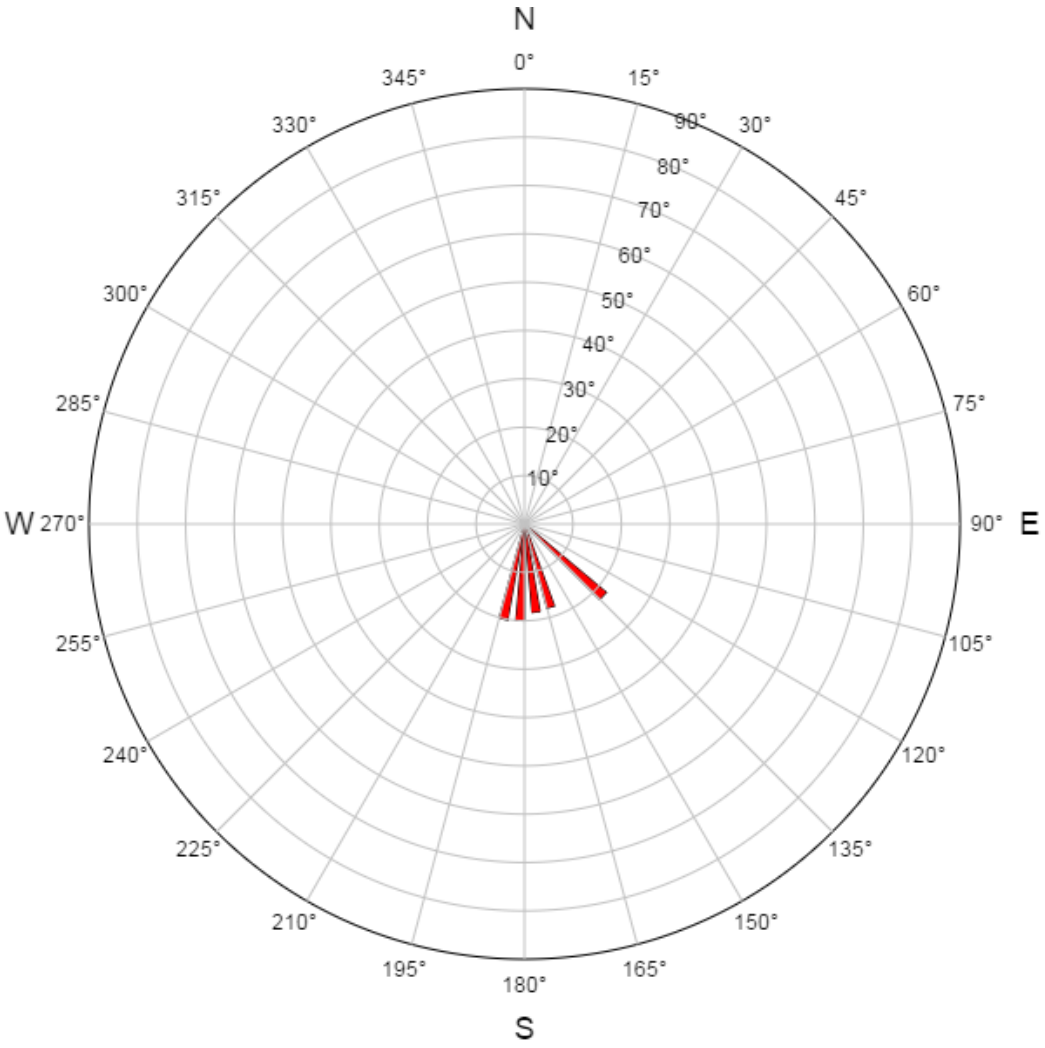

Figure 44: Rose diagram based on all the dip data collected for Fan A. There are some outcrops near the mid-fan area that dip slightly more to the east (≈ 135°); otherwise, the rest of the fan dips exclusively to the south (180 - 190°).

A detailed overview map was constructed for Fan A and its surrounding areas (Figure 45). In this map, the locations where the lithological logs were constructed are displayed. Each section will be presented in the following chapter.

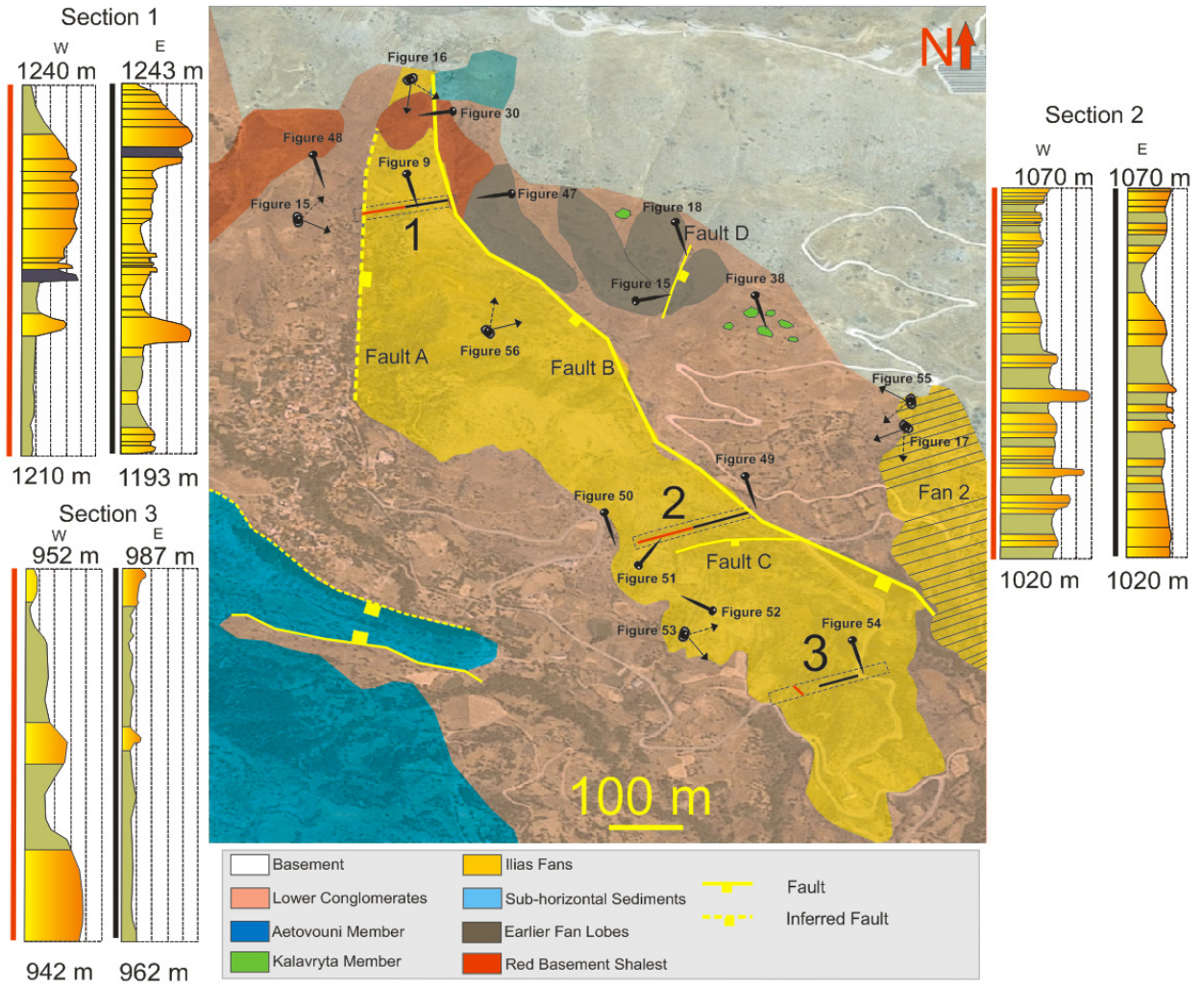

Figure 45: Shows a detailed geological map of Fan A and its associated lithological sections. Red (west) and black (east) lines within the dashed boxes on the map represent red and black labelled logs. Y-axis represents log interval in metres, and X-axis represents clast sizes (increasing towards the right). Notice the down-fan reduction of bed thickness and clast size from sections 1 to 3. Also note that the log intervals vary, based on exposed fan thickness. For a more detailed description of the logs, see Figure 46. The locations of all the figures related to Fan A are shown in this figure.

5.3.2 Sedimentary description

The lithological sections (Figure 46) were constructed in locations highlighting the facies differences from north to south. The sections best represent the clast size variabilities, while the bed thicknesses are not honoured properly. Only the well-defined bed boundaries are displayed in the logs, whereas there are many beds with ambiguous boundaries. The thickness intervals in the sub-sections below better represent the reality. The first section is based on the largest and complete outcrop close to the apex of the fan.

Section 1 – East

The first lithological section was made near the apex (Figure 47 and Figure 48).

- Clast-supported thick beds (0.4 - 3.0 m), with a Dip / DD of ≈ 20 - 22° / 190°S.
- Beds are thick, poorly defined and chaotic, both here and in the western log.
- Cobble-sized clasts, with a few instances of boulder-sized clasts. The sorting is moderate.
- Clasts are sub-rounded, exhibiting a high degree of reworking.
- It is not clear whether the beds have any grading, as the bed boundaries are obscure.
- From the bottom of the section to the top, the clast sizes increase slightly (in average 1 - 2 cm larger), while the bed thicknesses are quite constant.

Section 1 – West

- Beds are clast supported, but slightly thinner compared to their eastern counterparts (0.2 – 3.5 m). As seen in the lithological log, the dark coloured bed in Figure 46 is traceable from east to west.
- Cobble-sized clasts, with fewer occurrences of boulders than in the eastern section. The sorting is moderate.
- The clasts are sub-rounded.
- Grading is unclear, and the bed boundaries are diffuse.
- The bottom of the section is covered in soil, vegetation and loose sediments, and the log interval is not long enough to deduce any conclusive changes from bottom to top.

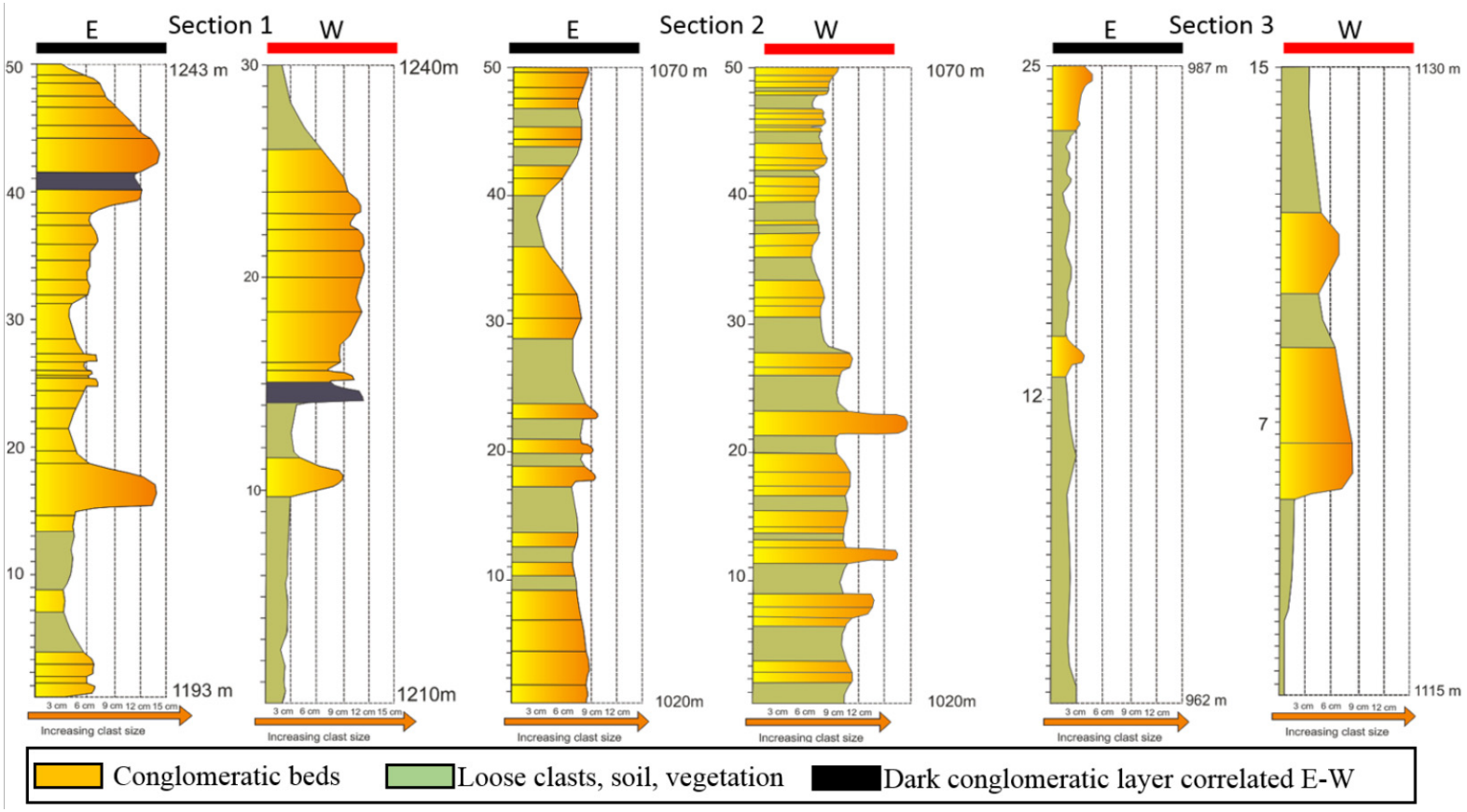

Figure 46: All the lithological logs for Fan A. Bed thicknesses and average clast sizes are emphasized, whereas contact types between beds are not, as most beds have been heavily eroded. All layers have a Dip / DD of ≈ 19 – 22° / 190°S. The conglomerates are polymictic and matrix supported. The beds are generally thinning from east to west, whereas the clast sizes and the two black layers are laterally correlatable. Vertically, the facies do not change much, but from north to south, the changes are clearly visible: finer sediments, thinning of beds and more vegetation.

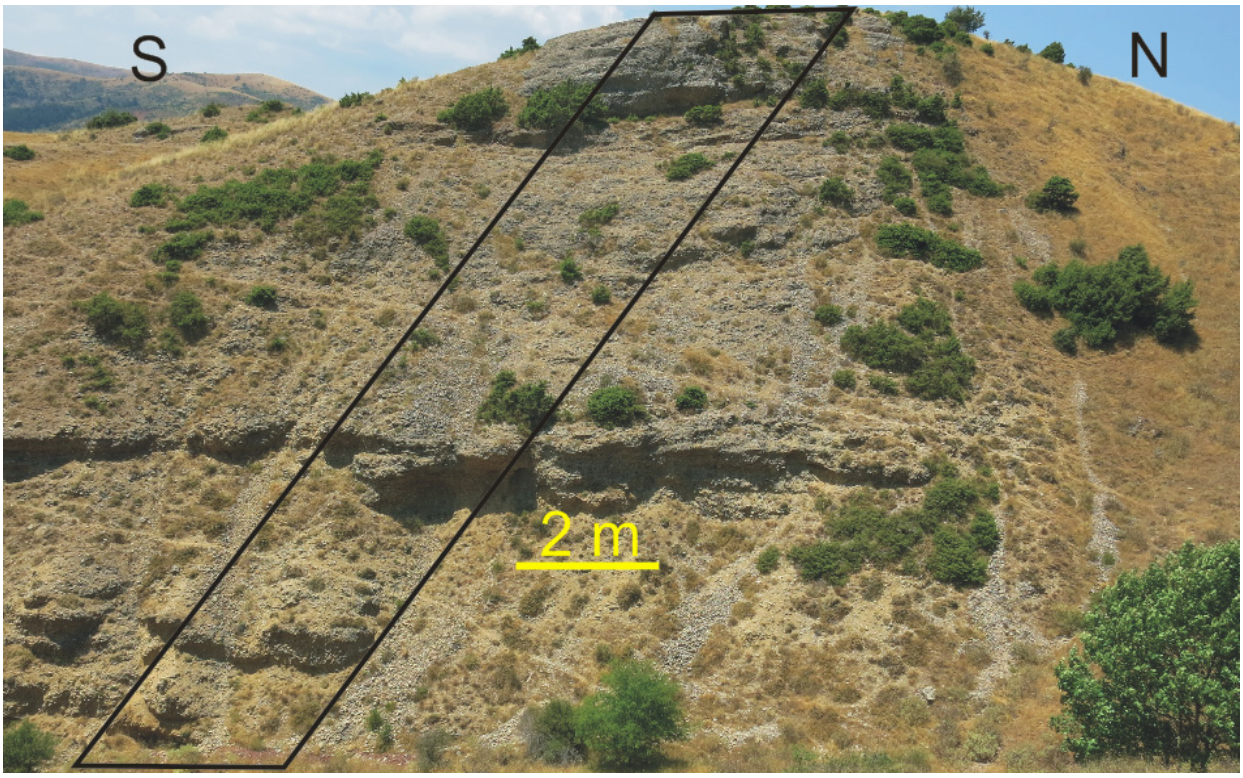

Figure 47: Field photo of Section 1 – East. It is the most complete package of exposed conglomerates in proximity to the apex of Fan A, which is why it was chosen. The location of this photo is shown in Figure 45.

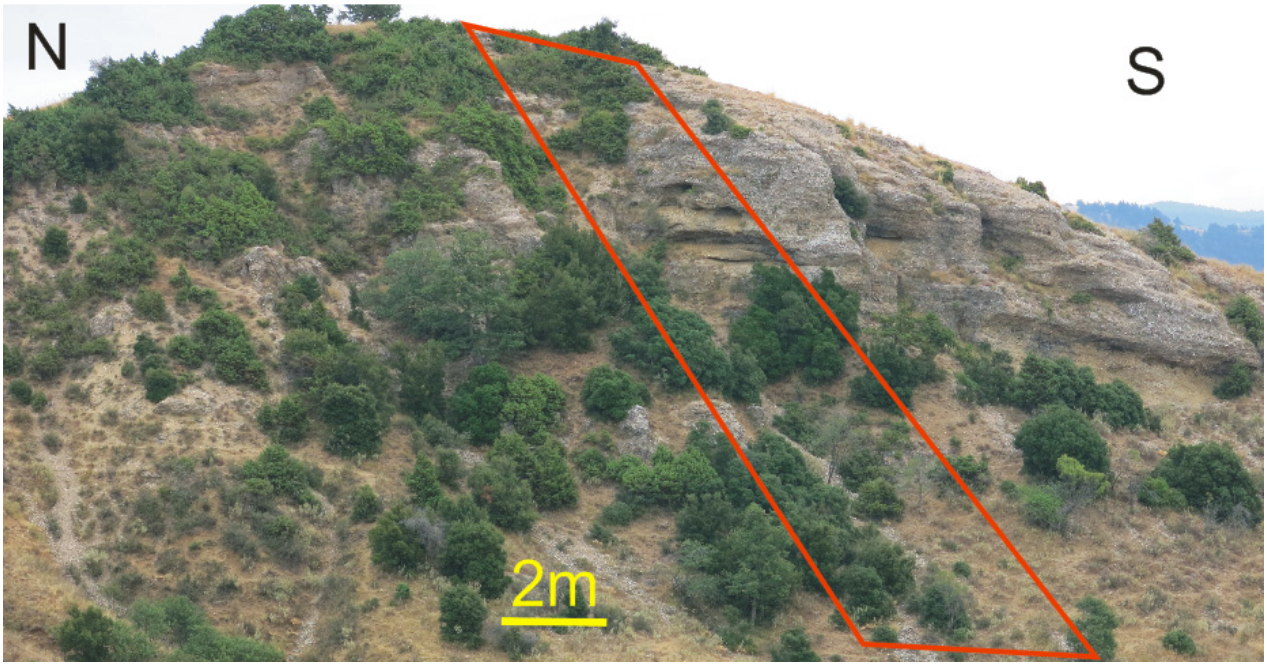

Figure 48: Shows Section 1 - West. There are greater amounts of vegetation and soil on this side of the fan, hence the relationship between Fan A and the sediments to the west are unclear. The location of this photo is shown in Figure 45.

The second pair of logs is made near the middle of Fan A, in an interval with numerous well-defined beds (Figure 49 and Figure 50). Finer conglomeratic beds with sand intervals occur in this area than in Section 1. The western part of this section has better exposed beds with clearer bed boundaries, and appears to be less eroded than its eastern equivalent.

Section 2 – East

- The beds here are matrix-supported, except for a few coarse and clast-supported beds. The beds are 10 - 50 cm thick, and has a Dip / DD of ≈ 17 - 18° / 190°S.
- Bed boundaries are generally unambiguous and beds are less chaotic.
- The clasts are pebble to cobble-sized and well sorted.
- Clasts are generally rounded.
- The beds show no obvious grading.
- The beds are thinning from base to top, whereas the clast sizes are consistent.

Section 2 – West

- Thinner bed thicknesses than in Section 2 – East. They are in the range of 5 - 40 cm. The beds are matrix supported and have a Dip / DD of ≈ 17 - 18° / 190°S.
- Clasts are pebble to cobble-sized, except for a few boulder-sized clasts in the coarsest beds.
- The clasts are rounded and well sorted, except for the coarsest and thickest beds that contain sub-rounded clasts and moderate to good sorting.
- Graded beds are not observed.
- The clast sizes decrease from base to top.

Figure 49: Composite photo of Section 2 – East from bottom to top. Notice the degree of erosion compared to Section 1, and the lack of thick and pronounced conglomeratic beds anywhere but at the base. The location of this photo is shown in Figure 45.

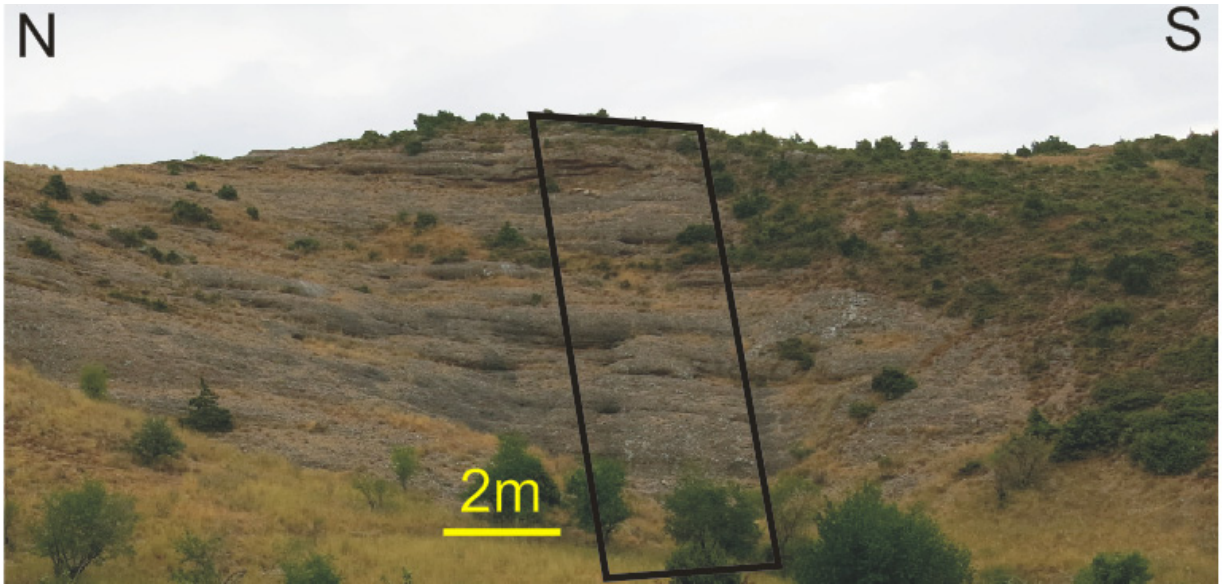

Figure 50: Field photo showing Section 2 - West. Notice that the bed boundaries are clearer in the west compared to east, with good exposure and less soil and gravel intervals. The location of this photo is shown in Figure 45.

Several beds are observed with imbrication in a southern direction in Section 2 (Figure 51), which is a good paleoflow indicator. Near Section 2 – West, beds can be observed thinning from north to south (Figure 52).

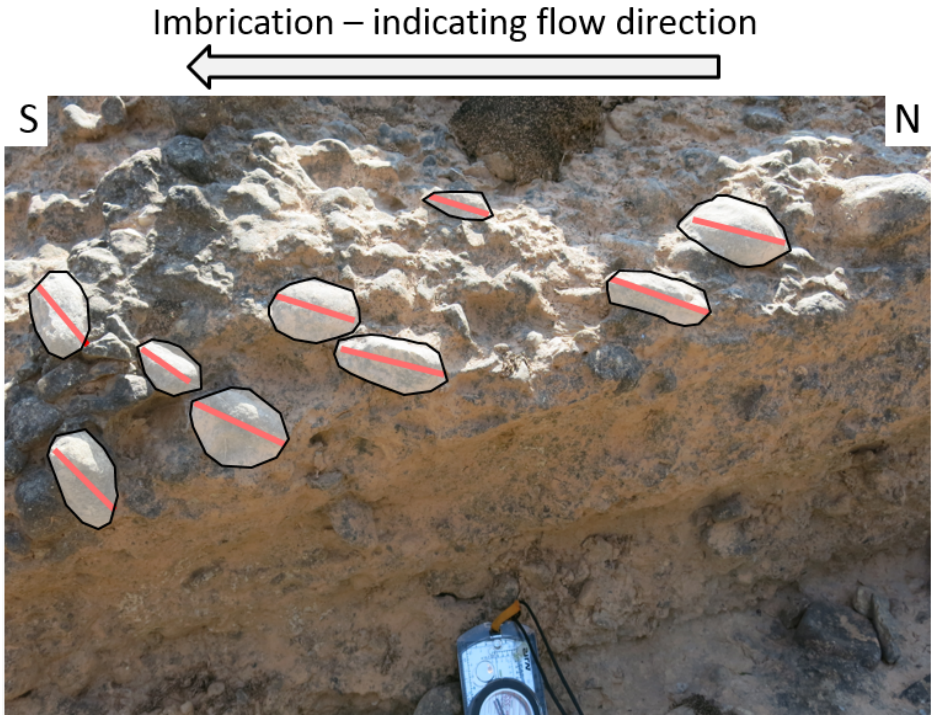

Figure 51: Imbrication to the south observed near Section 2 of Fan A. The location of this photo is shown in Figure 45.

Figure 52: Thinning of beds from north to south near the mid-fan area. The location of this photo is shown in Figure 45.

A third and final pair of logs were constructed further south (Figure 53 and Figure 54). The log intervals are smaller here, as the fan is much thinner this far south. There is only ≈ 30 m from the base to the top of the fan in this location. The vegetation and unconsolidated sediments dominate, with only a few conglomeratic beds exposed. Vegetation is much more likely to settle in finer sediments and less consolidated deposits, as such the southern ≈ 30 % of the fan is covered by a lusher flora than what is found northwards. The vegetation has changed from grass and occasional juniper bushes to larger trees and lusher bushes and plants. Bed thicknesses and clast sizes have decreased significantly.

Section 3 – East

- Matrix-dominated deposits dominate Section 3. The two conglomeratic packages in this section consist of 10 – 80 cm thick beds, with a Dip / DD of ≈ 18° / 180°S.
- These conglomerates are very well sorted and generally composed of pebble-sized clasts.
- The clasts are well rounded and show a high degree of reworking.
- No grading is observed.
- There are no clear trends or differences from bottom to top of section.

The western log was constructed differently from the other logs. In this area, there are only two exposed conglomeratic beds, and the log was made so these deposits would be recorded, in a smaller interval of 15 m. Such a small interval is not a sufficient section to represent any conclusive lithological changes. These are however the coarsest conglomerates in the area, and this interval is used to represent the maximum clast size in the southern area of Fan A. Thus, this log represents variabilities in a N-S direction for the fan as a whole.

Section 3 – West

- These 20 – 80 cm thick conglomeratic beds are matrix supported, with a Dip / DD of ≈ 18° / 180°S.
- Beds are moderately to well sorted, and are composed mainly of small cobble-sized clasts and pebbles.
- The clasts exhibit good sorting, but are not as well sorted as the conglomerates in the eastern section.
- No grading is observed within the individual beds.
- The beds at the base of the section are coarser than the beds at the top, suggesting a general fining upwards trend in this log interval.

Figure 53: Shows Section 3 – West, in the southern parts of Fan A, and how a lithological log similar to Section 1 and 2 were impractical to construct due to the sheer amounts of vegetation and lack of outcrops. Within the red box, the only 15 m interval of clear and exposed conglomerates this far south is exposed, and as such this interval was logged. The location of this photo is shown in Figure 45.

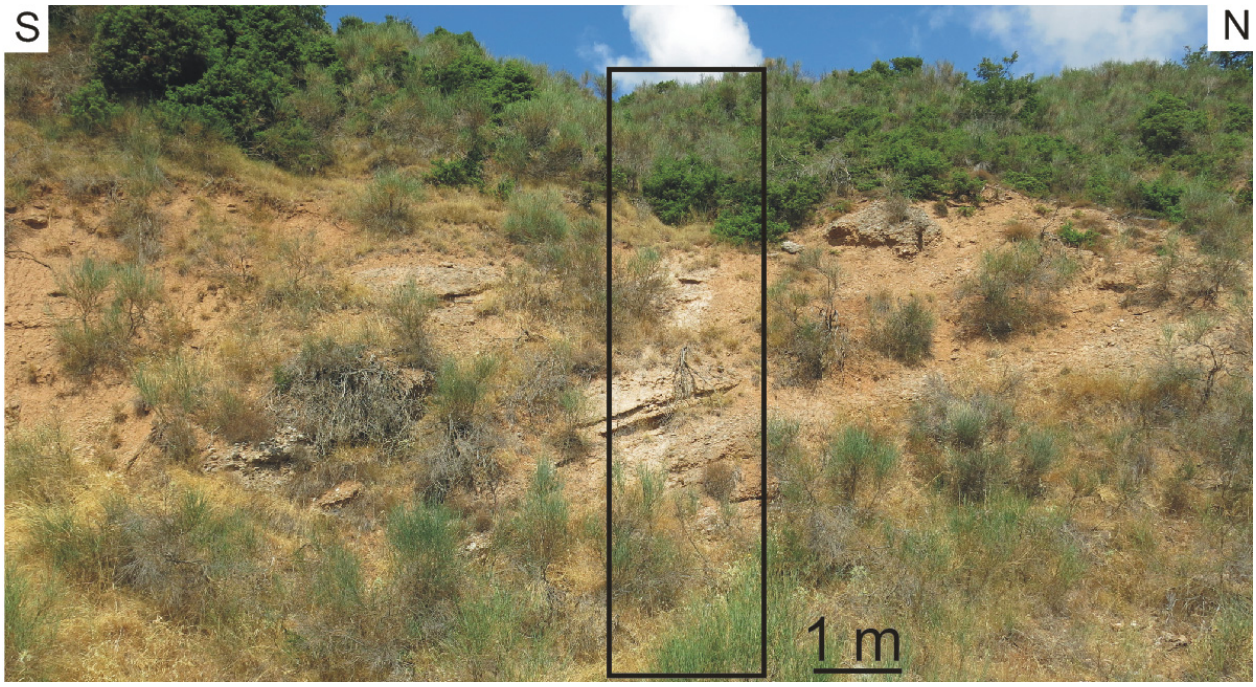

Figure 54: Shows Section 3 - East, and how the southern parts are not ideal for lithological logs. Streamflow deposits dominate this section. The location of this photo is shown in Figure 45.

5.3.3.1 Bedding geometries

The beds of Fan A appear to be building out from north to south (Figure 55). The beds are terminating downwards, and this gives the fan a progradational nature that is notable in the area between Section 1 and 3.

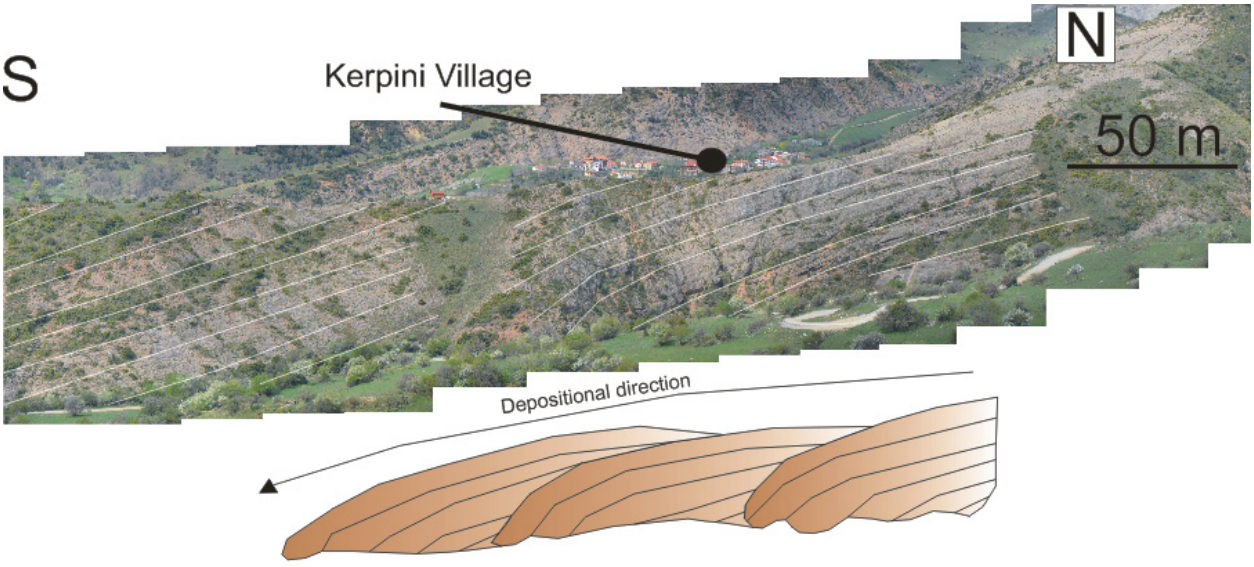

Figure 55: Panorama photo taken from Fan B, viewing the mid-fan area of Fan A, it shows the bedding geometries. Below, a simplified sketch of how the fan has built out through time. The location of this photo is shown in Figure 45.

5.3.3.2 Earlier Lobes

Four individual lobes are identified immediately east of Fan A (Figure 56). They cover an area of 600 m from west to east, and 350 m from north to south. The basement contact is traced 50 - 100 m north of the lobes, and the basement is outcropped where Fault D is located, thus the underlying unconformity has to be shallow. The maximum thickness of the lobe closest to Fan A is estimated to ≈ 100 m from base to top, and the thickness is decreasing eastwards. The beds are poorly defined and chaotic, poorly sorted, consist of large cobble and boulder-sized clasts, (20 - 30 cm) and have a Dip / DD of ≈ 20° / 200°S. The lobes terminate towards Fan A and Fault B.

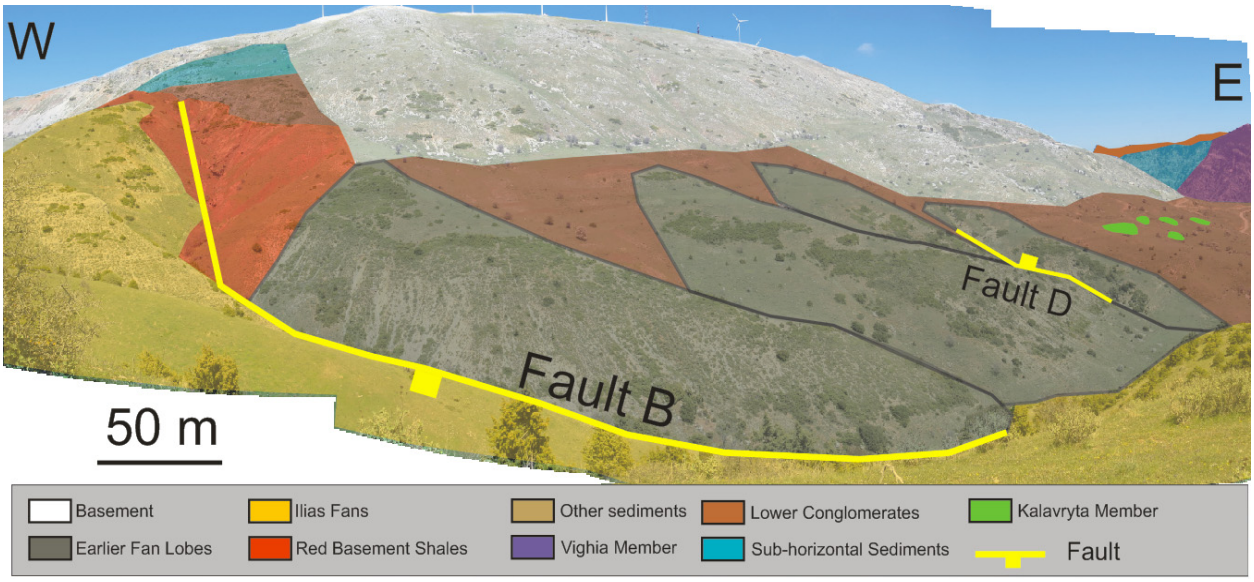

Figure 56: Individual lobes located immediately east of Fan A, believed to be earlier events. Scale is relevant to the base of the nearest lobe. The location of this photo is shown in Figure 45.

5.3.3 Fan A summary

From north to south, there is a clear trend concerning bed thickness, clast sizes, type of deposits, sorting and rounding. The beds are thinning from the apex in the north towards the south, clast sizes are decreasing significantly, and in the southernmost areas; unconsolidated sediments and sandy beds dominate. The beds show a higher degree of maturity, better sorting and clasts are more reworked in a southern direction. All of these observations support a general depositional direction from north to south.

E-W trends are not as apparent due to the narrow nature of the fan. However, observations suggest that there is an increase in maturity from east to west, but not nearly as conclusive as for the N-S trends.

5.3.4 Facies interpretation

Near the apex, the facies are characterized by a high textural heterogeneity. The deposits are clearly dominated by mass movements rather than channelized flows. These thick, poorly defined and coarse beds were interpreted as debris-flow deposits. Approximately 500 m south of the apex, the beds are thinner and more well-defined, with occasional sand lenses. Conglomeratic textures are more homogenous, and the deposits are clearly derived from episodic events. These deposits are classified as sheetflood deposits, and make up a large part of Fan A. Further south, in the most distal area, the fan consists of coarse sand facies and unconsolidated sediments covered by lush vegetation. The depositional energy has decreased significantly, and these deposits are the result of finer sediments transported as a suspended load. Only a few conglomeratic beds are outcropped, consisting of pebble sizes and thin beds, and these southernmost distal facies are interpreted as streamflow deposits. Based on all these interpretations, a facies distribution map was constructed for Fan A. The interpreted depositional direction is shown as well as the faults and locations of lithological sections (Figure 57).

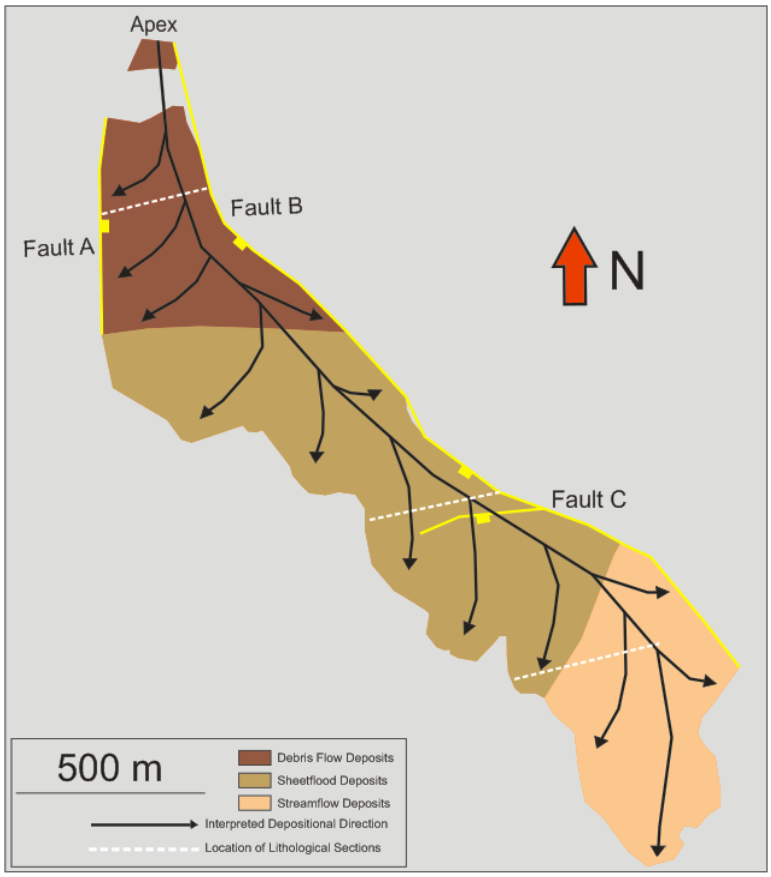

Figure 57: Facies distribution map for Fan A, showing the facies, depositional directions and faults.

5.4 Fan B

Fan B is one of the two smallest fans together with Fan D, and lies in close proximity to Fan A. The relationship between the two fans is difficult to determine due to high amounts of overlying vegetation in addition to a small river covering the contact (Figure 58). It consists of one minor lobe of no particular importance, and one main lobe (Figure 60). Fan B exhibits a similar Dip / DD as Fan A. The fan extends 750 m from north to south and 250 m from east to west, and initiates close to the unconformity contact in the north. It is approximately 30 m thick, based on the exposed contact at the base of the fan (Figure 61). Soily intervals are prominent, and clear bedding is scarce. However, Fan B has good exposure along the western boundary, which is mainly where the sediments were described. The average clast size is ≈ 12 - 13 cm (smaller than indicated in previous studies). Lithological logs were constructed vertically, but the lateral variabilities were difficult to capture as only the western side of the fan is properly exposed. Road construction close to the apex have destroyed some of the most proximal outcrops, resulting in an uncertain location of the apex as well. The clast composition of Fan B is almost identical to that of Fan A. It is dominated by 80 % limestone clasts, 18 % red/grey chert, and 2 % green chert/limestone clasts.

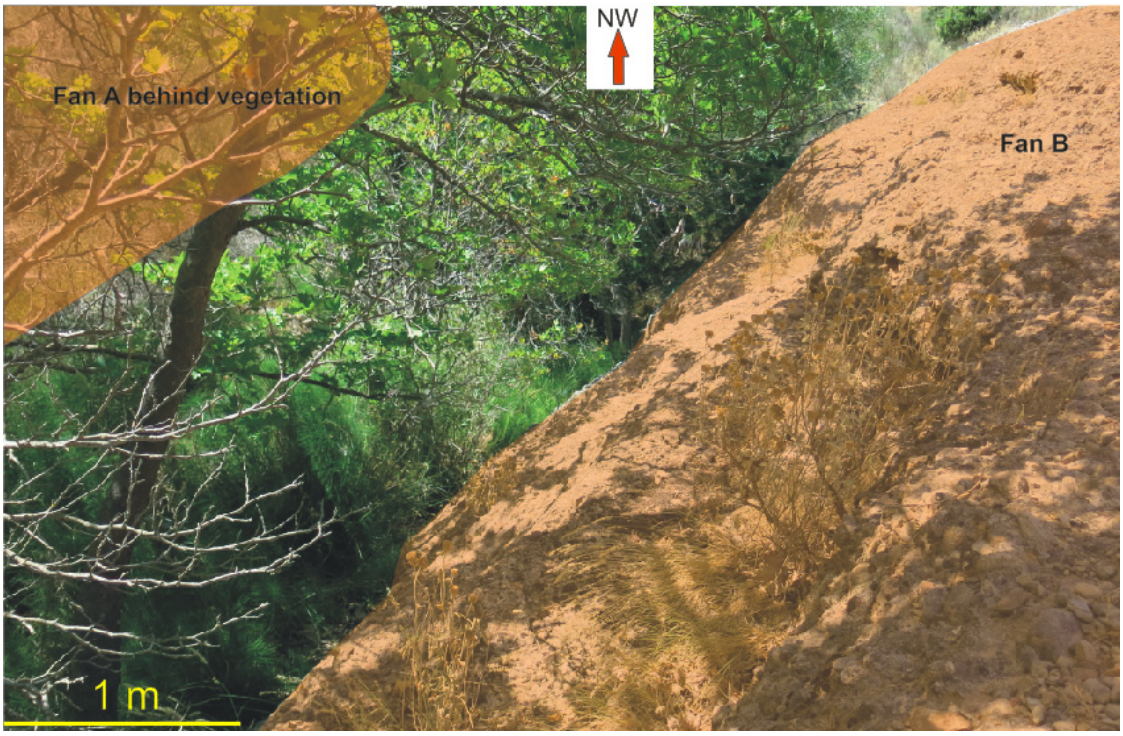

Figure 58: Photo from the southwestern base of Fan B that shows the location of the hidden relationship between Fan A and Fan B. The contact is partly eroded and completely covered by vegetation and a small river. The location of this photo is shown in Figure 45.

5.4.1 Structural description

The beds of Fan B have a general Dip / DD of 20 - 22° / 200°SSW. There is no bounding fault identified to the west, but the west-dipping Fault E intersects the fan. The dips are displayed in a rose diagram (Figure 59)

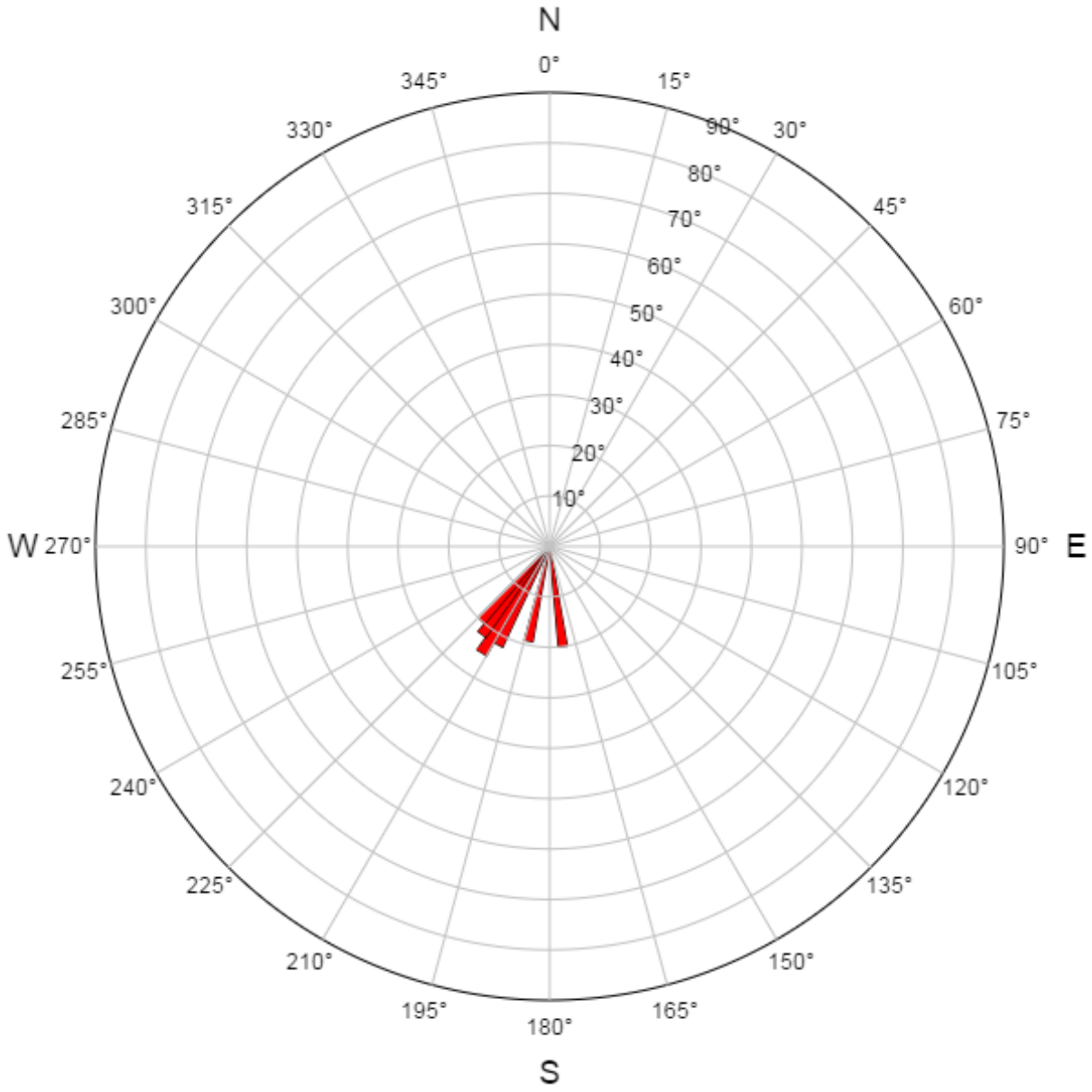

Figure 59: Rose diagram for fan B. This fan tends to dip slightly more to the west than Fan A.

A detailed overview map of Fan B was constructed (Figure 60), showing the location of the lithological sections (Figure 63), the extent of the fan, and how the unconformity is traced.

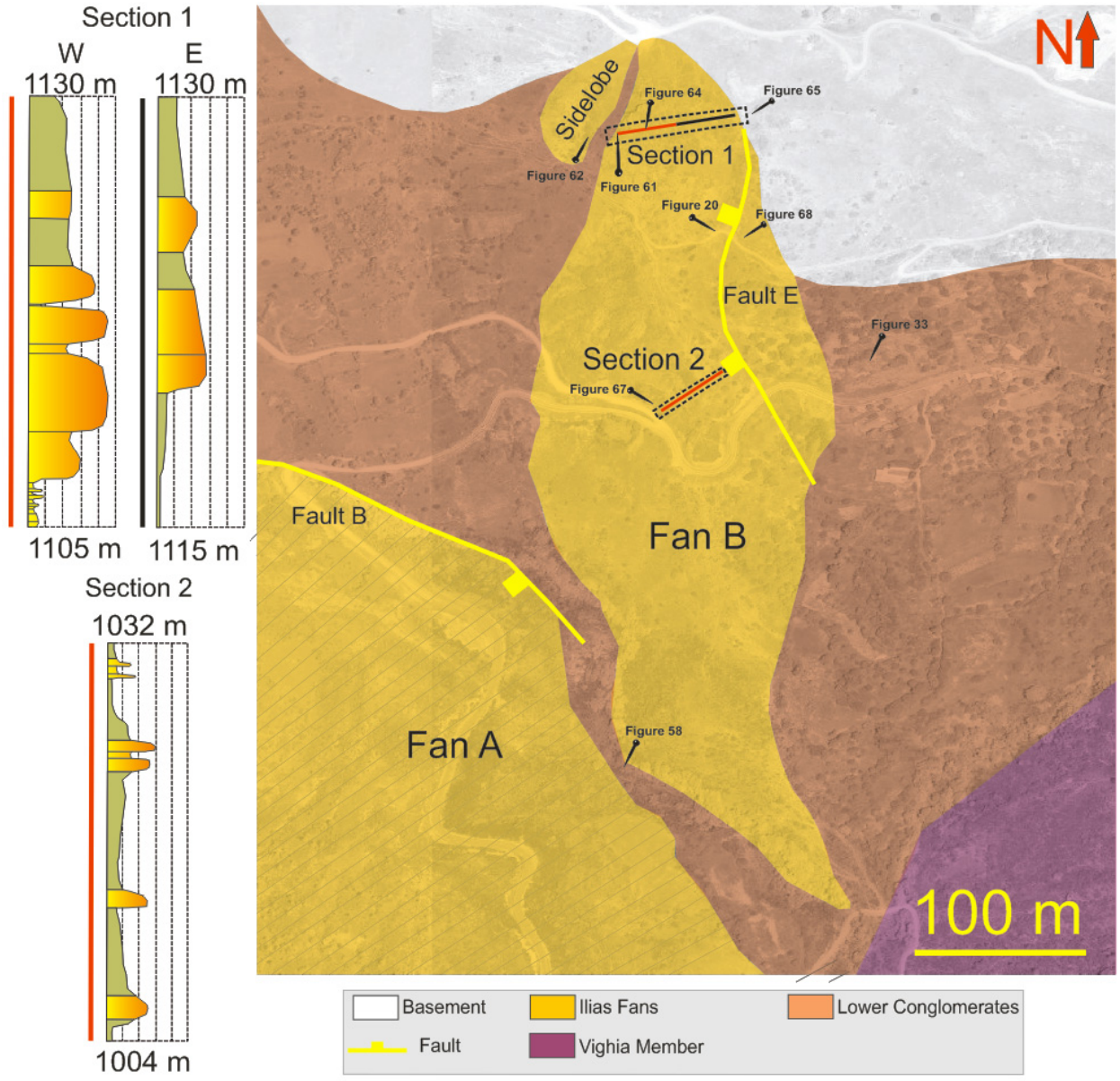

Figure 60: Shows a detailed geological map of Fan B and its associated lithological sections. Red and black lines within the dashed boxes on the map represent red and black coded logs. Notice the down-fan reduction of bed thickness and grain size. For a more detailed description of the logs, see Figure 63. The locations of all the figures in this area are shown as well.

5.4.2 Sedimentary description

Section 1 - West is located close to the northern boundary of the fan (Figure 62). At the base, there are thin layers with fine and coarse sand followed by a sharp change to thick and coarse beds. Occasional sand lenses (Figure 64) and intervals of finer facies occur throughout this log interval.

Section 1 – West

- Bed boundaries are difficult to establish, but the conglomeratic beds are quite thick in this western section, ranging from 0.5 - 3.0 m, often separated by sandy intervals of coarse sand. They are clearly clast-supported. The beds have a Dip / DD of ≈ 20 - 22° / 200°SSW.
- On average, the clasts are cobble-sized (10 - 12 cm), and of moderate sorting.
- The clasts are generally sub-angular.
- No graded beds are observed in this log interval.
- The log interval is fining from the coarsest conglomeratic layer at the base and to the top, transitioning into pebble to small cobble-sized conglomerates at the top of the section. This gives the log interval a fining upwards trend.

At the base of this log interval, different-natured beds are outcropped (Figure 61). These deposits are underlying the coarse conglomerates of Fan B, and consist of thin beds (1 - 5 cm) of fine deposits (fine to coarse sand), that dip 20° to the south. This contact will be further discussed in Sub-chapter 6.1.

Figure 61: Shows the relationship between fine sediments at the bottom of Fan B and with the first conglomeratic bed of Fan B. Notice the parallel dips of 20°. Compass for scale (10 x 6 cm). The location of this photo is shown in Figure 60.

The eastern side of Fan B is poorly exposed. Due to the structural orientation of the fan, this log interval is ten metres smaller than the western log. As such, lateral comparisons are inconclusive. Loose clasts, eroded beds, soil and vegetation dominate this log interval (Figure 65)

Section 1 – East

- Beds are clast-supported, but bed thicknesses and Dip / DD are hard to determine due to poor exposure, and are assumed to be similar to Section 1 - West. Bed thicknesses are estimated to be ≈ 0.3 - 2.0 m.
- Clast sizes generally range from ≈ 8 - 9 cm, smaller than in the western log interval, and they appear to be of moderate to well sorting.
- The clasts are sub-rounded.
- No graded beds are observed.
- The coarsest beds are located at the base of the log interval, and the finest at the top. However, there are no good outcrops to draw any conclusions regarding trends.

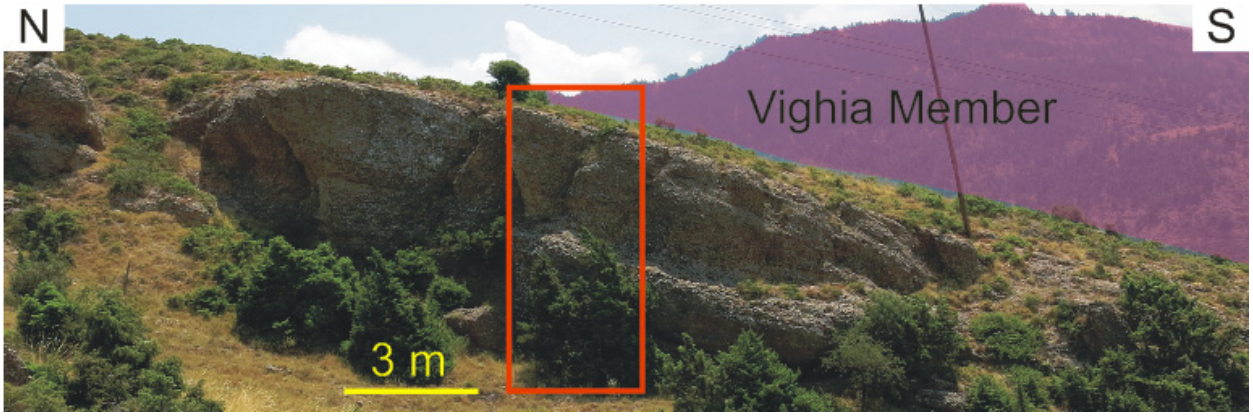

Figure 62: Shows Section 1 – West. At the base of the red box, the outcrop of Figure 61 is located. The location of this photo is shown in Figure 60.

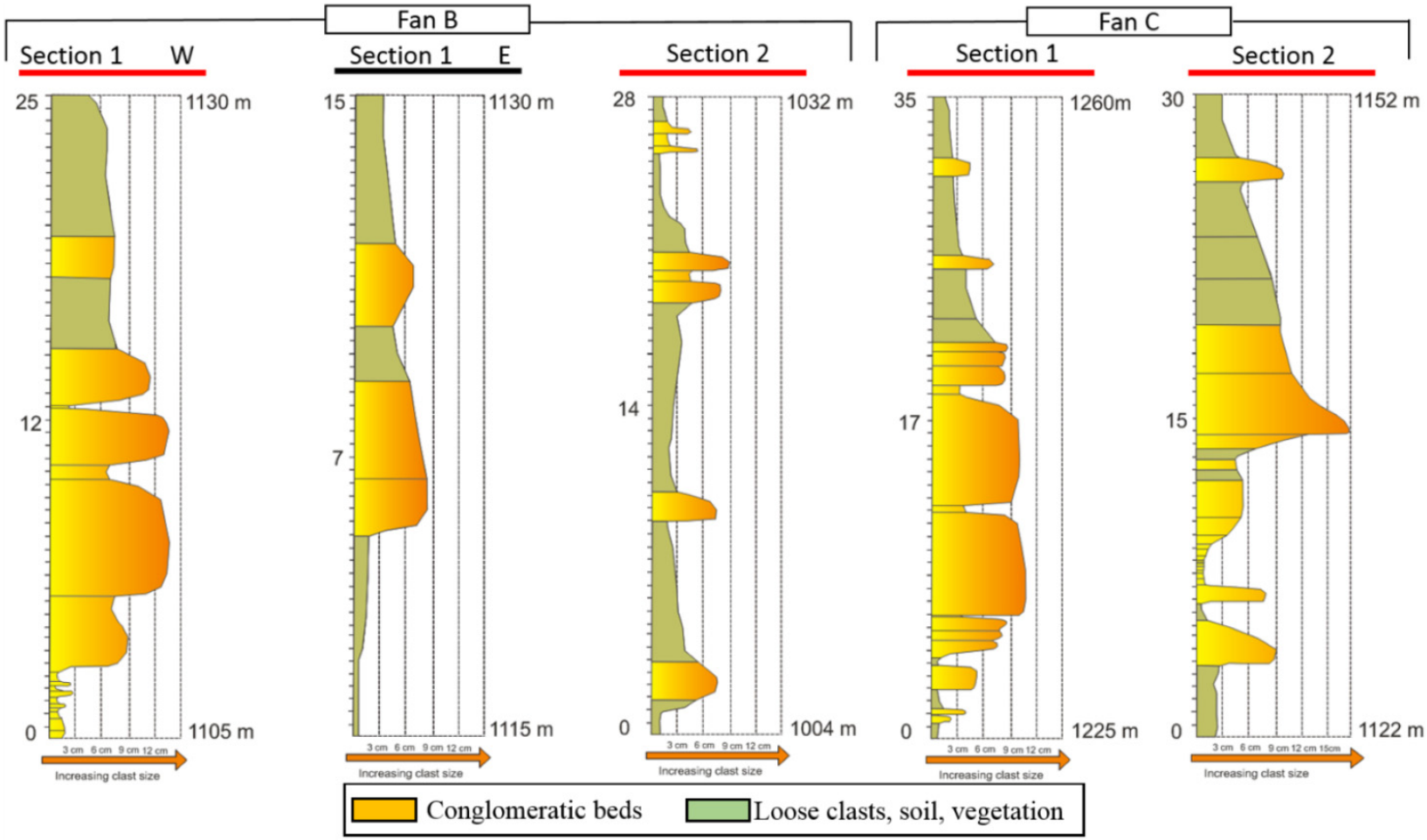

Figure 63: Detailed lithological logs for Fan B and Fan C. Notice in Fan B how the beds and clast sizes decrease drastically from section 1 to 2. In Fan C however, there is no decrease in clast sizes from Section 1 to Section 2 (north-west to south-east). However, there is a small change in bed thicknesses.

Figure 64: Shows the typical facies found in Section 1 – West in Fan B, with one of the many sandy intervals, coloured orange. Compass and pen for scale. The location of this photo is shown in Figure 60.

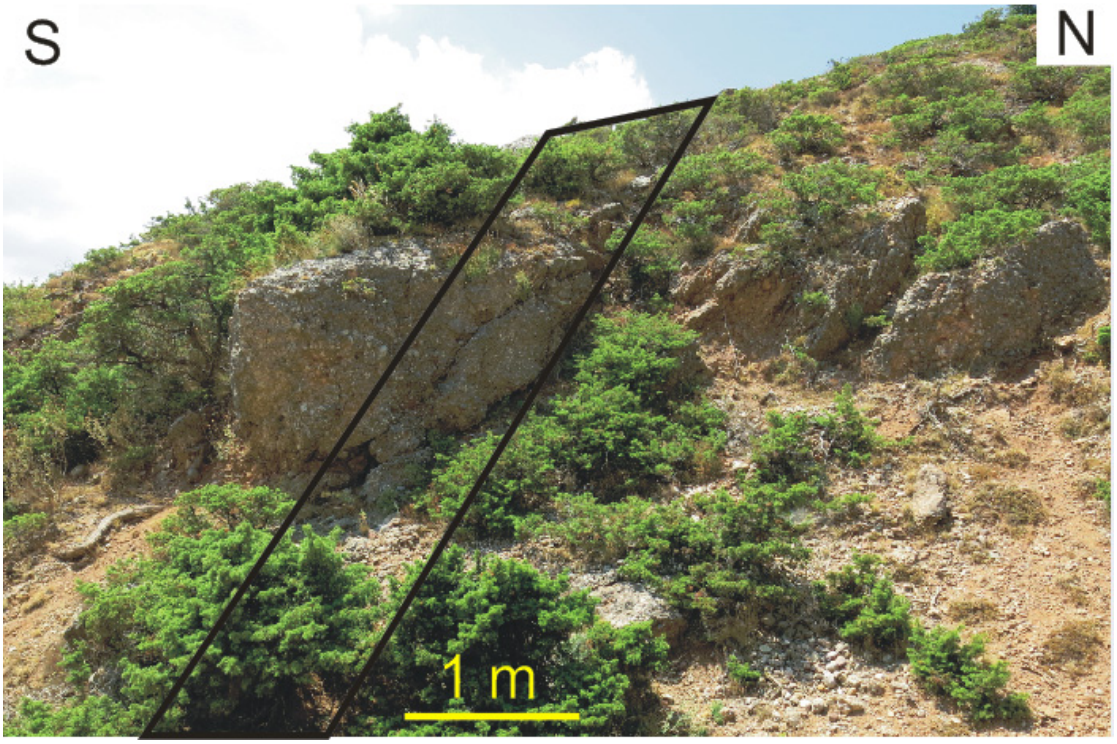

Figure 65: Shows Section 1 – East, with the most complete conglomeratic outcrop in this section. The location of this photo is shown in Figure 60.

Section 2

The second and final lithological section was made around the mid-fan area (Figure 66). No further than hundred metres from the apex, differences can already be observed. Finer, less consolidated and more homogenous facies are found in this log interval. Large packages of unconsolidated sediments dominate this section, with thin conglomeratic beds (5 – 30 cm) and fine clasts (mostly pebble-sized) (Figure 67). Further down in proximity to where the fan terminates, tall and impenetrable vegetation dominate the steep and eroded area. Creation of further lithological logs to the south was not possible due to inaccessibility. Such amounts of vegetation indicate fine lithologies and soily intervals. An eastern equivalent to this log interval was not possible to construct, as the eastern side has no exposed conglomerates (Figure 66).

- The conglomeratic beds are clast-supported, 0.2 - 2.0 m thick, and have a Dip / DD of 20° / 200S.
- Conglomerates are well sorted, and consist mainly of pebble-sized clasts ranging from ≈ 4 - 6 cm. There are a few coarser beds, as seen in the lithological log; with cobble-sized clasts ranging from ≈ 6 - 8 cm.
- Clasts are sub-rounded to rounded and well sorted.
- No graded beds are observed in this log interval.
- There are a few finer conglomeratic beds at the top of the section, but the exposure is too poor to deduce any definite variability from top to bottom of Section 2.

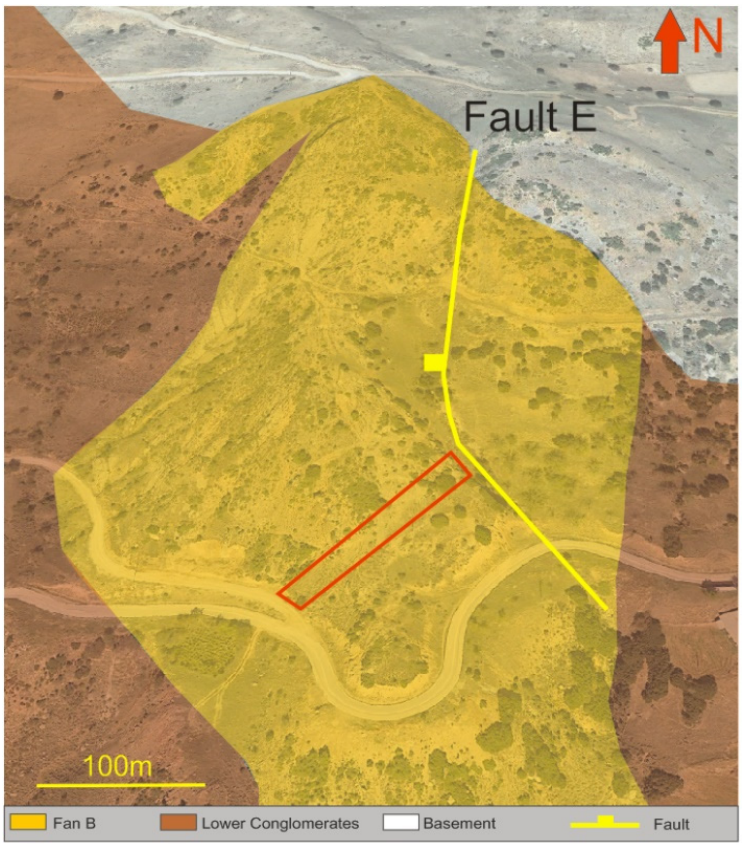

Figure 66: Satellite image from Google Earth used to show the location of Section 2 within the red box. Fault E is also included in the map.

Figure 67: Shows the fine and unconsolidated nature of the deposits near the base of Section 2. The location of this photo is shown in Figure 60.

5.4.3 Fan B summary

From north to south, the beds are thinning, clast sizes are decreasing, and deposits transition from proximal to distal deposits. In the southernmost areas, the deposits are comprised of fine sands and unconsolidated sediments with lush vegetation on top. The beds show higher maturities towards the south, as sorting improves and the roundness increases. It was not possible to make a figure for the bedding geometries of this fan due to poor exposure over a distance. Even though Fan B is smaller than Fan A, they share many similar N-S trends and characteristics.

5.4.4 Facies interpretation

To the north, in proximity to the unconformity contact, coarse and poorly defined beds with a high textural heterogeneity are overlying the fine sediments at the base. These deposits are clearly dominated by mass movement in a setting with a high depositional energy. These are interpreted as debris-flow deposits. On top of these debris-flows there are thinner beds with occasional sand lenses, exhibiting a greater textural homogeneity. These deposits are episodic and more channelized, and are interpreted as overlying sheetflood deposits. A hundred metres further south, all the conglomerates have transitioned into facies similar to the overlying sheetflood deposits. East of Fault E, coarse and fine sand beds are interbedded with unconsolidated sediments and soil in addition to a few fine conglomeratic beds (Figure 68). These low-energy muddy facies are interpreted to be streamflow deposits. The streamflow deposits are found on the eastern and western edges of the fan, as well as in the very southern vegetated area.

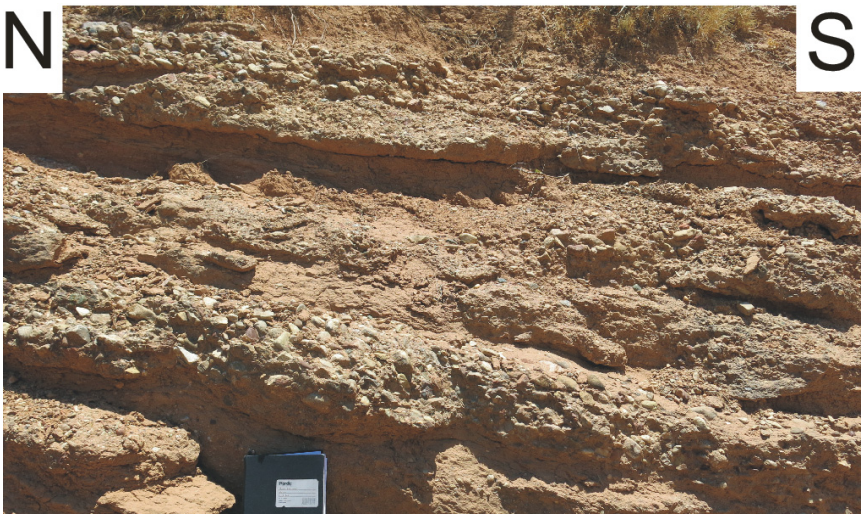

Figure 68: Distal deposits in the immediate footwall of Fault E, interpreted as streamflow deposits. Book for scale. The location of this photo is shown in Figure 60.

Based on all these observations, a facies distribution map was constructed for Fan B. The interpreted depositional direction is shown as well as the faults and locations of lithological sections (Figure 69).

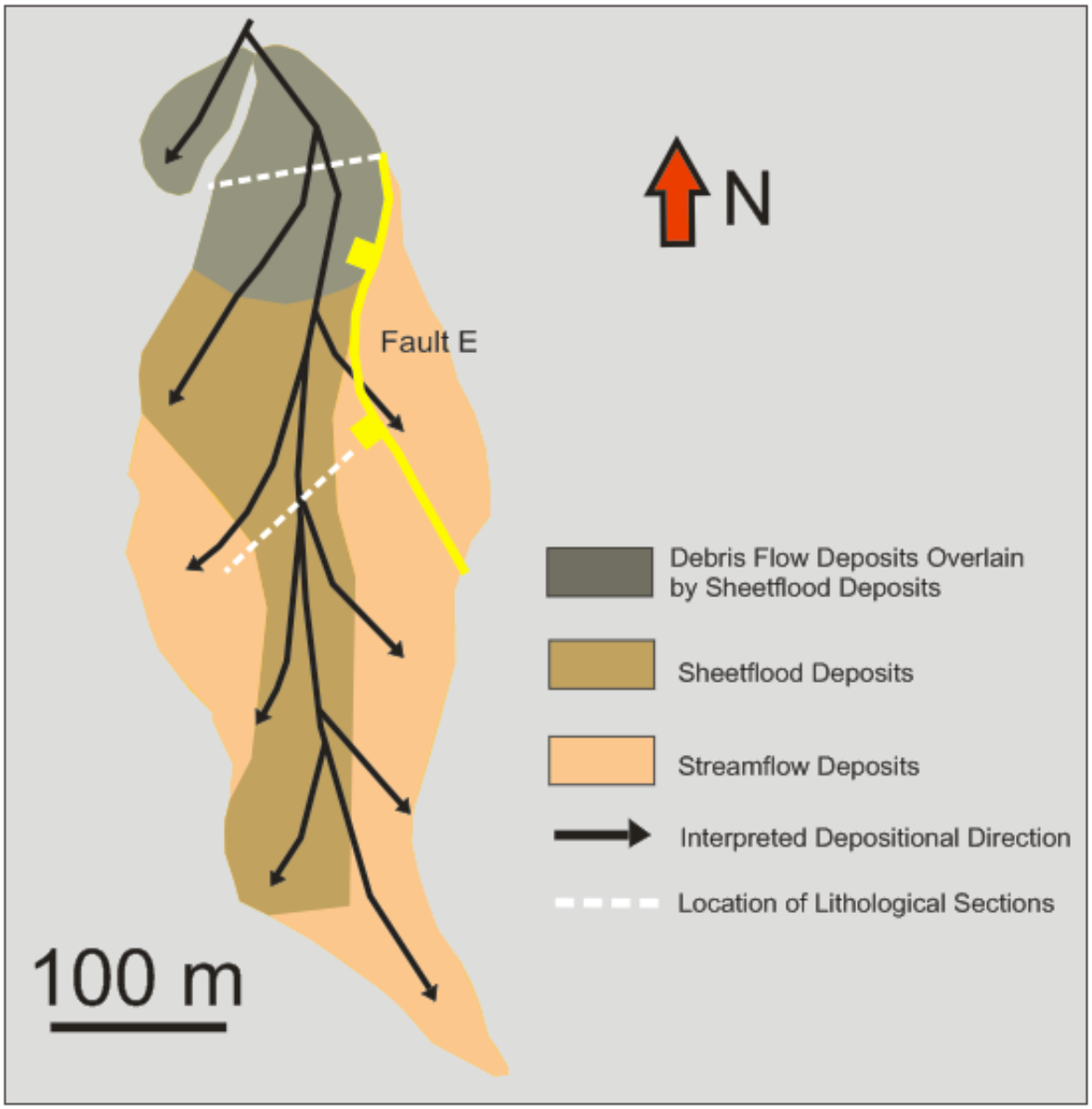

Figure 69: Facies distribution map for Fan B, as well as the interpreted depositional direction.

5.5 Fan C

Fan C is much more complicated than what previous studies suggest. It is located in the eastern region of the Kerpini Fault Block, and terminates against Roghi Mountain (Figure 70). Fan C extends for approximately 800 m in a NW-SE direction, and 500 m from SW-NE along its longest axes. Due to its narrow nature, it covers an area of only 0.20 km^2. Fan C is deposited approximately on the unconformity plane. The fan is estimated to be at least 40 m thick, based on the interpolated unconformity plane from Fault H. When viewed from a satellite image, its geometrical shape looks similar to both Fan A and B, with the apex sitting near the unconformity contact in the north. It appears that Fan C is deposited from NW towards SE, but this is not the case (Figure 71). It consists of one well-constrained main lobe with coarse and defined beds (Figure 70). This main lobe is well exposed, but the state of exposure is worse to the east. The coarsest conglomeratic beds are 0.5 - 3 m thick, with clasts up to large boulder sizes (>30 cm). Several finer conglomeratic and sandy deposits are found to the northeast. These differ from the Lower Conglomerates, and are believed to be distal side lobes of the main fan. The same vegetation grows on these finer deposits and the main lobe. The fan has a near-horizontal dip in the area to the northwest, and the dip gradually steepens towards the southeast. The clast composition of Fan C is 80 % limestone clasts, 15 % red/grey chert clasts and 5 % green chert and limestone clasts.

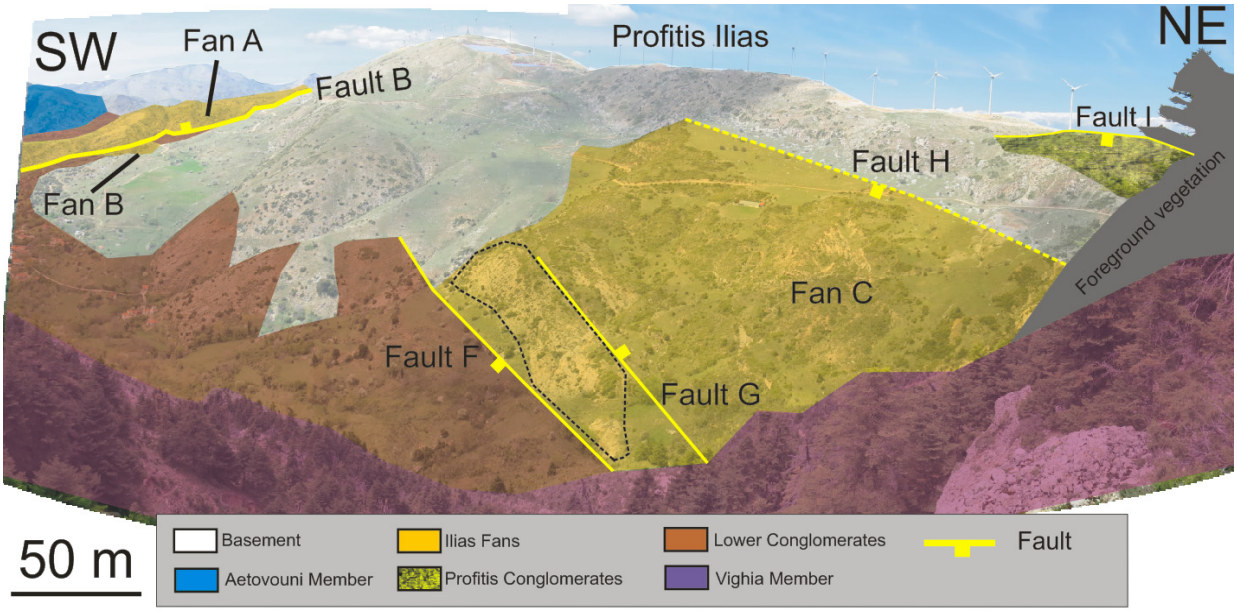

Figure 70: Panorama photo taken from Roghi Mountain, that shows the extent of Fan D, its faults, and how the lithological contacts span out in field view. The Roghi Fault is not drawn on this figure, as it disappears behind the Vighia Member. But as seen in Figure 71, it is the south-eastern boundary of the fan. The main lobe of Fan C is outlined with a dashed black line. The location of this photo is shown in Figure 71.

5.5.1 Structural description

Stuvland (2015) included an outcrop to the northwest as part of his sub-horizontal sediment outcrops (within dashed circle in Figure 71), and as seen in Figure 73, the beds are indeed sub-horizontal. The structural orientation of Fan C will be discussed in Sub-chapter 6.2.1.

Fault F (Figure 21) most likely down-faulted parts of Fan C in the south, exposing the coarsest beds near Section 2. An internal north-dipping Fault G was identified (Figure 22) as well. The key question is whether the linear feature inferred as Fault H bounds the fan in the north, or not. All the dip measurements are represented in a rose diagram (Figure 72).

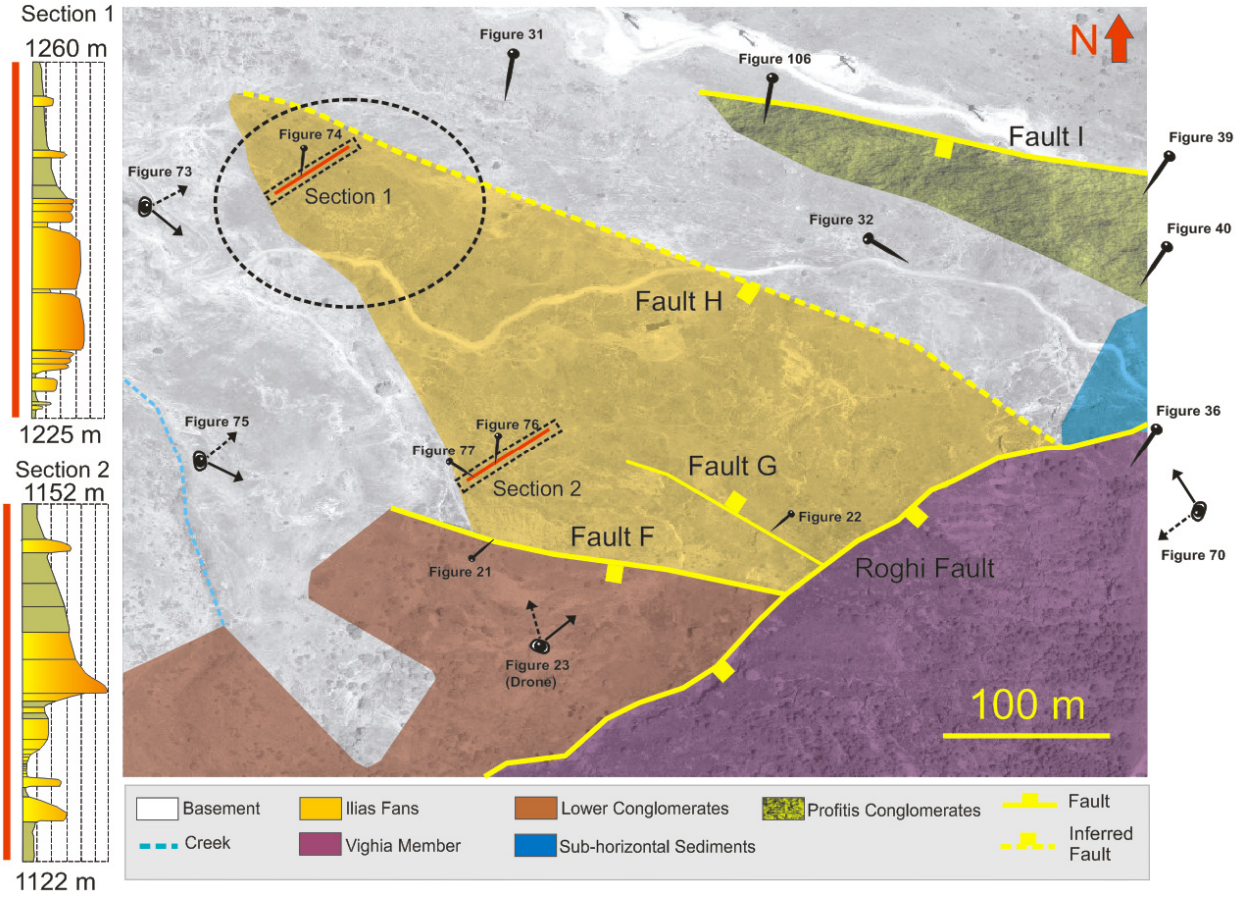

Figure 71: Satellite photo from Google Earth, showing a detailed geological map of Fan C and its associated lithological sections. Notice the similarities between Section 1 and 2 and the complex faulting in the area. The sub-horizontal layers are found within the black dashed circle, close to Section 1. For a more detailed description of the lithological logs, see Figure 63. This figure also shows the locations of all the figures located in this area.

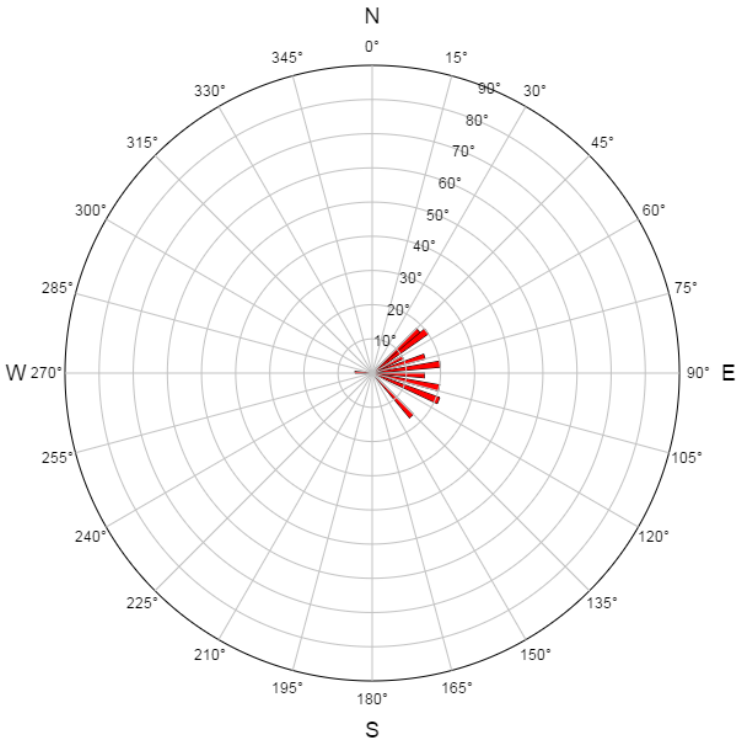

Figure 72: Rose diagram constructed based on all the collected dip data for Fan C. The outcrops furthest to the northwest dip slightly west, whereas the rest of the fan dips to the east.

5.5.2 Sedimentary description

Fan C is structurally orientated in such a way that creating lithological sections from the western base of the fan and up was sufficient. This fan does not have a convex geometry, and consequently an eastern log is not possible to make along the main lobe. The first lithological log was made in the northwest, where the beds are thick and defined (Figure 73). The conglomeratic beds are interbedded with lenses of fine and coarse sand (Figure 74).

Section 1

- Beds are clast-supported, ≈ 0.5 - 3 m thick, and have a Dip / DD of ≈ 5° / 270W at the exact log location. The Dip / DD changes rapidly to ≈ 10 - 12° / 90E within 50 - 100 m further south.
- The average clast size is ≈ 10 cm, (small to medium sized cobbles), and the sorting is generally good.
- Clasts are sub-rounded.
- No beds with an obvious grading were observed in this log interval.
- From base to top in this log interval, the conglomeratic beds exhibit a general thinning and fining trend.

Figure 73: Field photo showing Fan C to the northwest and the location of Section 1. The section was constructed here due to the extensive outcrops. Notice the sub-horizontal dip of the sediments, close to centre of the red polygon. The location of this photo is shown in Figure 71.

Figure 74: Photo from Section 1 showing a typical sand lens (coloured yellow), that was found within some of the finer conglomeratic facies of Fan C. The location of this photo is shown in Figure 71.

The second and final lithological log was constructed near the basement contact in the south-western part of the fan (Figure 75). This log interval contains some of the coarsest clasts found in the study area (>30 cm), and the steepest beds found in Fan C (15 - 22°). What is unique about the facies in this section is the sudden change between boulder-sized clasts to thin and sandy beds (0.5 - 3.0 cm) (Figure 76).

Section 2

- Conglomeratic beds are 0.5 - 3 m thick, clast supported, and have a Dip / DD of ≈ 15 - 20° / 90E. The sand beds are much thinner, ranging from 0.5 - 3 cm.
- The conglomerates are quite coarse in general (≈ 16 cm), but some boulders reach sizes up to 35 cm.
- Clasts are generally sub-angular.
- There are several normal graded beds (Figure 77), with a clear fining upwards trend.
- The coarsest beds are located around the middle of the log interval, both under- and overlain by thinner and finer beds. However, more soily and unconsolidated deposits occur towards the top of the section.

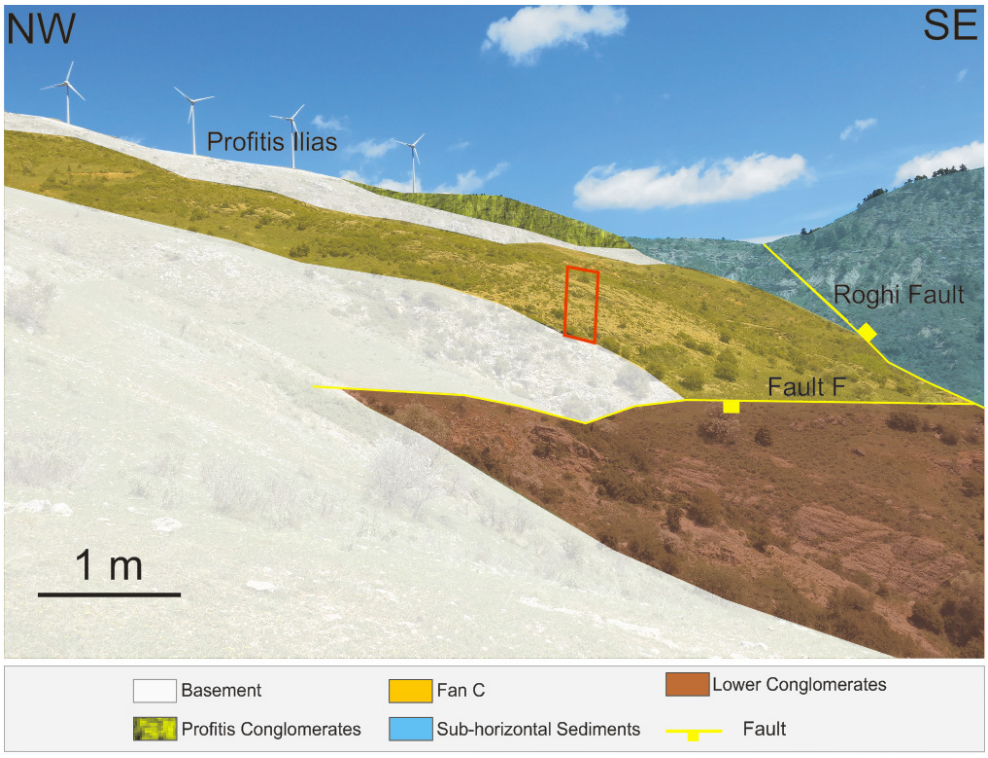

Figure 75: Shows the south-western part of Fan C, where the second and last lithological section was constructed (within red box). The location of this photo is shown in Figure 71.

Figure 76: Anomalous facies previously not observed in any of the fans, but found in several outcrops in Fan C. Very thin layers of coarse sand (≈ 1cm), overlain by boulder sized conglomerates. Similar facies were observed in the Profitis Conglomerates (Figure 106). Compass for scale. The location of this photo is shown in Figure 71.

Figure 77: Shows a fining up section at the very southern base of Fan C. Book for scale. The location of this photo is shown in Figure 71.

5.5.3 Fan C summary

Structurally, it appears as if the fan is deposited from NW-SE, contrary to sedimentological trends. There are no clear transitions from proximal to distal facies along a NW-SE direction (the structurally perceived depositional direction). There are clear thinning and fining trends from southwest to northeast, where the beds transition from meter-thick beds of boulder sized conglomerates to loose and unconsolidated sediments and centimetre-thick sand beds. These observations support a depositional direction from southwest to northeast. It was not possible to make a good figure featuring bedding geometries for this fan, as the exposure is poor.

5.5.4 Facies interpretation

In the southwest, the coarsest, most immature and poorly defined beds with a high textural heterogeneity are located. These thick, angular, chaotic and poorly sorted deposits were interpreted as proximal debris-flow deposits. To the northeast (and northwest), there is a clear decrease in depositional energy as the flow has lost its energy down-slope. These deposits are more mature, and consist of finer conglomeratic beds with frequently occurring sand lenses. These are interpreted as sheetflood deposits. Hundred metres further away from the apex, the depositional energy has decreased even more. The facies have transitioned into loose and unconsolidated sediments with centimetre thin beds ranging from mud sizes to coarse sand. Finer sediments have been transported as suspended load, and these deposits were interpreted as streamflow deposits. A facies distribution map was constructed for Fan C (Figure 78), clearly showing the SW-NE trend.

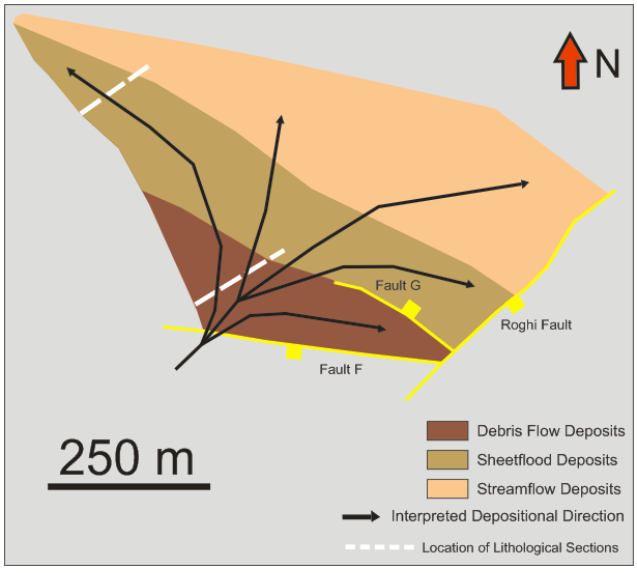

Figure 78: Facies distribution map for Fan C, showing the interpreted depositional direction and the faults as well.

5.6 Fan D

Fan D is deposited to the east of the Roghi Fault in a complex setting. It is best observed from the eastern side of the Vouraikos River Valley, and protrudes from the topography as a significant unit in the valley side (Figure 79). The Late Fan has deposited on top of Fan D and the surrounding area, thus eroding away parts of Fan D and reducing its state of exposure. The overlying Vighia Member to the south has also affected the extent of the fan. Fan D sits unconformably on the basement, which is believed to be quite shallow in this location, as the plane of the unconformity can be observed directly north of the fan (Figure 42). The fan is elevated ≈ 60 m compared to the surrounding deposits. Considering the shallow depth of the basement, Fan D is estimated to be 60 - 100 m thick. It extends ≈ 1 km from east to west, and ≈ 200 m from north to south (0.2 km^2). It is composed of two main lobes: Lobe I and Lobe II (Figure 80 and Figure 82), and these will be compared in the following subchapters.

There are steep drops to the north and south of the fan, making access very difficult. As such, it was not deemed safe to construct proper lithological logs. A general survey was done instead, as it was possible to walk on the fan ridge, and study it from a distance where it was dangerous to get close. Fan D is composed of 85 % limestone, 10 % red chert and 5 % grey chert.

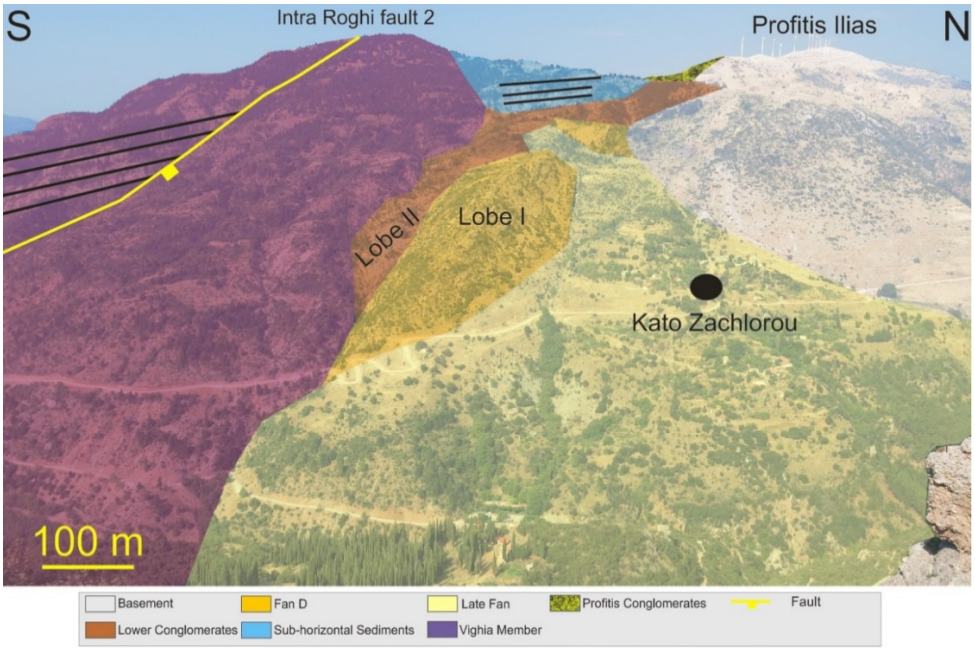

Figure 79: Photo of Fan D taken from the other side of the Vouraikos Valley, displaying Lobe I and II. Shows how the Late Fan has deposited, and eroded Fan D into two parts. The Intra Roghi Fault 2 can be seen to the south. The purple area north of the fault is what Sigmundstad (2016) refers to as segment V of Roghi Mountain, and this will be further discussed in Sub-chapter 6.3. The location of this photo is shown in Figure 43.

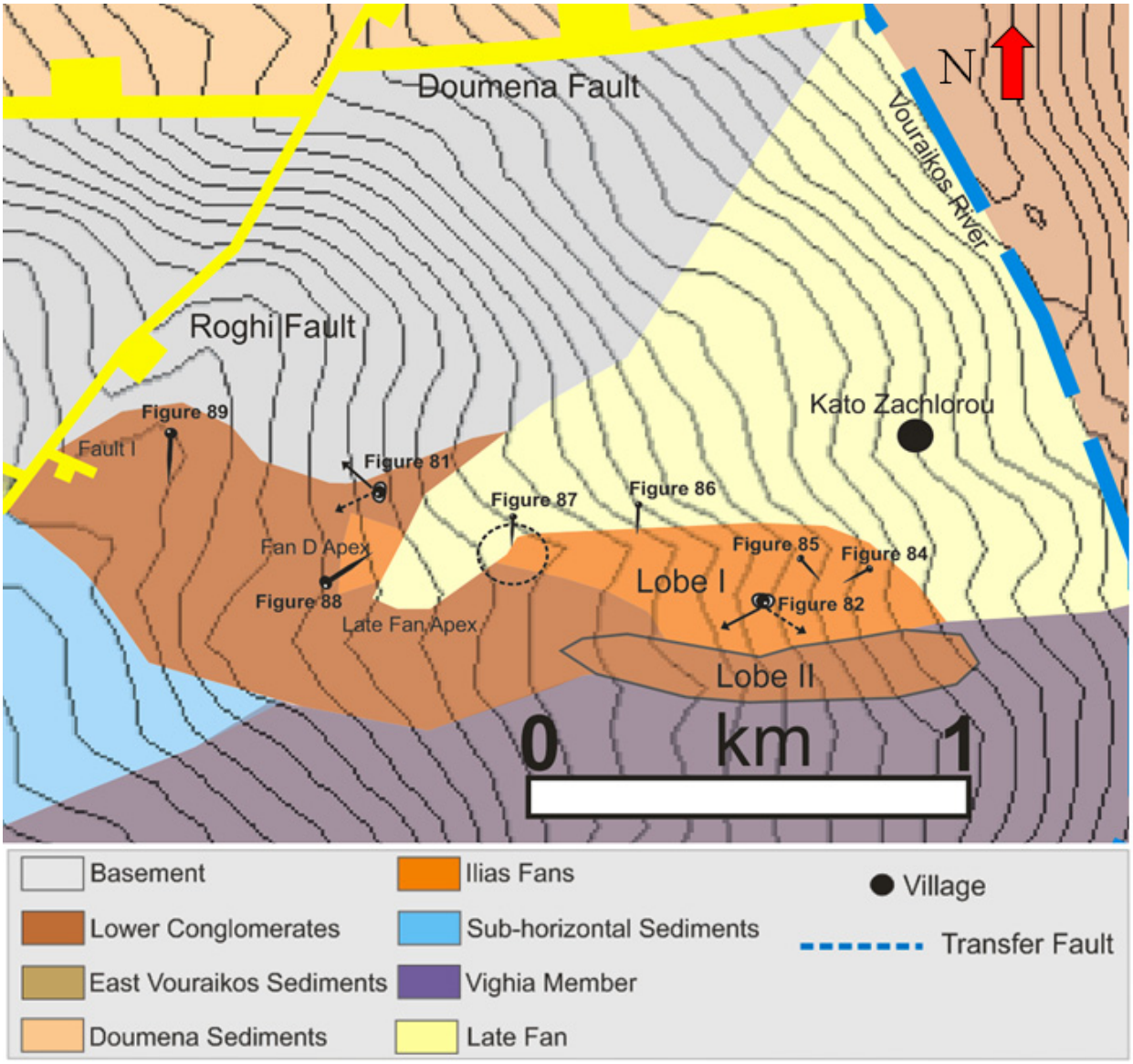

Figure 80: Zoomed in map-view of Fan D and its surrounding features. It shows the locations of all the figures related to Fan D. The locations of all the photos taken from the east of the Vouraikos River Valley are shown in Figure 43.

To the west of Fan D near the top of the valley side, Sub-horizontal Sediments and Lower Conglomerates are outcropped. It is difficult to map the boundary between these two stratigraphic units, but it was traced to where the Sub-horizontal Sediments are no longer exposed (Figure 81).

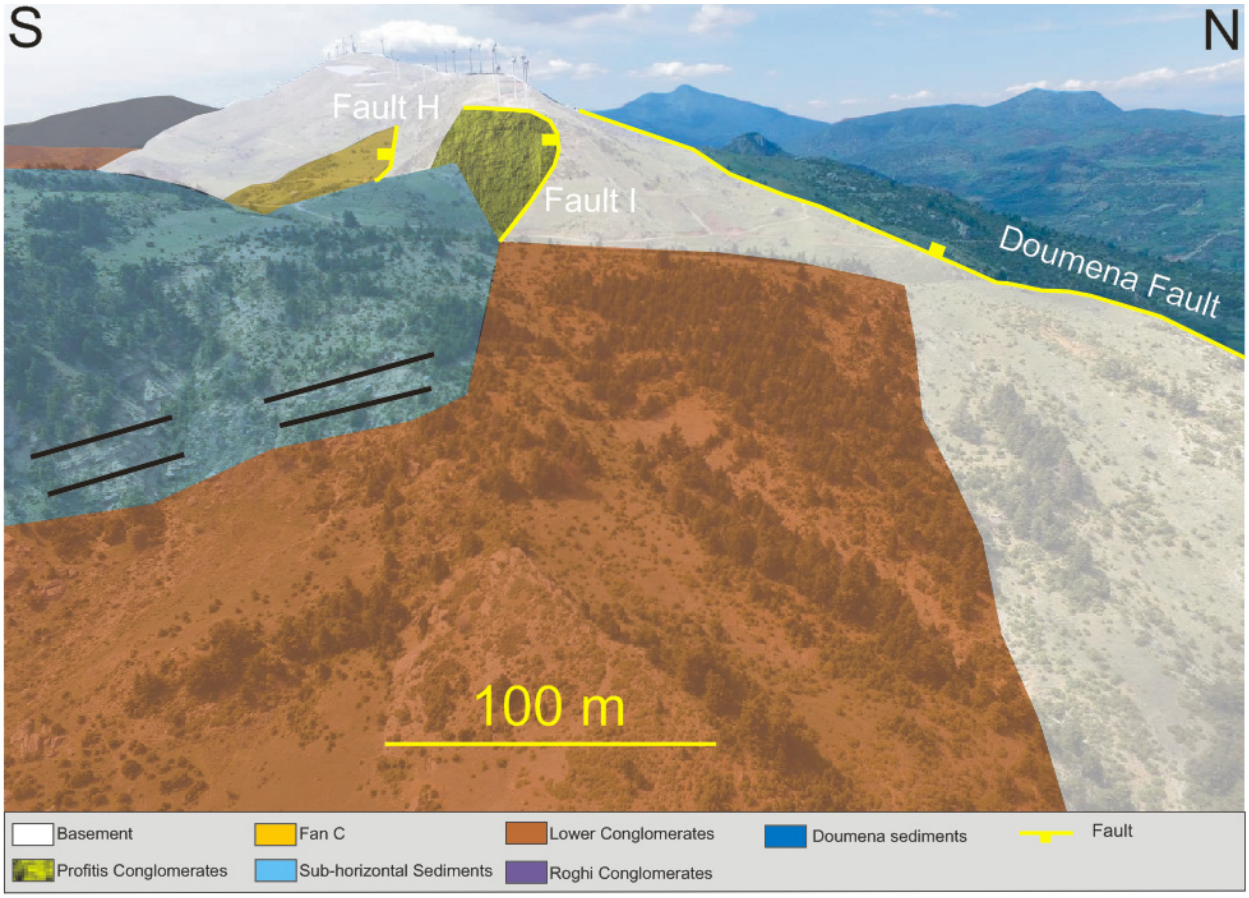

Figure 81: Drone photo over the area overlying Fan D to the west, featuring a glimpse into the Doumena Fault Block. The location of this photo is shown in Figure 80.

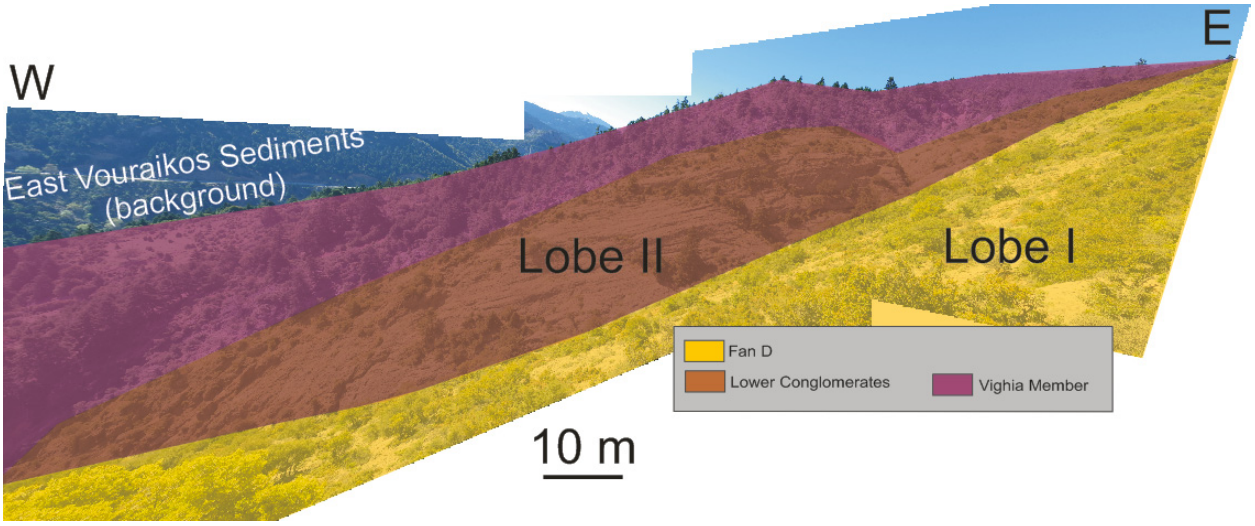

Figure 82: Panorama photo showing that Lobe II has a similar structural nature and depositional geometry. However, Lobe II has a much finer clast size than Lobe I. Scale is relevant to Lobe II. The location of this photo is shown in Figure 80.

5.6.1 Structural description

The beds have a Dip / DD of 30° / 110°E. There are no obvious fault surfaces cutting or bounding Fan D. Fault possibilities will be discussed in Sub-chapter 6.3.3. The dip data for Lobe I of Fan D is represented in a rose diagram (Figure 83), where the steep dip to the southeast is displayed. Lobe II was inaccessible, and dip measurements were only possible from a distance. The general Dip / DD of Lobe II was measured to 22° / 160°SSE, which is ≈ 10° gentler than in Lobe I, and oriented more to the south.

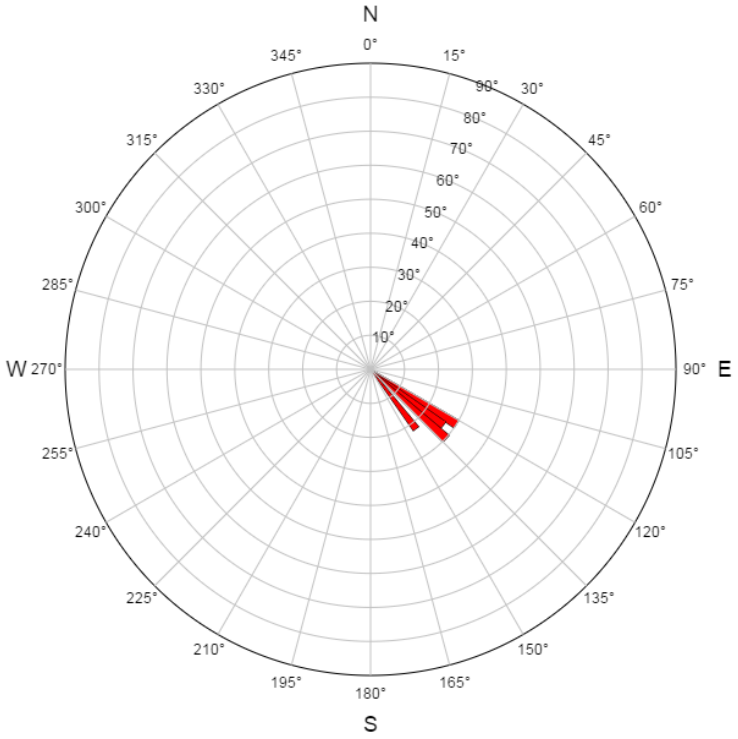

Figure 83: Rose diagram constructed based on all the dip data collected from Fan D.

5.6.2 Sedimentary description

As no proper lithological log was constructed, this sedimentary description is limited to the few observations that could be made in such an inaccessible area. Lobe I was studied up close, and Lobe II could only be observed from afar. The largest (Figure 84) and most angular clasts (Figure 85) are found from the eastern base of the fan and westwards, all the way up to the Late Fan contact (Figure 87). Walking from the base and up yielded little (if any) lithological differences. The conglomeratic clasts are large (≈ 25 cm in some beds) and angular from the eastern base to the western contact of Fan D. The sorting is poor, bedding is poorly developed. The largest complete conglomeratic section can be observed in the north (Figure 86), where the thickest and coarsest

deposits are located (up to 10 m in thickness). Here, the conglomerates are moderately sorted and slightly smaller in clast size (≈ 15 cm in general).

- The beds are clast supported, 0.5 - 2.0 m thick (up to 10 m in the northern cliff face).
- Clasts are boulder-sized, ranging from 20 - 45 cm in size.
- The largest clasts are sub-rounded, but in general the clasts are sub-angular.
- No graded beds are observed in this fan.
- There are no conclusive trends from east to west, but the bed thicknesses appear to decrease rapidly from north to south.

Figure 84: Shows the large boulders typical for the coarse deposits found throughout Fan D. The location of this photo is shown in Figure 80.

Figure 85: Shows the angular nature of the Fan D clasts. The location of this photo is shown in Figure 80.

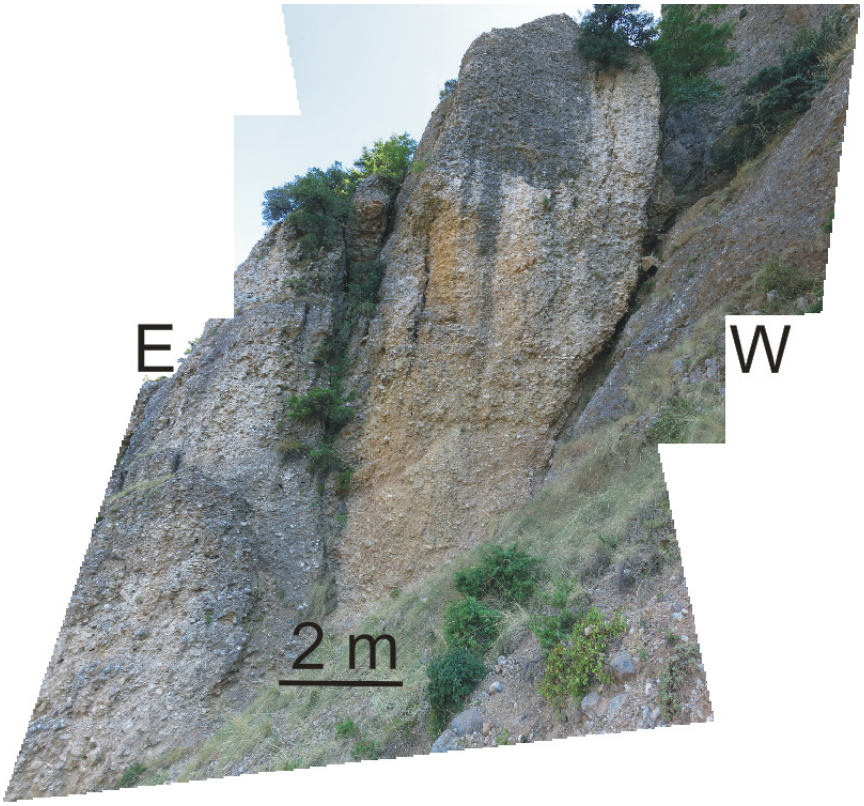

Figure 86: Shows the northern vertical cliff side of the fan with its massive outcrops. The bed boundaries are poorly defined, clasts are cobble to boulder-sized. The sorting is poor, matrix is quite coarse (pebbles, 3 - 4 cm) and the clasts are matrix-supported and sub-angular. The location of this photo is shown in Figure 80.

Towards the western limit of Fan D, there is a drastic change into much finer facies (Figure 87). This is a different stratigraphic unit, interpreted as the Late Fan (dashed black circle in Figure 80).

Figure 87: Shows the nature of the facies on the western limit of the main Fan D, which is a drastic change from what is observed elsewhere in the fan. The location of this photo is shown in Figure 80.

To the west of the Late Fan apex, another large conglomeratic outcrop is located (Figure 88). These conglomerates have the same chaotic texture as Fan D, with thick and poorly defined beds, poorly sorted and large conglomeratic clasts (15 - 25 cm). This outcrop was interpreted as the westernmost Fan D outcrop, possibly the apex.

Figure 88: Shows the facies of the western Fan D outcrop (possible apex), separated from the main lobe by the Late Fan. The location of this photo is shown in Figure 80.

At the very top of the valley side, thick and sub-angular conglomerates are poorly exposed (Figure 89). When comparing these conglomerates to the Profitis Conglomerates (only 300 m apart), they lack the interbedded coarse sand beds typical for the Profitis Conglomerates, and exhibit larger clast sizes (20 - 30 cm sized clasts). The Roghi Fault is separating this outcrop from the Profitis Conglomerates. The most similar facies to this outcrop is found in Fan D, which is 300 m to the east, and ≈ 150 m lower in elevation. The outcrop was classified as Lower Conglomerates, and one possibility is that Fan D was sourced from this area, as it is located at a higher elevation in the same valley side.

Figure 89: Shows the conglomerates that are a possible source for Fan D, with similar facies as the fan, although not outcropped clearly. Shoe tip for scale. The location of this photo is shown in Figure 80.

5.6.3.1 Bedding geometries

Fan D have similar bed geometries as those of Fan A (Figure 55). They build out from NW to SE, giving Fan D a progradational nature. Lobes I and II have comparable bedding geometries, although Lobe II exhibits gentler dips.

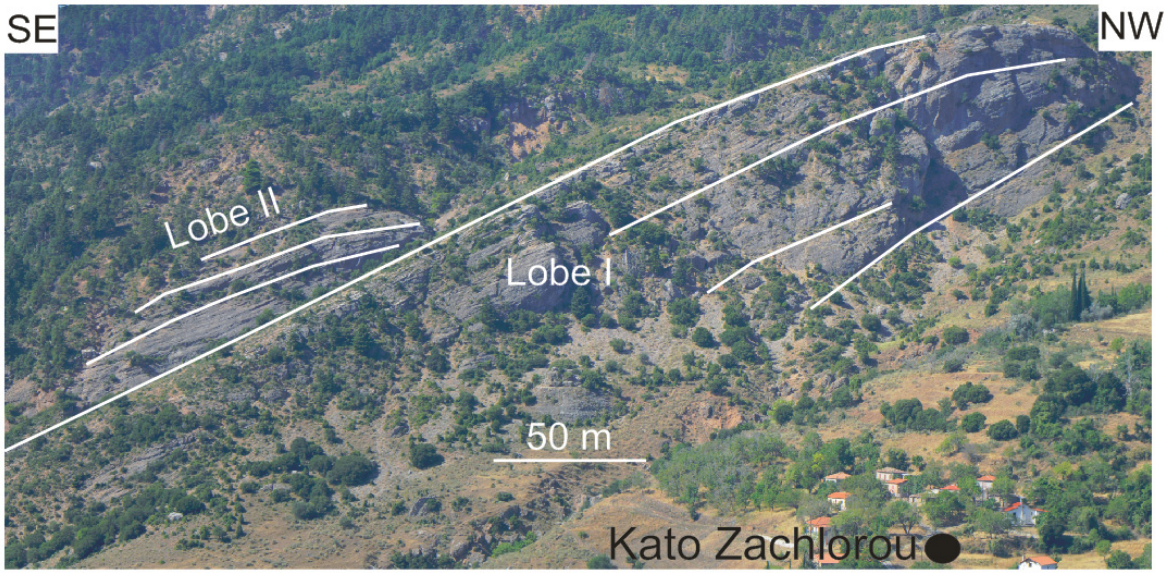

Figure 90: Simplified figure showing how the beds of Lobe I and Lobe II are building out from NW to SE. The location of this photo is shown in Figure 43.

5.6.3 Summary

There are no fine and sandy deposits observed in Lobe I or Lobe II. The thin beds with occasional sand lenses are absent, and the fan is entirely composed of thick beds with coarse clasts. From west to east, there is no clear decrease in bed thickness, but clast sizes are slightly increasing. The beds are dipping 30° to the east, and the interpreted depositional direction is from east to west, as there are no observations that would suggest otherwise. Lobe II was only observed from a distance. However, it is clearly more thinly bedded, dips more to the south, and is comprised of finer clasts with a better sorting than Lobe I. Due to these differences, Lobe II is interpreted as a different stratigraphic unit, not belonging to Fan D. There is a complete absence of green clasts in the clast composition of Fan D. This is an indicator that Fan D has a different source than Fan A, B and C, as they all contain green clasts. Additionally, Fan D is ≈ 10° steeper than the other fans, and consist of larger and more angular clasts.

5.6.4 Facies interpretation

Chaotic, poorly defined beds of a high textural heterogeneity were observed throughout the fan. There are no waterlain deposits, and no observations suggest a low depositional energy anywhere in the fan. Mass movements dominate all the deposits, with no real signs of channelized flows. These deposits were all interpreted as debris-flow deposits. Based on these field observations, a facies distribution map was constructed for Fan D. As this fan is entirely composed of debris-flow deposits, the map is quite simple (Figure 91). The interpreted depositional direction was included together with the ridge of the fan.

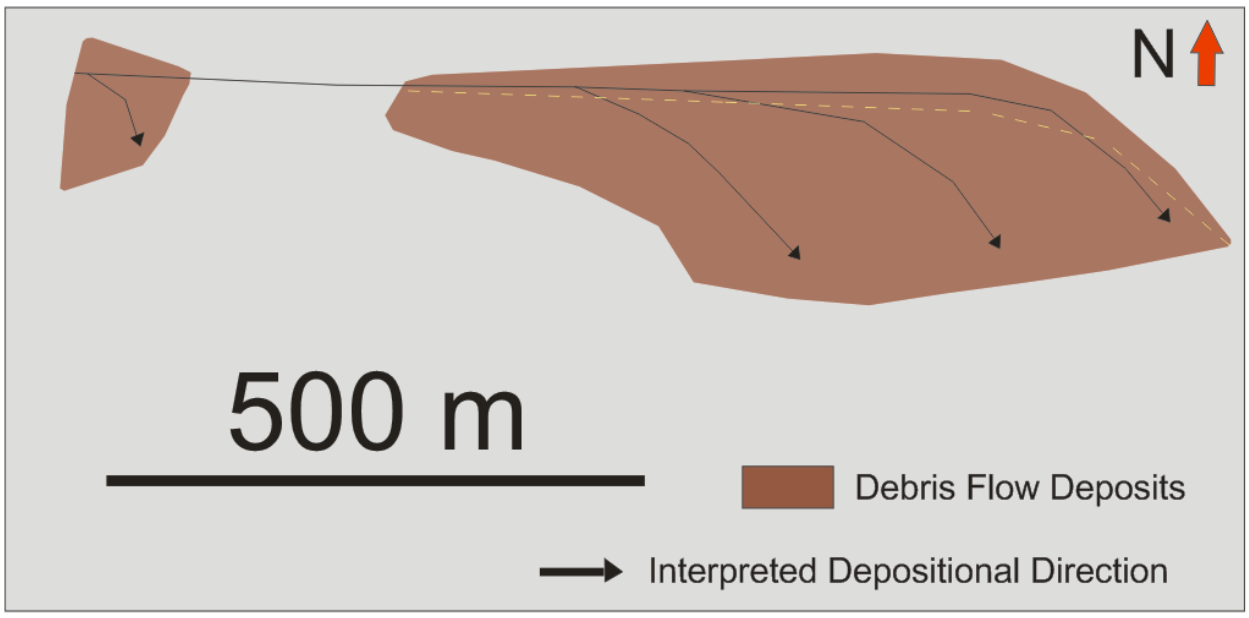

Figure 91: Facies interpretation map constructed for Fan D. The dashed yellow line in the figure represents the ridge of the fan, which was the only possible path to take from base to top.

5.7 Summary of fans

To summarize, Fan A and Fan B are honouring the general observations made by Syahrul (2014) and Hadland (2016). Observations suggest that these two fans are deposited from north to south, and exhibit several decisive alluvial fan characteristics. Fan C is located in the very eastern part of the study area, more than a kilometre away from Fan B. It dips to the east, and is a more complex unit. Observations during this study contradict observations made by Hadland (2016). The fan appears to be sourced from an apex in the south, and the structural orientation of the fan is difficult to explain. Fan D is deposited to the east of the Roghi Fault, and appears unrelated to the other fans. Similarly to Fan C, it dips to the east, but at a ≈ 10 - 15° steeper dip. The clast composition and homogenous facies distribution are further arguments that Fan D is unique. The area where Fan D is located is an intricate one, with several stratigraphic units deposited in proximity to each other in a complex relationship.

Chapter 6: Discussion

This chapter will discuss the key observations from the previous chapters, and attempt to address some of the geological problems that have been raised by previous master students from the University of Stavanger (Syahrul, 2014; Rognmo, 2015; Stuvland, 2015; Hadland, 2016). This is a detailed study of units that are only briefly described previously, and areas that have not been investigated in detail. As such, some of the observations made during this thesis contradict previous observations, and this study aims to improve and update some of the already existing data in the Kerpini Fault Block. The cross sections will also be discussed, in addition to transfer faults, XRD results, Profitis Conglomerates, and whether the Lower Conglomerates can be correlated with the Kalavryta Member. The objectives are relisted below, and this chapter will address them.

- Resolve whether the proposed fans are alluvial fans and if so; classify them, and
- Determine their relative timing concerning faulting and other stratigraphic units in the Kerpini Fault Block.

The main goal of the study was to confirm the alluvial fans, and this will be addressed first. The relative timing will be discussed in Sub-chapter 6.9.

6.1 Fan A and Fan B

In this sub-chapter, the classification, source and relative timing of Fan A and Fan B will be discussed. There are many similarities between these two fans. They more or less have the same structural orientation, consist of the same facies and clast composition, and lie in close proximity to each other.

6.1.1 Fan A - classification and sourcing

Fan A is an extensive unit with a complicated history affected by several stages of faulting. As shown in the facies interpretation for this fan, it is clearly deposited from north to south. The facies maturity trend is unambiguous from the apex and southwards, where the clast sizes decrease and the beds are thinning. The facies transitions from debris-flows to streamflows, due to the decrease in depositional energy and flow velocity. It is evident that this stratigraphic unit is an individual alluvial fan, as there are no observations that suggest otherwise. Due to the larger proportion of sheetflood deposits compared to debris-flow and streamflow deposits, the fan classifies as a sheetflood-dominated fan.

It is difficult to say anything conclusive about the source of the fan. There are several possibilities as to where the fan can be sourced from. Hemelsdaël *et al.* (2017) included Fans A, B and C in the same stratigraphic unit sourced from the Kalavryta Fault Block in the south (Kalavryta Member), but based on the results from this study this theory seems highly unlikely. It is reasonable to assume that Fan A is sourced from the north, supporting the suggestion by Syahrul (2014) and Hadland (2016) that it is a footwall-derived fan. Although this is the most likely theory, it is difficult to defend it, considering how extensive Fan A is and the sheer amount of sediments required from the north to deposit such a large unit. The Doumena Fault is located ≈ 1 km north of the apex of Fan A, and it is unlikely that the fan sediments are sourced from the fault. The area between the fault and Fan A is simply too small to accommodate such large amounts of sediments.

6.1.2 Fan B – classification and sourcing

Based on the interpreted depositional direction and the facies distribution, Fan B is clearly sourced from the north. The coarsest and thickest debris-flow deposits are found in the north, overlain by sheetflood deposits. Streamflow deposits are located to the south, and along the distal outline of the fan. It appears in the facies distribution map that there is an equal amount of streamflow

deposits, but only the area covered is shown in the map, whereas volume is not properly represented (Figure 69). This fan classifies as a sheetflood dominated fan based on the greater volume of sheetflood deposits. The main difference between Fan A and Fan B is that the debris-flow deposits of Fan B are overlain by sheetflood deposits. This is not the case for Fan A. The size difference between the two fans is also significant, but this is mainly due to Fan B having less accommodation space.

6.1.3 Relative timing

The lower unit at the base of Fan B is interpreted to be composed of waterlain deposits prior to Fan B, and it is not observable in any of the other fans. It indicates important evidence when considering the relative timing between Fan A and B, and major faulting in the area (Figure 61). The fine sediments at the base are low-energy and waterlain deposits, and consequently must have deposited on a flat (or 1-2° dipping) surface, before being tilted to the present day 20° dip. The overlying conglomeratic beds of Fan B are parallel to the underlying waterlain beds, suggesting that the fan was also deposited on a flat or very gently dipping surface. This is critical evidence that Fan B was deposited prior to the activation of the Doumena Fault, or in the very earliest stages of fault activity as syn-Doumena Fault strata.

Based on the short distance between Fan A and Fan B, the same structural orientation and the similar clast composition, it is assumed that the two fans deposited around the same stage in the evolution of the Kerpini Fault Block. The contact between the two fans is covered by vegetation, and consequently it was not possible to determine which fan is overlying the other without proper excavation and digging. Thus, the relative timing between the two fans remains speculative. Similarly to Fan B, the dips of the conglomeratic beds of Fan A are interpreted as structural dips and not depositional dips.

6.1.4 Earlier Lobes

The lobes east of Fan A was interpreted as earlier lobes based on the observation that they terminate towards Fan A (Figure 56). They are interpreted as resulting deposits from initial erosional events from conglomerates that were located near the Profitis Ilias (most likely conglomerates of the Kalavryta Member). At a later stage in time, Fault B initiated and created a large accommodation space together with Fault A to the west of the Earlier Lobes. This caused the sediment deposition to shift from east to west, and allowed for Fan A to deposit.

6.2 Fan C

In this sub-chapter, the classification, source and relative timing of Fan C will be discussed.

6.2.1 Classification and sourcing

Fan C is much more complex than previously suggested (Hadland, 2016). Of all the four fans, Fan C was the most difficult to classify as an alluvial fan. Due to the large amounts of sheetflood deposits, this fan classifies as a sheetflood dominated fan.

Based on its geomorphology in map view, the fan appears to be sourced from the northwest (Hadland, 2016). However, due to a SW-NE facies trend and the eastern dip direction of the beds, an interpretation where deposition occurred from the southwest is preferred for Fan C. The Kerpini Fault is believed to have tilted the fan, and later the Doumena Fault tilted it even further. The Roghi Fault in the south appears to have tilted the beds more towards the east. The beds of Fan C have their present day structural configuration because of these faulting events. The present-day configuration of Fan C is illustrated and explained in Figure 92.

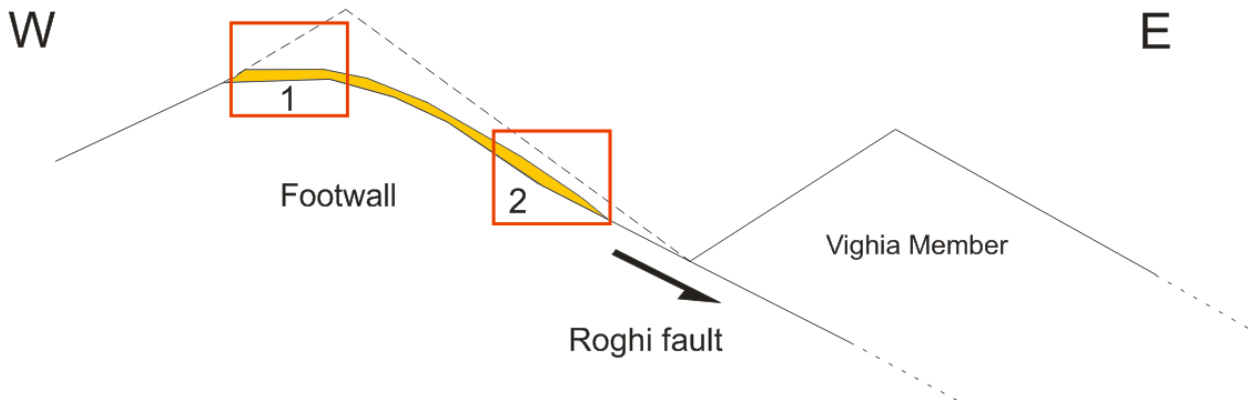

Figure 92: The dashed line represents the eroded sediments from the Kerpini Fault Block, and the orange package is the re-deposited Fan C. The coarsest clasts (2) are present in a steeper slope closer to the fault, whereas the most distal parts (1) are located on a much gentler surface. This is a result of later tilting events, which is responsible for the present-day configuration of Fan C. The figure is very simplified, and the dip of the Roghi Fault is exaggerated to illustrate the scenario.

6.2.2 Relative timing

It is difficult to determine the relative age of Fan C. It is interpreted to have been deposited after the Roghi Fault became active, and most likely while it was still active. Due to its structural orientation it must have deposited before the Kerpini Fault became inactive, and prior to the Doumena Fault. Fan C is affected by more than one major tilting event, as evident by its present-day orientation. Fan A and Fan B however, appear to be affected only by one major tilting event

(the Doumena Fault). As such, Fan C is interpreted as having been deposited before Fan A and Fan C. It also terminates towards the Vighia Member, which is interpreted as one of the earliest stratigraphic units in the Kerpini Fault Block (Hadland, 2016). This is further discussed in Sub-chapter 6.9.4.

6.3 Fan D

In this sub-chapter, the classification, source and relative timing of Fan C will be discussed.

6.3.1 Classification and sourcing

Fan D is considered unrelated to the other three fans. Fan D is sourced from the west. There are no streamflow or sheetflood deposits in Fan D. The fan is composed entirely of debris-flow deposits, and as such this is the only fan that classifies as a debris-flow dominated fan.

6.3.2 Relative timing and Late Fan influence

Fan D is more or less parallel to the basement unconformity, and as such it was likely deposited very early in the evolution of the Kerpini Fault Block. It is unconformably underlying the Vighia Member, which was one of the earliest stratigraphic units in the area of study (Sub-chapter 6.9.4). The Vighia Member is deposited from south to north, and originally dipped to the north, but was tilted to a southern dip by the activity of the Kerpini Fault in the south. Seeing as Fan D is dipping more steeply than the Vighia Member, it can be assumed that it was tilted to the south prior to the Vighia Member. Fan D is interpreted to be influenced by the Roghi Fault, and subsequent footwall erosion on the western valley side of the Vouraikos River Valley.

The latest addition to the stratigraphic column in the area of study is the Late Fan, which has influenced Fan D (Figure 93). What triggered the deposition of the Late Fan is unknown. One possibility is a steady erosion of the valley side by rainwater, and that an area of Fan D near its apex was eroded away. This erosion created a sediment pathway for the Late Fan to deposit, until the limited accommodation space in the area was filled.

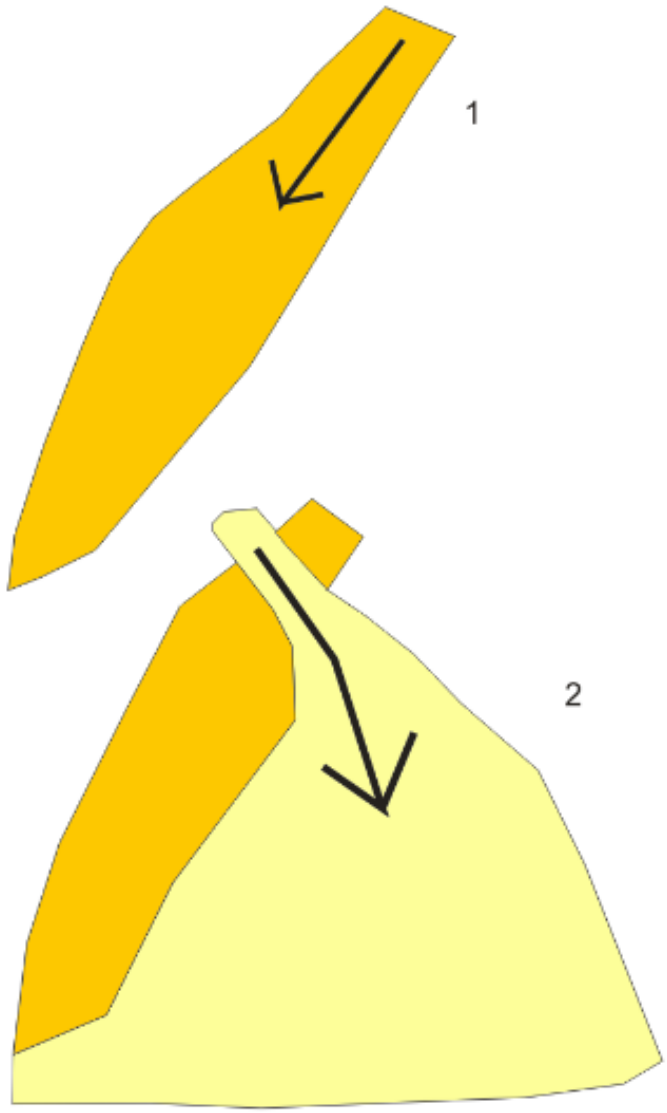

Figure 93: Simplified figure showing one possible interpretation as to how Lobe I of Fan D deposited first and was later influenced by the Late Fan.

6.3.3 Fault possibility

No bounding fault was observed for Fan D, but there is one fault possibility to the south, marked with a dashed yellow line in Figure 94. This fault could have downfaulted Lobe I relative to Lobe II. Across this fault, there is a sharp lithological change and a completely different vegetation. The incision where the inferred fault is traced is a sharp feature in the topography, with beds dipping differently on either side of the contact. However, not enough conclusive evidence is present to interpret a fault in this contact. It is interpreted to be a natural incision in the topography due to erosion.

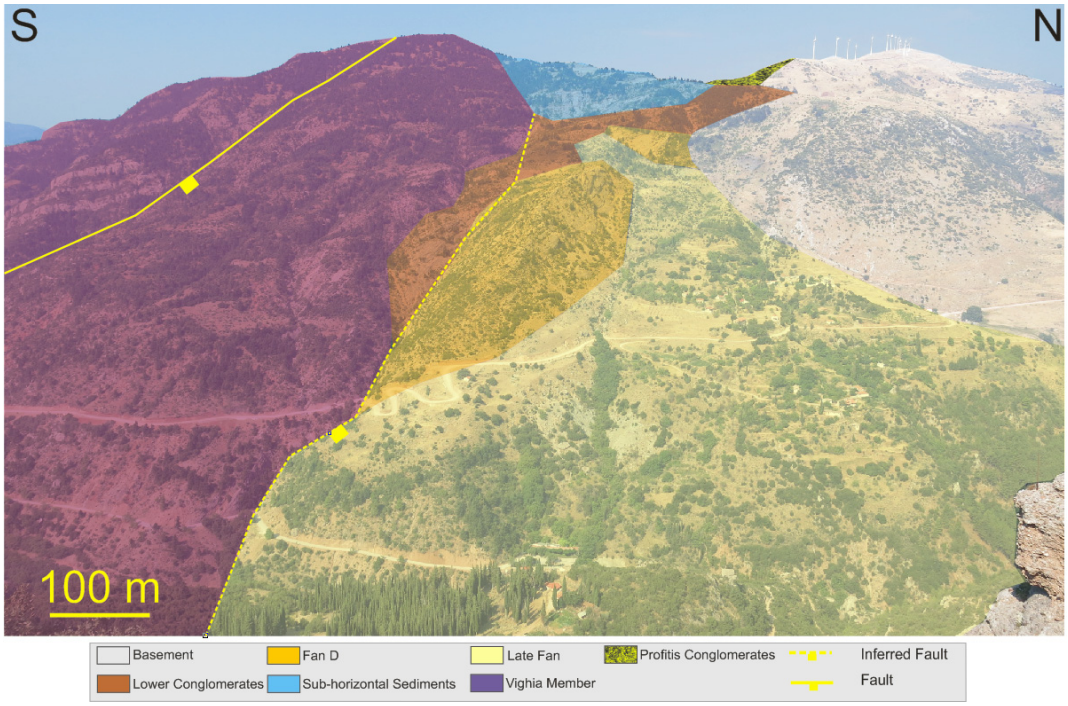

Figure 94: Shows one interpretation of a possible fault bounding Fan D to the south. Intra Roghi Fault II is shown in the south. The location of this photo is shown in Figure 43.

6.3.4 Lobes I and II

Lobe I and Lobe II are deposited in a similar manner, but Lobe II is interpreted as a different stratigraphic unit than Fan D due to the finer facies, gentler and more southern dip, and completely different vegetation growing on top of it. Lobe II is covered by fir trees and juniper bushes, whereas Lobe I is covered by birches and smaller plants. There are at least three possible interpretations:

1. Lobe II is a prograding feature of Fan D, deposited at a different time with a different source material, which explains the fine facies and more southern dip. It was later overlain by the Vighia Member. However, if it was indeed a prograding feature, one would not expect completely different facies from the first lobe.
2. Lobe II is one of the most distal deposits of the Vighia Member, which explains the fine facies and more southern dip. However, it fails to explain why Lobe II dips significantly more towards the east than the Vighia Member.
3. Lobe II belongs to the Lower Conglomerates, which was later overlain by the Vighia Member. This explains the difference in facies and dips. However, it is difficult to explain how the Lower Conglomerates would deposit at such a dip, and with such a geomorphology.

Any of these three interpretations are possible, but option 3 was preferred to differentiate between Lobe I, Lobe II and the Vighia Member, as three different stratigraphic units.

6.4 Cross sections

As there is quite a lot of stratigraphic units in the study area with a wide spread, eight different cross sections were made (Figure 95). These cross sections intersect most of these units, and show how the study area is interpreted in the subsurface. Five were made from north to south, and the remaining three were made from east to west (Figure 96 to Figure 103). The faults have unknown depths, and several have an unknown Dip / DD as well, but assumptions based on the structural descriptions have been made. All of the cross sections are described in the figure texts, for an easier overview.

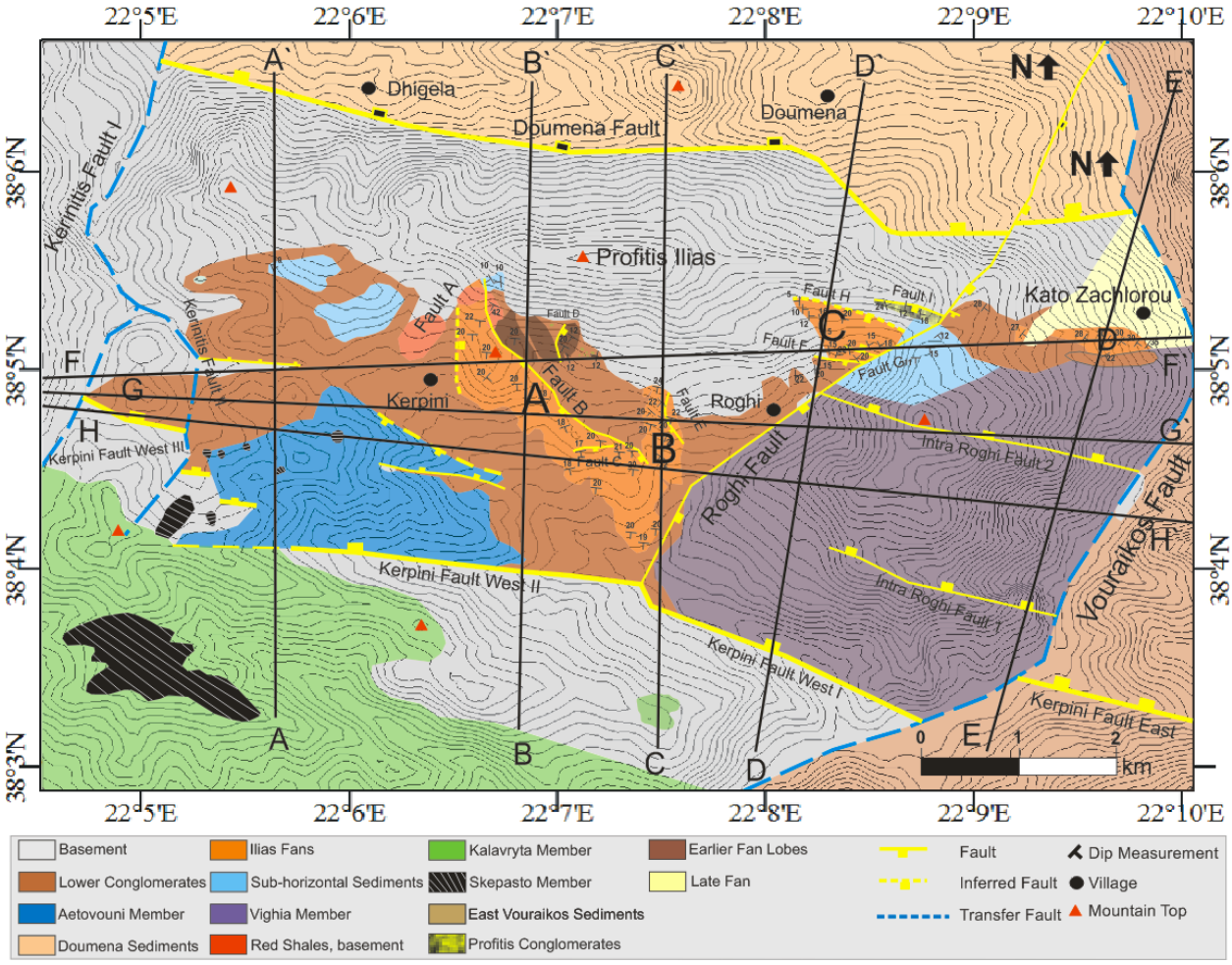

Figure 95: Shows the locations of the eight cross sections, A-H.

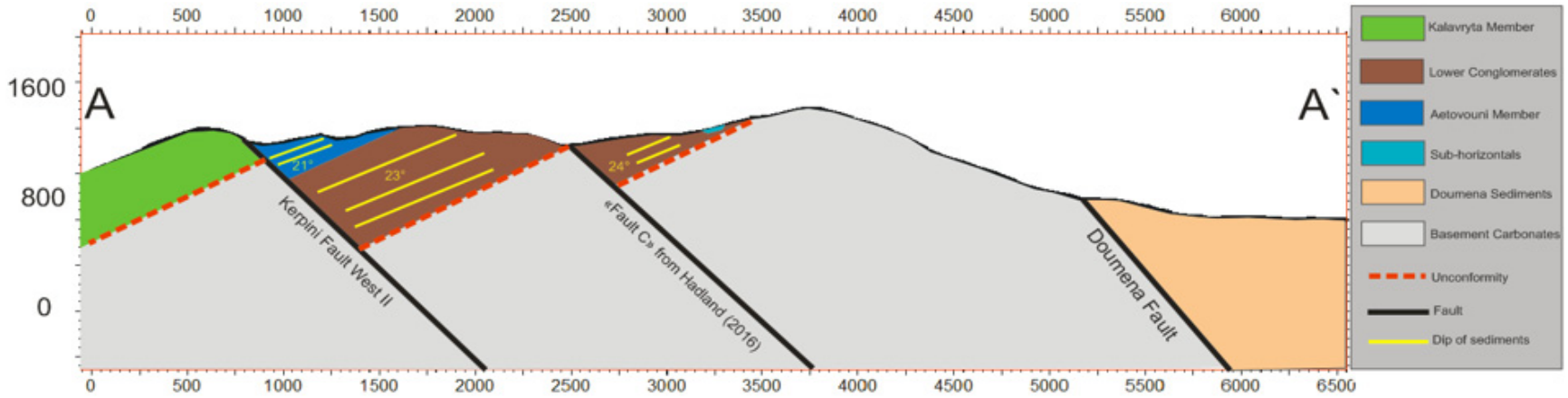

Figure 96: Shows the westernmost north-south cross section A-A`. The southernmost data here is credited Hadland (2016), as this area was not studied for this thesis.

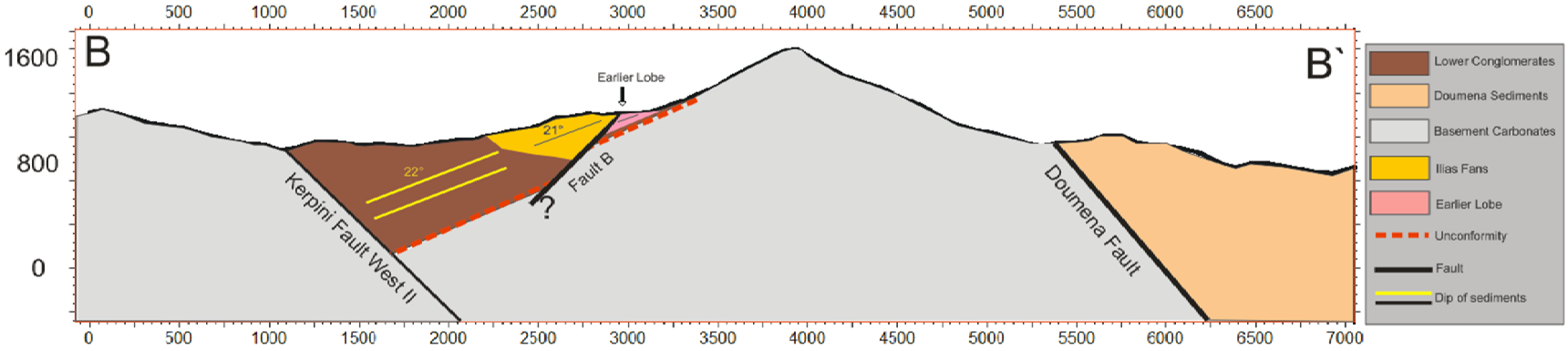

Figure 97: Cross section B-B`. This section goes through Fan A and is not perpendicular to Fault B. Fault B is believed to be quite steep (50 - 55˚), and such the dip in the cross section is apparent, as The Lower Conglomerates have a similar dip to the fan. The depth of the Lower Conglomerates is unknown, and the unconformity depth is assumed to jump to a shallower depth north of Fault B. Notice the earlier lobe immediately east of Fan A with a similar dip (coloured pink to be visible).

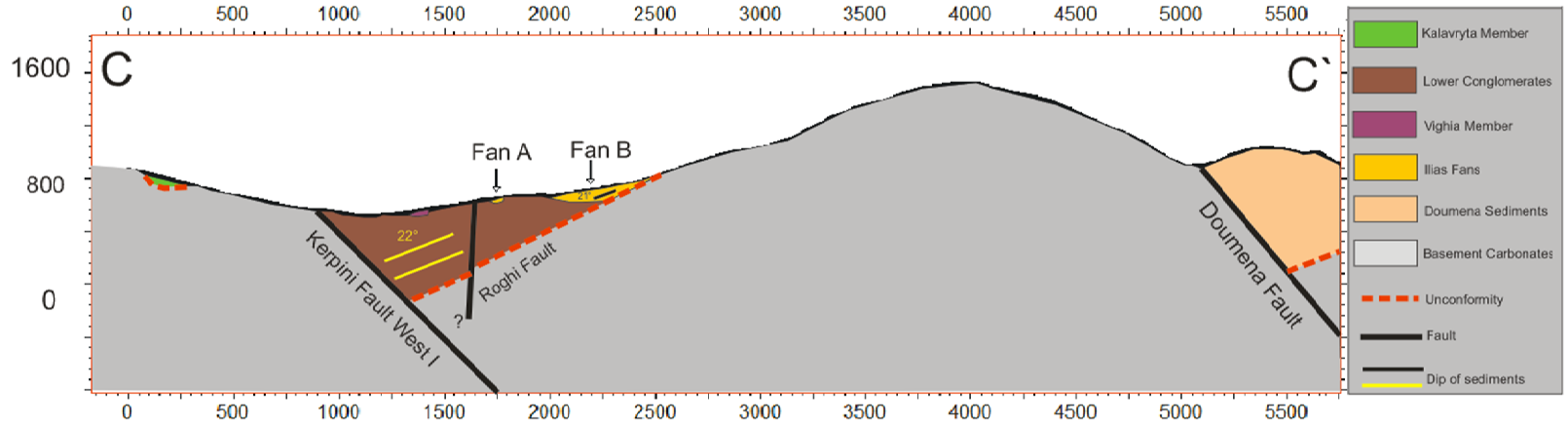

Figure 98: Cross section C-C` that barely intersects the Vighia Member and Fan A before it cuts through Fan B. The Roghi Fault, which is believed to be a transfer fault, dips quite vertically, and has a tiny offset in this location, as it is believed to die out in proximity to this location. The Kalavryta Member also outcrops in the very south, as seen here.

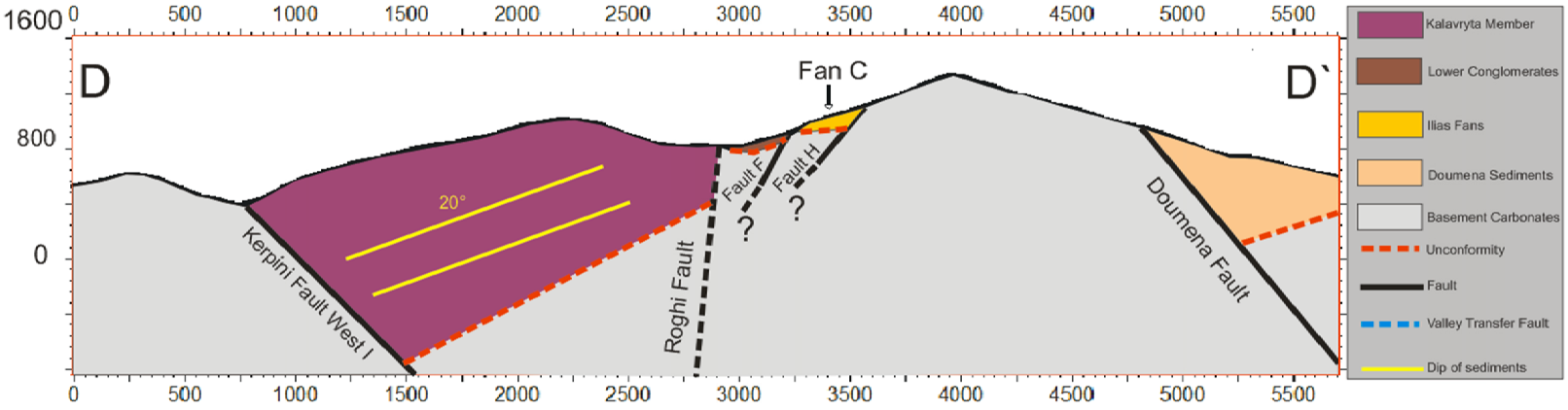

Figure 99: Cross section D-D`, which is the first cross section that intersects Roghi Mountain, and shows the thick conglomeratic package that is the Vighia Member. A tiny interval of Lower Conglomerates is also displayed, and faults F and H are visible in this section. The fault depths are unknown, and the depth of the unconformity is assumed to be shallow, as the unconformity contact is close to the location of the cross section.

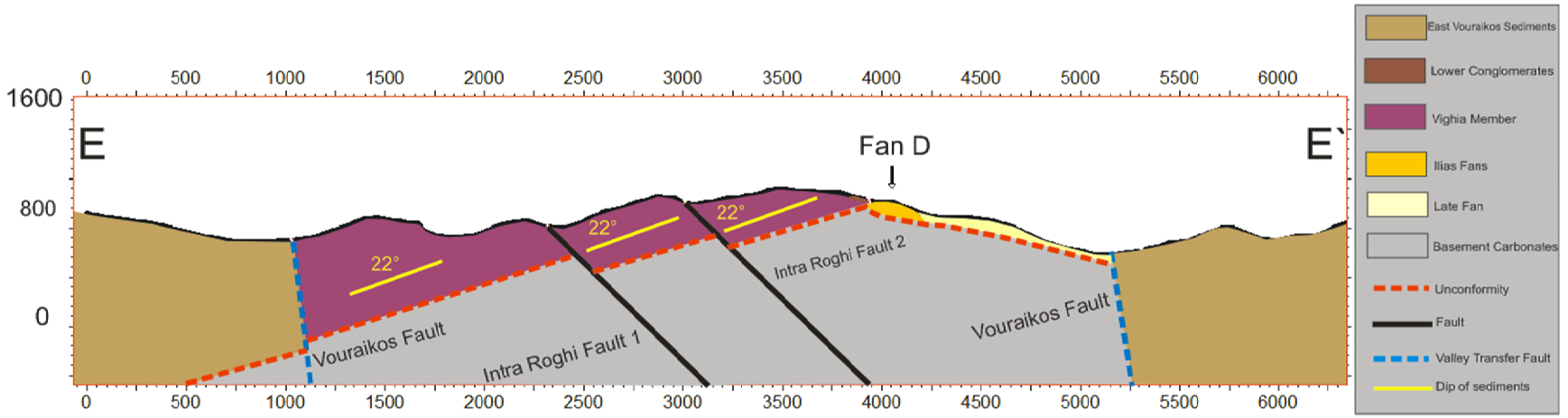

Figure 100: Cross section E-E`. This cross section goes through Roghi Mountain, and shows the two intra Roghi Faults where the unconformity is assumed to drop across each fault. Fan D is intersected to the north, and the Late Fan is also displayed here, assumed to be quite thin. The Vouraikos Fault displaces the basement far down, as it is not observable to the east of the valley.

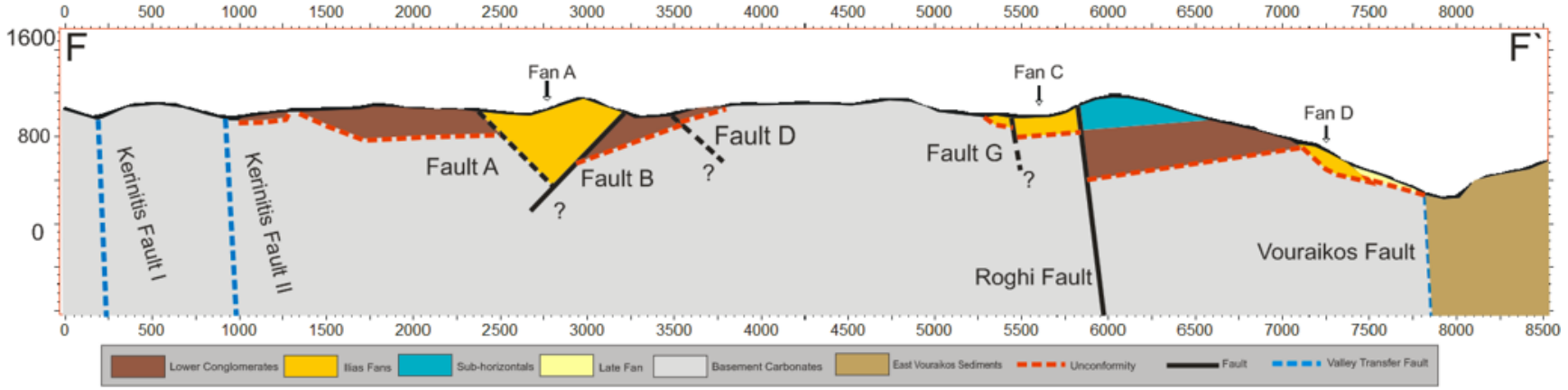

Figure 101*: Cross section F-F`, the first of three west-east cross section. This section intersects all the transfer faults and three of the Ilias Fans; A, C and D. Fault B is believed to be the dominating fault over Fault A, both of which has an unknown dip/depth. Fault D also has an unknown depth, but it displaces the basement, as observed in the field. Fault G has an unknown depth, but the unconformity is assumed to drop to a lower depth over the fault. The Roghi Fault dips slightly to the east, and displaces the unconformity to a lower but unknown depth. The Vighia Member is not intersected, but the sub-horizontal sediments can be seen on top of the Lower Conglomerates in this location. To the very east, it intersects Fan D, which is overlain by the Late Fan.*

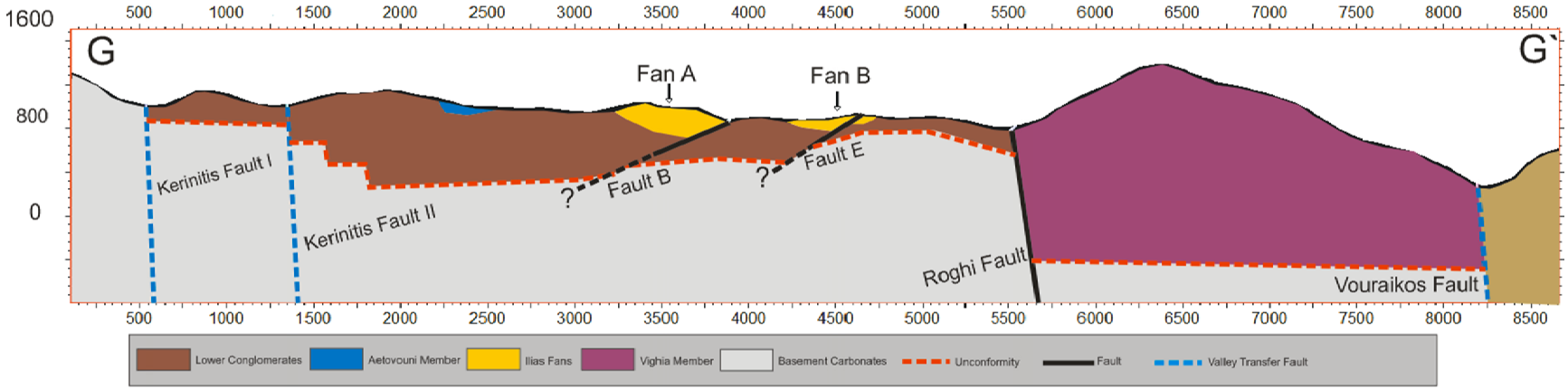

Figure 102: Cross section G-G`, the center east-west section. The thickness of the Lower Conglomerates increases to the east due to the steps of the Kerpini Fault. The displacement of the fault decreases to the west, where it terminates in the Kerinitis Fault 1. The cross section intersects Fan A around the mid-fan area, where it is thinner than in F-F`. Fan B is then intersected where the unconformity depth is unknown. However, it is assumed to jump to a higher level over Fault E. As aforementioned, the depths of fault B and E are unknown. The unconformity drops to a deep level over the Roghi Fault, and even further down in the Vouraikos River Valley.

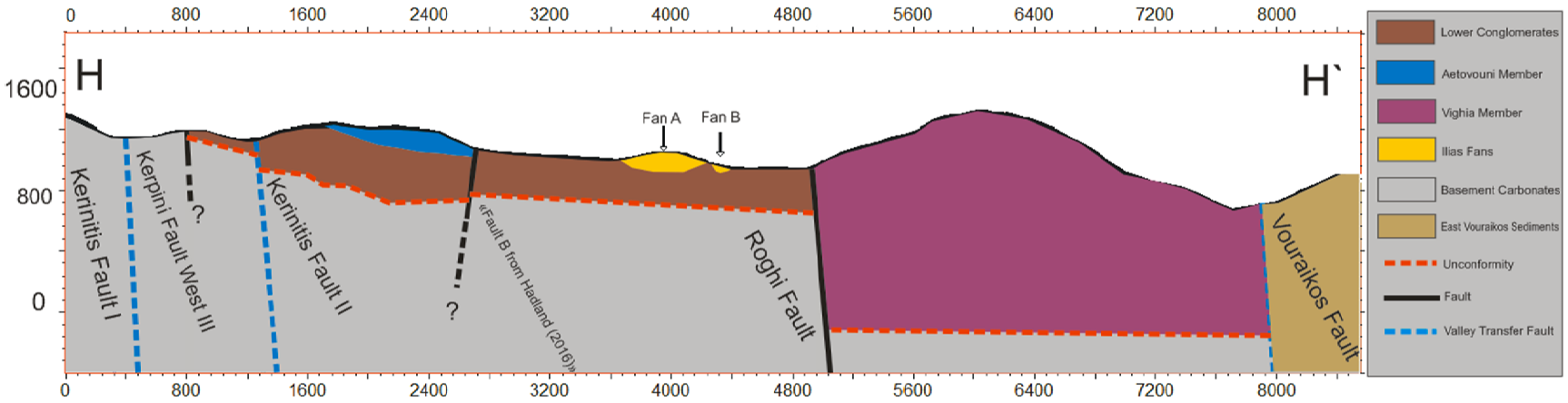

Figure 103: Cross section H-H`. The western data here is credited Hadland (2016). This section passes through the more distal areas of Fan A and B, where Fan B has nearly died out, and Fan A has thinned even further. As in the previous east-west sections, the unconformity drops in both the Roghi Fault and the Vouraikos River Valley.

6.5 Transfer faults

As previously discussed in Sub-chapter 2.2.1, there are transfer faults present in the major river valleys in the study area, Vouraikos in the east and Kerinitis in the west, and they both split into two (Figure 104). The rift segmentation is controlled by pre-existing transfer fault structures in the underlying pre-rift Pindos Basement (Ghisetti and Vezzani, 2005).

Syahrul (2014) suggested the presence of an additional transfer fault to the west of the Vouraikos Fault; the Roghi Fault. This fault was interpreted as having a near-vertical dip and a minimum displacement of 100-200 m. Dahman (2015) and Hadland (2016) supported the presence of this transfer fault, and there are some reasons as to why.

- Several faults terminate in this fault, and Fault I is observed stepping to the north. The Doumena Fault is believed to be stepping in this fault as well.
- There is a clear change in bed thickness and clast size across the fault.
- The fault creates accommodation space for the Vighia Member to deposit.
- The topography is clearly affected by what seems like a fault when viewed by satellite imagery, and its effect is seen as far south as the Kerpini Fault (Figure 13).
- There is a significant change in the basement unconformity elevation across the fault.

Essentially, the same arguments persist for all the transfer faults:

- Faults cannot be traced continuously across.
- Large lithological differences to either side.
- Unconformity elevation varies across.

The other main theory to explain the points listed above, is by a combination of paleo-topographic features and cross-faults. This is implausible at best. As shown in 5.2.1.1, the basement is generally not a flat and linear surface. It has local variations, but suggesting that these local variations are responsible for a ≈ 1000 m drop in the unconformity elevation over such a short distance (≈ 2 km) is farfetched. Combined with the discontinuous faults and the large lithological differences, the idea of transfer faults is more conceivable.

Figure 104: Google Earth satellite photo from south to north that shows how the Vouraikos and Kerinitis Transfer Faults split off in two different directions, quite similar to each other.

6.6 Kalavryta Member and Lower Conglomerates

As mentioned in Chapter 5, the Kalavryta Member of the Kalavryta Fault Block is correlatable with the Lower Conglomerates of the Kerpini Fault Block. The theory from Hadland (in prep) is that the Kalavryta Member was an alluvial fan deposited after the Kalavryta Fault activated. The fan extended far north, reaching the northern areas of the Kerpini Fault Block (Figure 105). According to Ford *et al.* (2013), this alluvial fan deposited across the Doumena Fault as well, but this is outside the scope of this thesis.

The Kerpini Fault initiated at a later stage, separating the Kalavryta Member in the Kalavryta Fault Block from the Kalavryta Member in the Kerpini Fault Block. The sediments defined as Lower Conglomerates in this thesis and the Kalavryta Member are considered the oldest sediments in their respective fault blocks, and they share many characteristics. As such, this is a plausible theory. They are both unconformably overlying the basement, chaotic and poorly sorted, distinguished by channel-like sand lenses, and appear to be related to an alluvial fan system. The sand lenses are present due to the widespread channelization that are believed to have occurred at the surface of the fan of the Kalavryta Member.

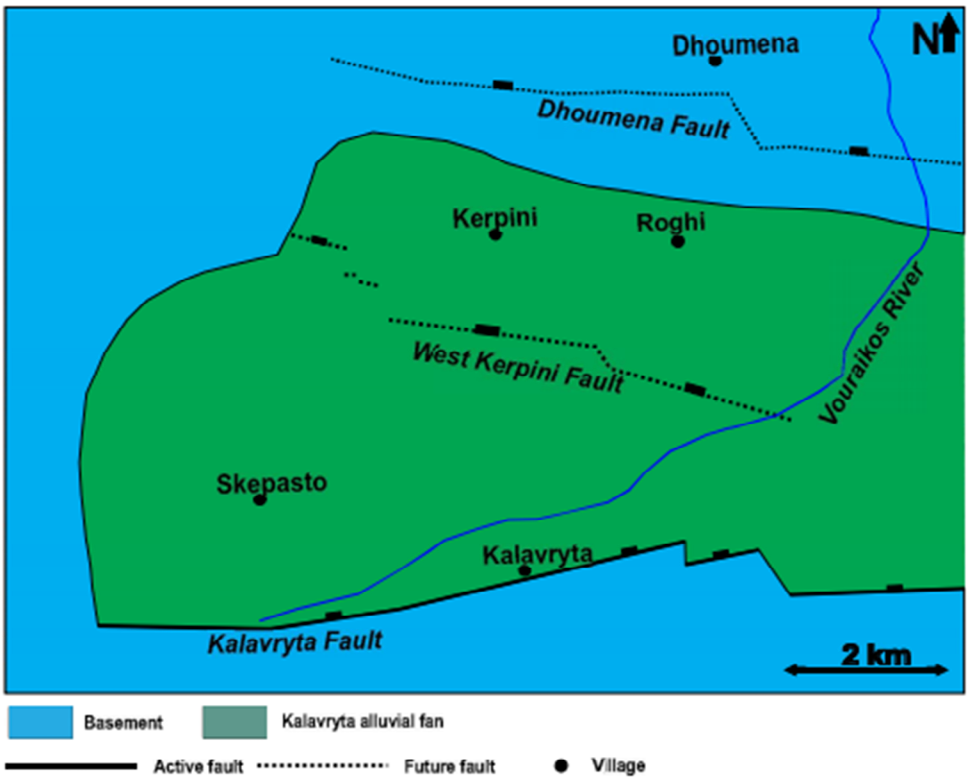

Figure 105: Proposed development of the Kalavryta Member (Hadland, in prep).

6.7 Profitis Conglomerates

The Profitis Conglomerates is a unique unit as described in 5.2.8. However, there are several similarities with the south-western conglomerates of Fan C:

- The same thin sandy facies occur in both outcrops (Figure 106 and Figure 76)
- Beds of both outcrops have the same east-dipping structural orientation
- The coarse conglomeratic beds are poorly defined, chaotic and poorly sorted

Figure 106: One of the many thinly layered sand intervals in the Profitis Conglomerates outcrop. The location of this photo is shown in Figure 71.

These combined characteristics and short distance between the two units suggest that Fan C may relate to the Profitis Conglomerates. However, this theory poses a problem. Fan C is thinning towards the northeast, where the most distal deposits are located. If this thinning trend was extrapolated to the Profitis Conglomerates, one would expect to find distal facies and not the coarse and chaotic beds that make up the Profitis Conglomerates outcrop. As such, they are classified as two different stratigraphic units.

6.8 XRD results

One green chert clast, and one red chert clast was analysed, as mentioned in Sub-chapter 4.2.2.3. This was done in order to say something about the depositional environment of the red and green clasts, and discuss why no green clasts are present in Fan D based on the results. The resulting mineral spectra were analysed in an XRD lab by a specialist, and the results are very dominated by quartz, as expected by a chert lithology. The problem, however, was that quartz was so prominent that all the other peaks in the spectrum disappeared in comparison. As such, no certain conclusion could be reached as to what colours the chert red and green. However, numerous red chert clasts that had begun to turn green were observed. Consequently, the green clasts are interpreted as having previously been red.

There are a few possibilities as to what causes this, such as influence by chlorite, reduced iron or glauconite. The influence of iron is most likely the cause of red colours in the shales and chert, but the green colour could be due to either of the possibilities. The XRD-analysis shows no minor peaks for glauconite, but there were minor shows of chlorite, which seemed like the most plausible explanation. Even though no conclusion was reached regarding the red and green colours, the clasts were confirmed to be chert without any doubt.

6.9 Evolutionary model

A step-by-step evolutionary model in a 2D map view was constructed to postulate on the relative timing of faults and stratigraphic units. A 3D model was attempted, but it quickly cluttered up, and the view became obstructed by all the elements in the figure. Based on interpretations discussed in every stage, a simplified seven-stage 2D model was constructed to postulate about the relative timing of the stratigraphic units in the fault block. A generalized chronostratigraphic overview is also presented to show the relative timing of faulting and sedimentation (Figure 107).

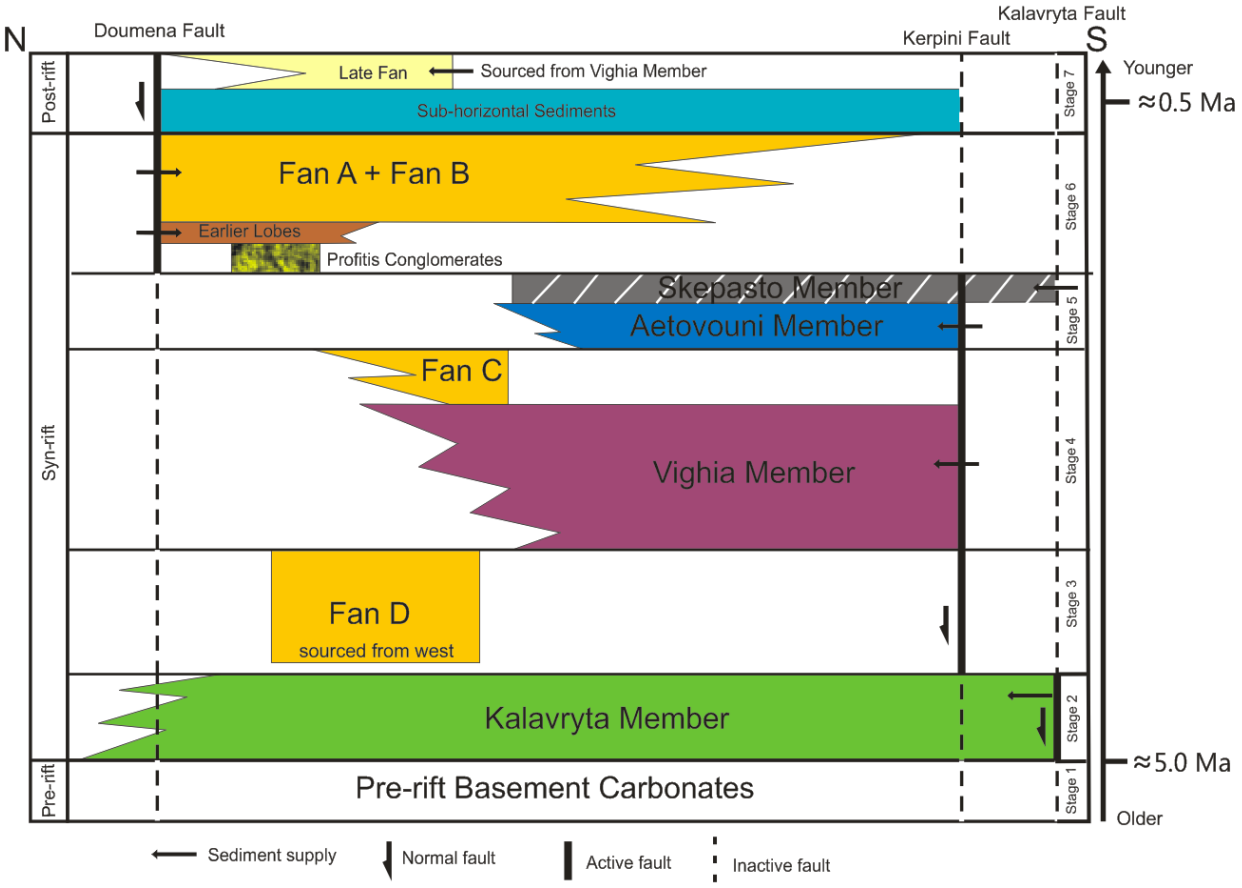

Figure 107: Chronostratigraphic chart showing the relative age relationships in the Kerpini Fault Block.

6.9.1 Stage 1

It is believed that the transfer faults were already present before the major north-dipping faults became active in the study area (Figure 108), and that the Doumena and Kerpini Faults stepped across pre-existing transfer zones rather than being affected by transfer faults at a later stage. The argument is that the segments on either side of the transfer faults have developed in a very different manner, as previously discussed. Oppedal (in prep) studied the various river valleys in a regional sense, and he supports the theory that the transfer faults are pre-existing structures. It is not certain how far south the Roghi Transfer Fault extends. In the geological map it terminates in the Kerpini Fault, but it is believed to extend further.

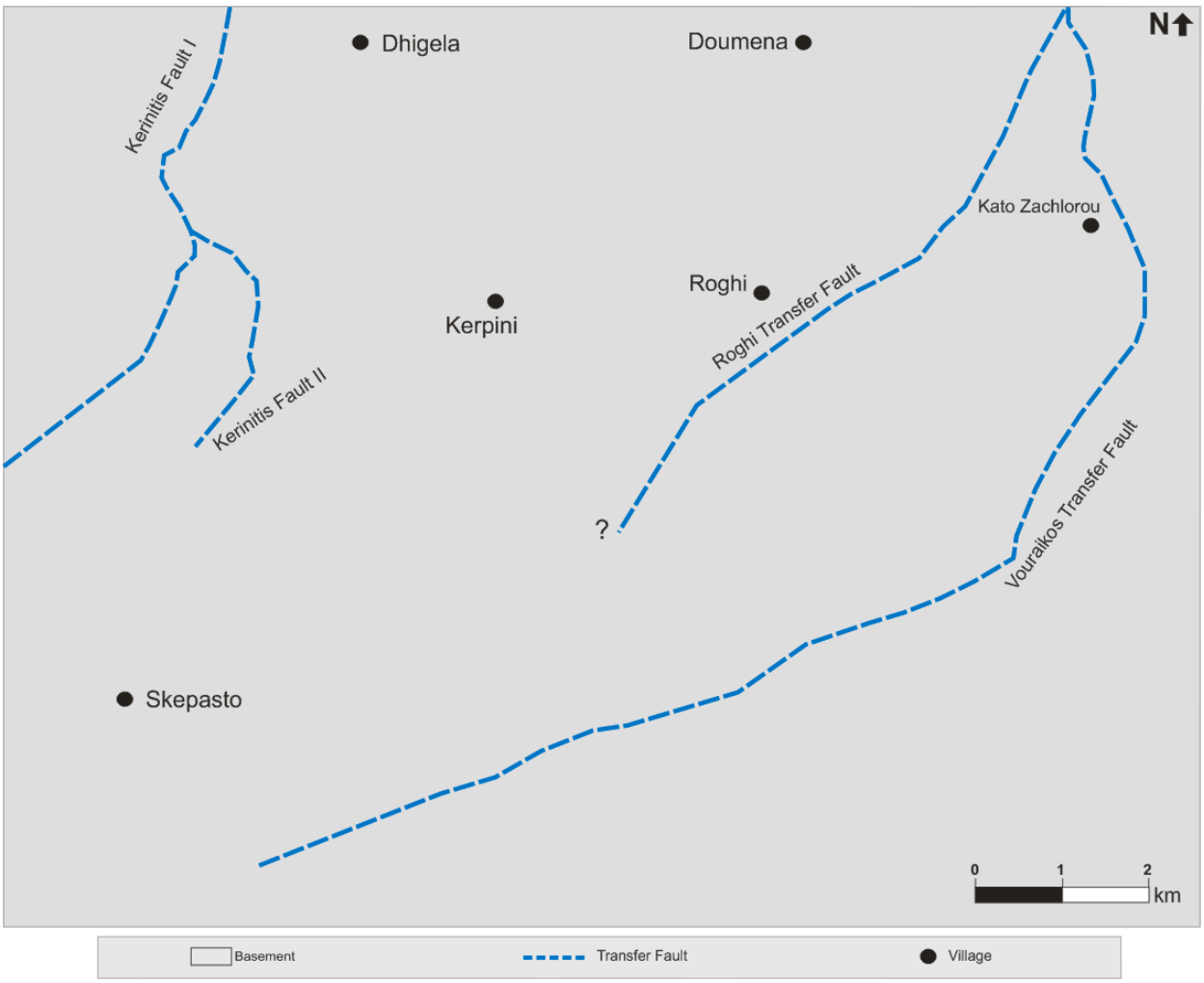

Figure 108: Shows the area of study prior to syn-rift deposition. The map extends further to the west, east and south, to include the Kalavryta Fault Block in the next stage.

6.9.2 Stage 2

There are some earlier events to the south of the Kalavryta Fault Block, but they are not important for the geology in the area of study. The first major north-dipping fault of importance was the Kalavryta Fault (Figure 109). This fault initiated early in the rift system, and consequently the Kalavryta Member deposited as a large and extensive alluvial fan from south to north. It is unknown whether it is sourced from multiple points or not. The Kalavryta Member is assumed to have been heavily affected by channelization due to the fluvial/alluvial character of the member.

Figure 109: Shows the active Kalavryta Fault in the south, and the subsequent deposition of the Kalavryta Member. It has a wide extent, and covers most of the Kerpini Fault Block that will later be confined to the north. Sand lenses observed in the field are derived from a widespread channelization across the fan surface.

6.9.3 Stage 3

After the Kalavryta Member deposited, the Kerpini Fault activated and cut it in half (Figure 110). This confined the Kalavryta Member to at least two fault blocks (Kerpini Fault Block and Kalavryta Fault Block). This is confirmed based on the presence of the Kalavryta Member in the immediate footwall to the Kerpini Fault. In Figure 110, all the erosional stages of the Kalavryta Member is simplified and combined into one figure. Thus, the unconformity in this figure represents the present day unconformity. This is done due to the uncertain erosion and development of the Kalavryta Member through time. Regarding the Kerpini Fault, the step between Kerpini Fault West and Kerpini Fault East is believed to happen first, followed by the western steps. This is also simplified and drawn to its present day configuration, as the development of this fault has been thoroughly described before (Syarhul, 2014; Hadland, 2016). Fan D deposited early in the development of the fault block. This is based on the observations that the unconformity is very shallow under Fan D, and that it is underlying all the surrounding strata.

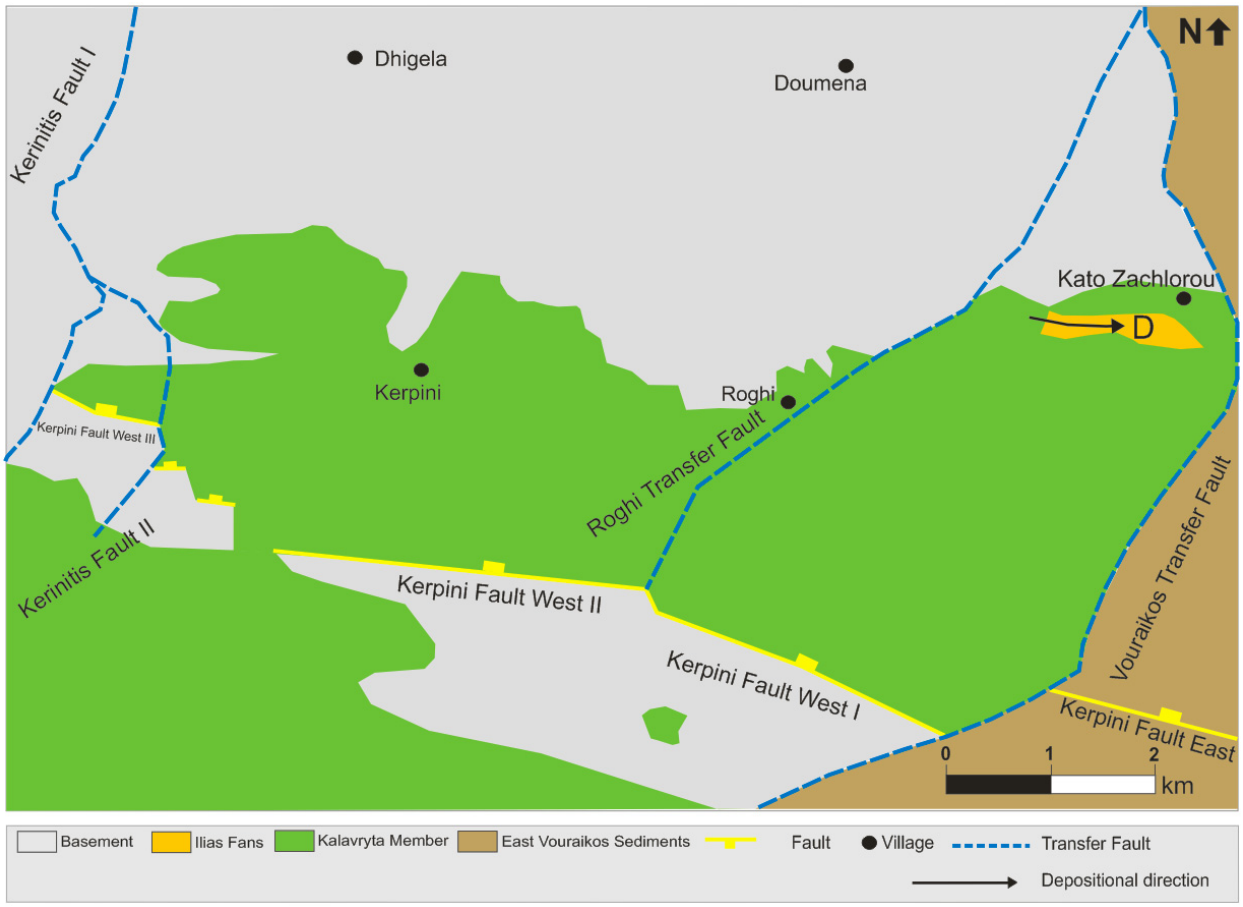

Figure 110: Shows how Fan D deposited in the northeast and activation of the Kerpini Fault.

6.9.4 Stage 4

The Vighia Member was mainly sourced from two entry points (Bjåland, 2016; Sigmunstad, 2016) (Figure 111). The first source point was between Kerpini Fault East, and Kerpini Fault West. The Vighia member is segmented by the Roghi and the Vouraikos Transfer Faults, which are the bounding faults for the Vighia Member. These faults are responsible for creating sufficient accommodation space for such a vast unit to deposit. The second source point was between Kerpini Fault West I and Kerpini Fault West II. The Vighia Member and Fan C are interpreted to be subsequent stratigraphic units relative to each other. This is based on the interpretation that Fan C is sourced from the south, and that some of the source material is derived from the Vighia Member. Another possible scenario is that Fan C deposited prior to the Vighia Member. In this scenario, the Roghi Fault caused footwall erosion and re-deposition of the Kalavryta Member (located in the footwall of the fault) as Fan C.

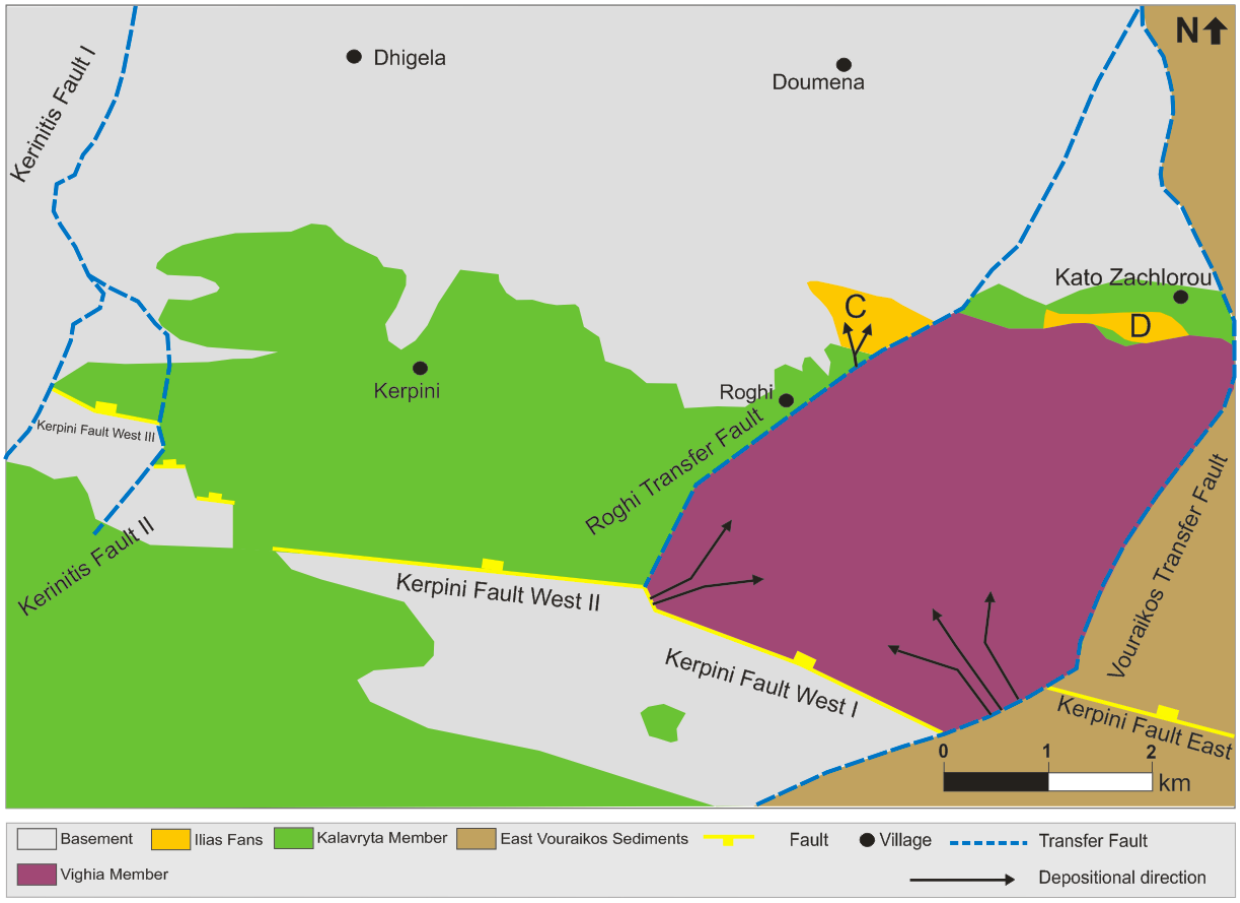

Figure 111: Shows how the Vighia Member deposited and is overlying Fan D. Fan C appear to have been deposited shortly after or at the same time as the Vighia Member.

6.9.5 Stage 5

The second step of the Kerpini Fault created a sediment pathway for deposition of the Aetovouni Member. This unit deposited in three different depositional stages marked with the numbers 1, 2, 3 (Figure 112) (Hadland, 2016), and is here summarized in one stage. The Aetovouni Member is overlain by the Skepasto Member, which is believed to be comprised of fluvial-derived deposits from the Kalavryta Fault Block.

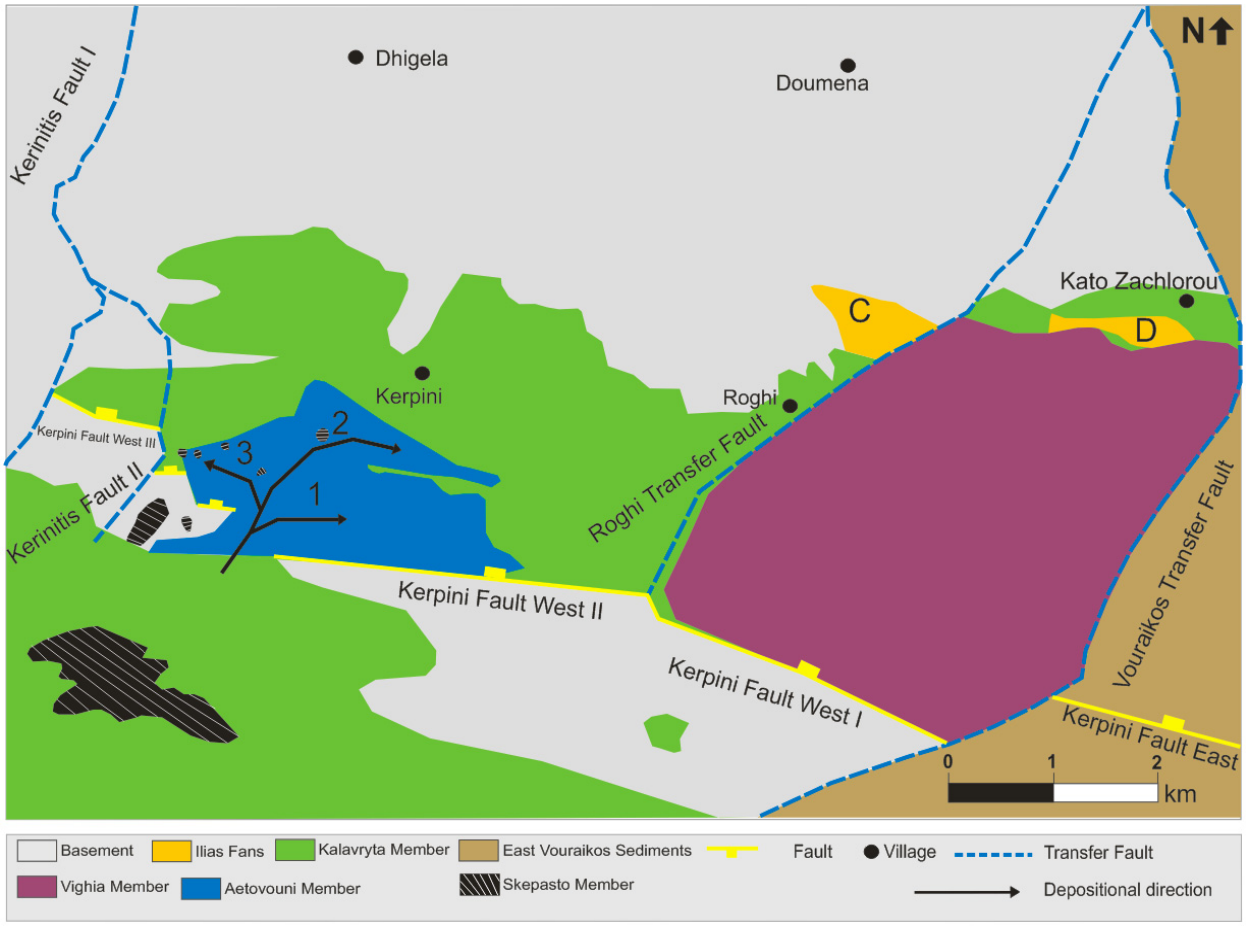

Figure 112: Shows how the Aetovouni Member deposited in the southwest, followed by the Skepasto Member.

6.9.6 Stage 6

After the deposition of the southerly derived stratigraphic units, the Doumena Fault became active. As previously mentioned, Fan A and Fan B have structural dips rather than depositional dips. They must have either been deposited prior to the Doumena Fault, or in the very earliest stages of it. The latter scenario is the most probable, as the Doumena Fault is believed to affect the deposition of these units. Fans A and B in addition to the Earlier Lobes and the Profitis Conglomerates deposited in an unknown sequence (Figure 113). One theory is that the Profitis Conglomerates deposited first, followed by the Earlier Lobes, then Fan A, and finally Fan B. It appears that the footwall-derived deposits from the north moves from old to young in an E-W direction. However, this is pure speculation, as no conclusive relationships between the units were observed in the field

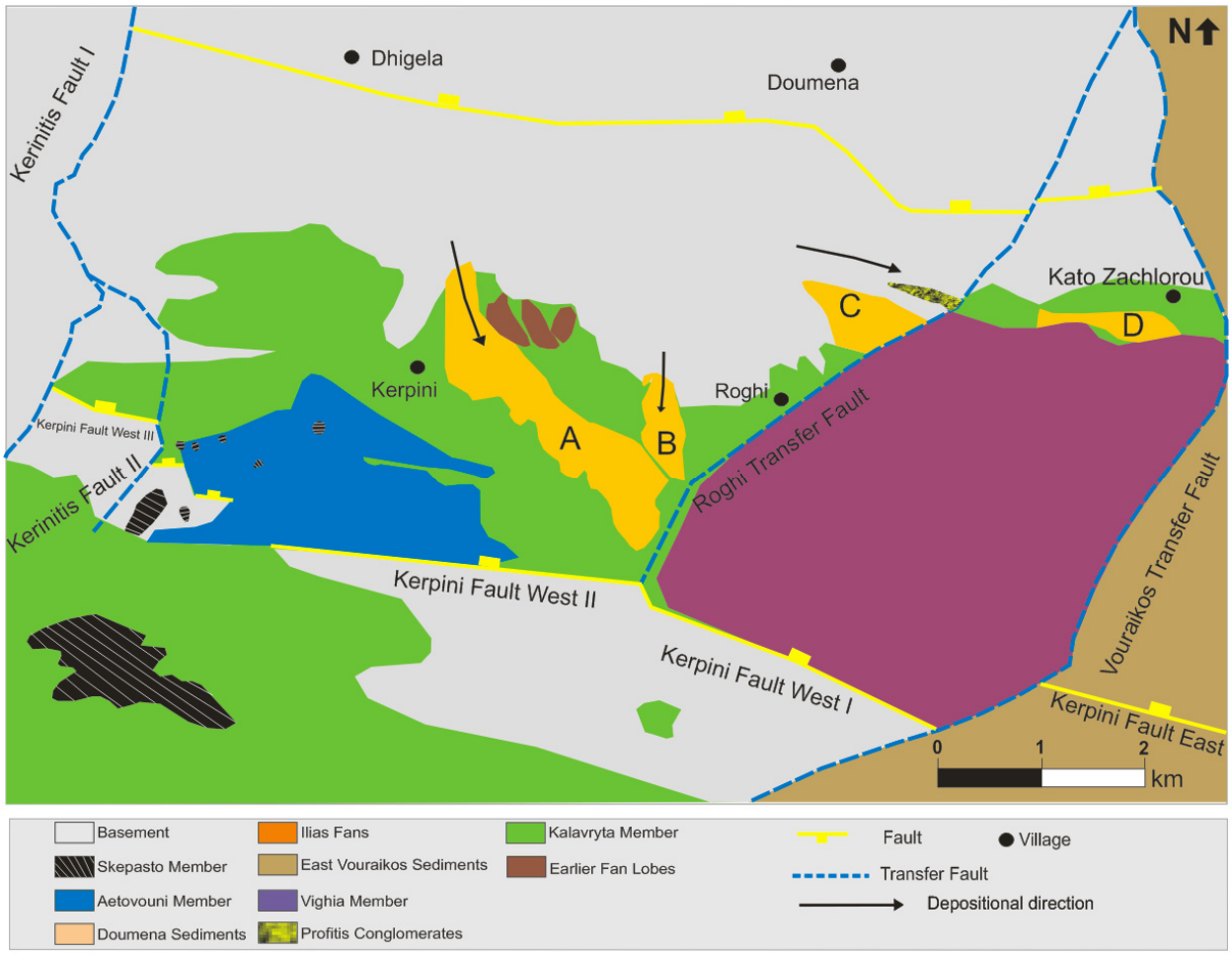

Figure 113: Shows how the Doumena Fault activates, and initiate the deposition of the Earlier Lobes, Fans A and B, and the Profitis Conglomerates.

6.9.7 Stage 7

The latest additions to the stratigraphic column are the Sub-horizontal Sediments, followed by the Late Fan (Figure 114). These are overlying all of their surrounding units, and it is evident that they deposited subsequently to the other stratigraphic units in the fault block. Stuvland (2015) did not reach a conclusion regarding the source of the Sub-horizontal Sediments. The Late Fan appears to be sourced from the south, possibly due to erosion of the Vighia Member.

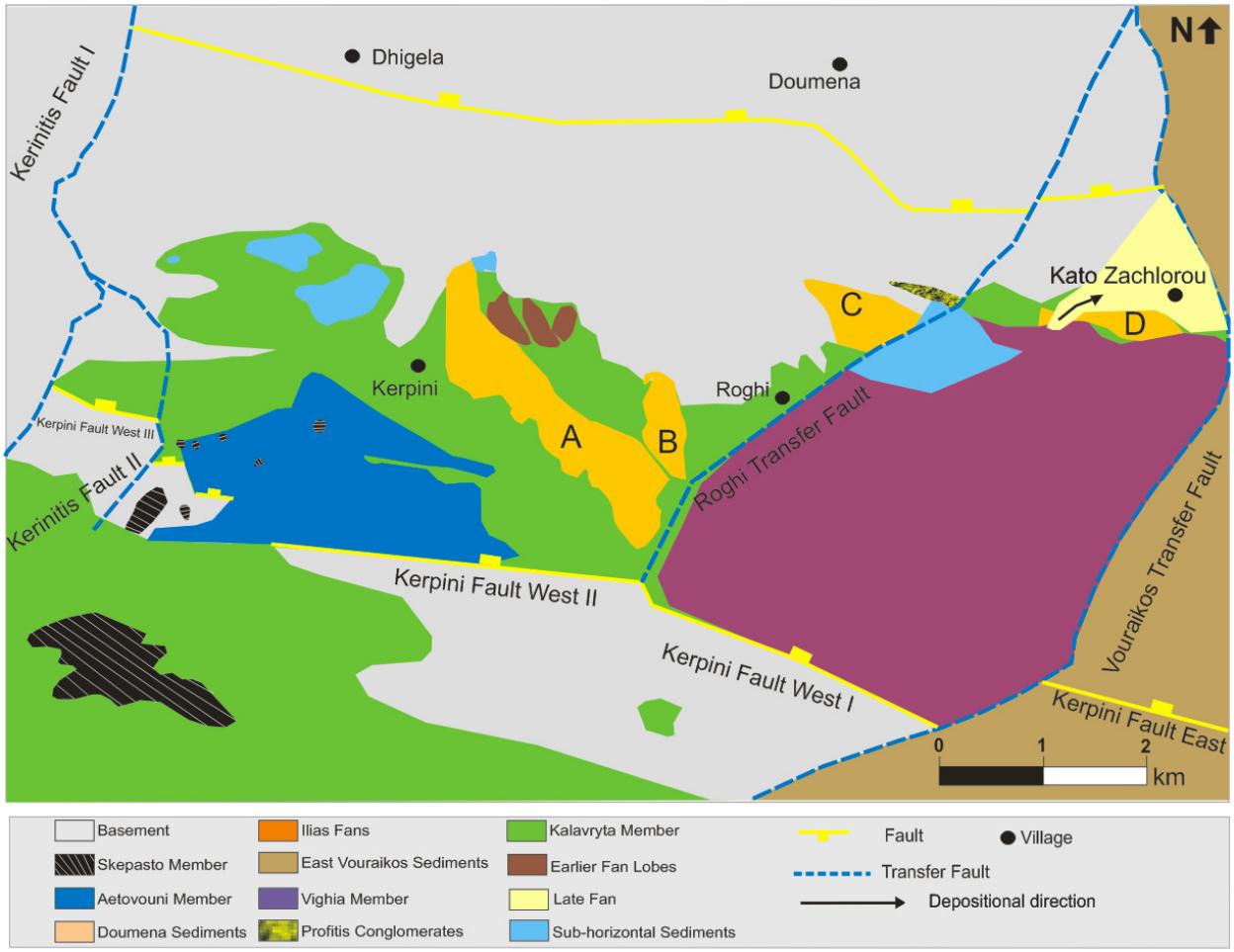

Figure 114: Shows how the Sub-horizontal Sediments deposited on top of the other stratigraphic units in the Kerpini Fault Block, followed by the Late Fan in the northeast.

Chapter 7: Conclusion

The Kerpini Fault Block has a complicated history. It consists of many different stratigraphic units in a complex relationship with each other. A generalized stratigraphic framework for the rift system as a whole (Ford et al., 2013) does not apply to the individual fault blocks and their respective details. This has been made clear based on several master theses done by students from the University of Stavanger (Syarhul, 2014; Dahman, 2015; Rognmo, 2015; Stuvland, 2015; Hadland, 2016; Bjåland, 2016; Sigmundstad, 2016). This study has contributed to a greater present-day knowledge of the fault block. It shows that to understand the sediment history within the various fault blocks; thorough and detailed outcrop studies are required.

The objectives of this thesis was to:

- Resolve whether the four units are alluvial fans and if so; classify them, and
- Determine their relative timing concerning faulting and other stratigraphic units in the Kerpini Fault Block.

Firstly, the proposed alluvial fans by Hadland (2016) are confirmed to be individual alluvial fans. He suggested that they were footwall-derived, and this is only a possibility for Fan A and Fan B, which appear to be sourced from the uplifted footwall of the Doumena Fault. Fan C is deposited from the south, in a different structural setting than the other two fans. Furthermore, Fan D is deposited from west to east, but whether the source material originates from the footwall of the Roghi Fault or from erosional events in the valley side, remains unknown.

There are pre, syn and post-fault strata within the Kerpini Fault Block. The Lower Conglomerates make up the pre-fault strata in the area of study, and they can be correlated with the Kalavryta Member. The syn-fault strata are comprised of the Aetovouni Member, Ilias Fans, Vighia Member, Skepasto Member and the Earlier Lobes. The post-fault strata consist of Sub-horizontal Sediments and the Late Fan.

Fans A, B and C are classified as sheetflood dominated fans based on their respective vertical and lateral facies variabilities. Fan D classifies as a debris-flow dominated fan due to a coarse and homogenous facies distribution. This fan is clearly characterized by a high-energy depositional environment dominated by mass movement of sediments, contrary to Fans A, B and C which are more affected by episodic movements and water influence.

Regarding the relative timing of the four fans, Fan D deposited first, followed by Fan C, and finally Fan A and Fan B at more or less the same stage in the evolution of the Fault Block. Fan D deposited in the earliest stages of the Kerpini Fault, prior to the Vighia Member and the Doumena Fault. Fan C deposited shortly after the Vighia Member or during the same time, prior to the activation of the Doumena Fault. Fans A and B deposited on a flat surface prior to or in the very earliest stages of the Doumena Fault, and was later tilted to their present day southern dips.

The results of this study have both confirmed and contradicted previous theories, and consequently contributed to a better present-day understanding of the Kerpini Fault Block. Further investigation into the Kerpini Fault Block is still needed to resolve some unanswered problems.

- The sourcing, provenance and transport distance of the four fans are still not properly understood. Conglomerates are complicated deposits, as they are often a result of reworked sediments. A detailed provenance study into the four fans coupled with proper sampling and sample analyses could potentially contribute to a better understanding of where the sediments are sourced from.

Reference list

Armijo, R., Meyer, B., King, G. C. P., Rigo, A., and Papanastassiou, D. (1996). Quaternary evolution of the Corinth Rift and its implications for the Late Cenozoic evolution of the Aegean. *Geophysical Journal International, 126*, 11-53.

Avallone, A., Briole, P., Agatza-Balodimou, A., Billiris, H., Charade, O., Mitsakaki, C.*, et al.* (2004). Analysis of eleven years of deformation measured by GPS in the Corinth Rift Laboratory area. *C. R. Geosci., 336*(4-5), 301-311. doi:10.1016/j.crte.2003.12.007

Bjåland, S., Stian. (2016). *Case Study of Roghi Mountain. Greece -Mapping and modelling of facies development within an alluvial sequence.* (M.Sc), University of Stavanger, Unpublished.

Blair, T. C., and McPherson, J. G. (1994). Processes and Forms of Alluvial Fans. In A. J. Parsons & A. D. Abrahams (Eds.), *Geomorphology of Desert Environments* (pp. 55): Springer Science

Blissenbach, E. (1954). Geology of alluvial fans in semiarid regions. *Geological Society of America Bulletin, 65*(2), 175-190.

Boothroyd, J. C. (1972). Coarse-Grained Sedimentation on a Braided Outwash Fan, Northeast Gulf of Alaska.

Collier, R., and Jones, G. (2004). Rift Sequences of the Southern Margin of the Gulf of Corinth (Greece) as Exploration / Production Analogues*. *Search and Discovery, 50007*.

Dahman, A. (2015). *The Vouraikos Valley: an example of rift segmentation in the Corinth Graben, Greece.* (M.Sc), University of Stavanger.

Drew, F. (1873). Alluvial and Lacustrine Deposits and Glacial Records of the Upper-Indus Basin. *Quarterly Journal of the Geological Society, 29*, 441-471.

Finnesand, S. (2013). *Analysis of Structural Control in Fault Interactions and their Sediment accumulation in the Gulf of Corinth rift, Greece.* (M.Sc), University of Stavanger, Stavanger.

Flotté, N., Sorel, D., Müller, C., and Tensi, J. (2005). Along strike changes in the structural evolution over a brittle detachment fault: Example of the Pleistocene Corinth-Patras rift (Greece). *Tectonophysics, 403*(1-4), 77-94.

Ford, M., Hemelsdael, R., Marco, M., and Palyvos, N. (2016). Rift migration and lateral propagation: evolution of normal faults and sediment-routing systems of the western Corinth rift (Greece). *Geological Society London Special Publications*. doi:10.1144/SP439.15

Ford, M., Rohais, S., Williams, E. A., Bourlange, S., Jousselin, D., Backert, N.*, et al.* (2013). Tectono-sedimentary evolution of the western Corinth rift (Central Greece). *Basin Research, 25*(1), 3-25.

Galloway, W. E., and Hobday, D. K. (1996). *Terrigenous Clastic Depositional Systems, Applications to Fossil Fuel and Groundwater Resources* (2nd edition ed.). Berlin, Heidelberg Springer - Verlag.

Ghisetti, F., and Vezzani, L. (2005). Inherited structural controls on normal fault architecture in the Gulf of Corinth (Greece). *Tectonics, 24*(4), 1-17.

Hadland, S. (2016). *Geological Mapping and Investigation into a Proposed Syn-rift Alluvial Fan Deposit in the Kerpini Fault Block, Greece.* (M.Sc), University of Stavanger.

Hemelsdaël, R., Ford, M., Malartre, F., and Gawthorpe, R. (2017). Interaction of an antecedent fluvial system with early normal fault growth: Implications for syn-rift stratigraphy, western Corinth rift (Greece). *Sedimentology*. doi:10.1111/sed.12381

Le Pichon, X., and Angelier, J. (1979). The Hellenic Arc and Trench System: A key to the neotectonic evolution of the Eastern Mediterranean Area. *Tectonophysics, 60*, 1-42.

Leeder, M. R., Mack, G. H., Brasier, A. T., Parrish, R. R., McIntosh, W. C., Andrews, J. E.*, et al.* (2008). Late-Pliocene timing of Corinth (Greece) rift-margin fault migration. *Earth and Planetary Science Letters, 274*(1-2), 132-141.

Lopes, G. C. (2015). *Geological Mapping of the South-central Gulf of Corinth Coastal Fault System - Greece.* (M.Sc), University of Stavanger, Stavanger.

Mastronuzzi, G., Sanso., P., and Stamatopoulos., L. (1994). Glacial landforms of the Peloponnisos (Greece). *Rivista Geografica Italiana, 101*, 77-86.

Moretti, I., Sakellariou, D., Lykousis, V., and Micarelli, L. (2003). The Gulf of Corinth: An active half graben? *Journal of Geodynamics, 36*(1-2), 323-340.

Morley, C. K. (1995). Developments in the structural geology of rifts over the last decade and their impact on hydrocarbon exploration. *J.J Lambise, Ed., Hydrocarbon Habitat in Rift Basins: Geological Society Special Publication, 80*, 1-32.

Oppedal, E. (in prep). *Rift Segmentation: Structural mapping in the Kerpini-Tsivlos and the Dhoumena Fault Blocks, Greece.* (M.Sc), University of Stavanger.

Pope, R. J., Hughes, P. D., and Skourtsos, E. (2015). The glacial history of Mount Chelmos, Peloponnesus, Greece. *Geological Society, London, Special Publications, 433*(1).

Rietbrock, A., Tiberi, C., Scherbaum, F., and Lyon-caen, H. (1996). Seismic slip on a low angle normal fault in the Gulf of Corinth: Evidence from a high-resolution cluster analysis of microearthquakes. *Geophysical Research Letters, 23*, 1817-1820.

Rognmo, T. (2015). *Sedimentary Infill in the Kalavrita Faulted Block, South-central Gulf of Corinth, Greece.* (M.Sc), University of Stavanger.

Royden, L. H. (1993). The tectonic expression slab pull at continental convergent boundaries. *Tectonics, 12*(2), 303-325.

Sigmundstad, E. (2016). *Detailed Structural Mapping and Correlation of a Thick Syn-Rift Sequence in the Kerpini Fault Block, Greece.* (M.Sc), University of Stavanger.

Skourlis, K., and Doutsos, T. (2003). The Pindos Fold-and-thrust belt (Greece): Inversion kinematics of a passive continental margin. *International Journal of Earth Sciences, 92*(6), 891-903.

Sorel, D. (2000). A Pleistocene and still-active detachment fault and the origin of the Corinth-Patras rift, Greece. *Geology, 28*, 83-86.

Stuvland, M. E. (2015). *Kalavryta and Kerpini Fault Block: Investigation into correlation and nature of sub-horizontal layers; Corinth Graben, Greece.* (M.Sc), University of Stavanger.

Syahrul, R. (2014). *Fault Controlled Sedimentation: A case study of the Kerpini Fault, Greece.* (M.Sc), University of Stavanger.

Taylor, B., Weiss, J. R., Goodliffe, A. M., Sachpazi, M., Laigle, M., and Hirn, A. (2011). The structures, stratigraphy and evolution of the Gulf of Corinth rift, Greece. *Geophysical Journal International, 185*(3), 1189-1219.

Tucker, M. E. (2011). *Sedimentary Rocks in the Field: A Practical Guide* (Vol. 4). Chicester: John Wiley & Sons.

Wentworth, C. K. (1922). A scale of Grade and Class Terms for Clastic Sediments. *The Journal of Geology, 30*(5), 377-392.

Wood, A. M. (2013). *The influence of fault geometric uncertainty on hydrocarbon reservoir and simulation models.* (Ph.D. Doctoral thesis), University of Leeds. Retrieved from http://etheses.whiterose.ac.uk/id/eprint/5885